Formation of ternary oxides in the gas phase.
Mass spectrometric and quantum chemical investigation

Von der Naturwissenschaftlichen Fakultät

der Gottfried Wilhelm Leibniz

Universität Hannover

Zur Erlangung des Grades

Doktorin der Naturwissenschaften

(Dr. rer. nat.)

genehmigte Dissertation von

Katerina Alexandrovna Kunkel, geb. Berezovskaya,

Diplom kandidata nauk, Diplom chimik (Russland)

Geboren am 29.10.1979 in Nowotscheboksarsk, Russland

2015

Referent: Prof. Dr. Michael Binnewies

Koreferent: Prof. Dr. Franz Renz

Tag der Promotion: 12.03.2015

Die vorliegende Dissertation wurde als kumulative Arbeit eingereicht. Grundlage dieser Arbeit sind die folgenden Publikationen:

1   K. Kunkel, E. Milke, M. Binnewies, **Formation and stability of gaseous ternary oxides of group 14-16 elements and related oxides of group 15 elements: mass spectrometric and quantum chemical study,** *Eur. J. Inorg. Chem.* 2015, 124-133.

2   K. Kunkel, E. Milke, M. Binnewies, **Formation of ternary lead-molybdenum oxides PbMoO$_4$, PbMo$_2$O$_7$ and Pb$_2$MoO$_5$ in the gas phase. Mass spectrometric and quantum chemical investigation,** *Int. J. of Mass Spectrom.* 374, 2014, 12-19.

3   K. Kunkel, E. Milke, M. Binnewies. **A mass spectrometric and quantum chemical study of the vaporisation of lead monoxide in a flow of gaseous arsenic and antimony trioxides** *Dalton Trans.*, 43, 2014, 5401-5408.

4   E. Berezovskaya, E. Milke, M. Binnewies. **The formation and stability of molybdenum-antimony and tungsten-antimony ternary oxides Sb$_2$MO$_6$, Sb$_2$M$_2$O$_9$, Sb$_2$Mo$_3$O$_{12}$ and Sb$_4$MO$_9$ in the gas phase (M = Mo, W). Quantum chemical and mass spectrometric studies**, *Dalton Trans.*, 41 (35), 2012, 10769-10776.

5   E. Berezovskaya, E. Milke, M. Binnewies. **Formation and stability of molybdenum-tellurium oxides MoTeO$_5$, Mo$_2$TeO$_8$, Mo$_3$TeO$_{11}$ and MoTe$_2$O7 in the gas phase. Quantum chemical and mass spectrometry determination of standard enthalpy of formation**, *Dalton Trans.* 2012, 41 (8), 2012, 2464-2471.

Contents

Preface and acknowledgements

This thesis is results of Ph.D study which was conducted at the Institute of Inorganic Chemistry at the Gottfried Wilhelm Leibniz University under the supervision of Prof. Dr. Michael Binnewies since May 2010 until November 2014.

Five research articles in which I have been participate as primary author are presented in this thesis. I wrote these articles with the kind support of co-authors. My contribution was preparation of samples, interpretation of mass spectra, conducting of quantum chemical calculations and analysing of results.

First of all, I kindly thank Prof. Dr. Michael Binnewies for his excellent and outstanding support during all my work, his readiness to discuss results of study. I feel extremely fortunate to work under his supervision and in his research group.

I thank all members of the Binnewies research group, particularly Dr. Edgar Milke for his technical support of mass spectrometric measurement. I also like to thank Dr. Ralf Köppe from Institute of Inorganic Chemistry, Karlsruhe Institute of Technology.

I would also like to thank my family, particularly my husband Stefan for his patience.

Abstract

The formation and stability of the row of hitherto unknown ternary oxides in the gas phase has been studied. The following novel 24 ternary gaseous oxides were detected:

- $MoTeO_5$, Mo_2TeO_8, Mo_3TeO_{11} and $MoTe_2O_7$ in $MoO_3 - TeO_2$ system;
- $PbMoO_4$, $PbMo_2O_7$, $PbMo_3O_{10}$ and Pb_2MoO_5 in $PbO - MoO_3$ system;
- $PbTeO_3$, $PbTe_2O_5$, Pb_2TeO_4 and $Pb_2Te_2O_6$ in $PbO - TeO_2$ system;
- $PbAs_2O_4$, $PbSb_2O_4$ and $Pb_3As_2O_6$ in $PbO - X_2O_3$ systems (X = As, Sb);
- Sb_2MoO_6, $Sb_2Mo_2O_9$, $Sb_2Mo_3O_{12}$, Sb_4MoO_9, Sb_2WO_6, $Sb_2W_2O_9$ and Sb_4WO_9 in $Sb_2O_3 - MO_3$ (M = Mo, W) system;
- Sb_2TeO_5 and $Sb_2Te_2O_7$ in $Sb_2O_3 - TeO_2$ system.

The gaseous species was identified in mass spectrometric experiments by the determination of m/z-values and isotopic patterns. Thermodynamic data for the ternary oxides were obtained experimentally by means of a mass spectrometric Knudsen-cell method and were confirmed by quantum chemical calculations. The structures of the gaseous oxides were obtained by means of quantum chemical calculations too. Several compounds exist in two stable isomeric forms in the gas phase. The appearance energies were obtained experimentally and compared with theoretical vertical ionisation energies.

Keywords: gaseous ternary oxides, mass spectrometry, quantum chemical calculations

Zusammenfassung

Die Bildung und Stabilität einer Reihe von bisher unbekannten ternären Oxiden in der Gasphase wurde untersucht. Die folgenden neuen 24 ternären gasförmigen Oxide nachgewiesen:

- $MoTeO_5$, Mo_2TeO_8, Mo_3TeO_{11} und $MoTe_2O_7$ in $MoO_3 - TeO_2$ System;
- $PbMoO_4$, $PbMo_2O_7$, $PbMo_3O_{10}$ und Pb_2MoO_5 in $PbO - MoO_3$ System;
- $PbTeO_3$, $PbTe_2O_5$, Pb_2TeO_4 und $Pb_2Te_2O_6$ in $PbO - TeO_2$ System;
- $PbAs_2O_4$, $PbSb_2O_4$ und $Pb_3As_2O_6$ in $PbO - X_2O_3$ Systems (X = As, Sb);
- Sb_2MoO_6, $Sb_2Mo_2O_9$, $Sb_2Mo_3O_{12}$, Sb_4MoO_9, Sb_2WO_6, $Sb_2W_2O_9$ und Sb_4WO_9 in $Sb_2O_3 - MO_3$ (M = Mo, W) System;
- Sb_2TeO_5 und $Sb_2Te_2O_7$ in $Sb_2O_3 - TeO_2$ System.

Die gasförmigen Spezies in den massenspektrometrischen Experimenten durch die Bestimmung von m / z-Werten und Isotopenmuster identifiziert. Thermodynamischen Daten für die ternären Oxide wurden experimentell mit Hilfe eines massenspektrometrischen Knudsenzellen-Verfahrens erhalten und quantenchemischen Berechnungen bestätigt. Die Strukturen der gasförmigen Oxide wurden durch quantenchemische Berechnungen erhalten. Mehrere Verbindungen existieren in zwei stabilen isomeren Formen in der Gasphase. Die Auftrittsenergien wurden experimentell bestimmt und mit den theoretisch berechneten vertikalen Ionisationsenergien verglichen.

Schlagwörter: gasförmige ternäre Oxide, Massenspektrometrie, quantenchemische Berechnungen

1 INTRODUCTION

The formation and stability of gaseous ternary oxides from individual metal oxides have been investigated in the present work.

Metal oxides have a very broad application area and represent an attractive class of materials whose properties cover the entire range from semiconductors to insulators and are interesting for many aspects of material science, chemistry, physics and engineering science. The area of application is quite wide: electronics [1-2], photonics [3-5], catalysis [6-7], chemical and biological sensors [8-10], thermionic emission [11], energy storage devices [12 -14], e.g. In the past few years many studies of the metal oxides were devoted to the synthesis, structural, physical and chemical characterization. A large number of scientific papers have been published on metal-oxide nanostructures and thin films. The chemical vapour deposition (CVD) [15 -17], physical vapour deposition (PVD) [18 -19] and vapour transport [20-22] technique are the main synthesis methods for growing nanostructures and thin films. Therefore it is important to study properties of the gaseous oxides and ternary oxides.

The vaporization and thermodynamic properties of many individual oxide systems and some ternary oxides have been widely studied. Very informative and detailed overview of the properties of the gaseous individual oxides is reported in the handbook of Kazenas et al. [23].

There are many studies devoted to the formation of ternary oxides in the gas phase too. However the investigation of the ternary systems is not complete. There are many systems which were not studied at all or were studied superficially. Many gaseous ternary oxide systems are presented in recent review of Lopatin et al. [24] and handbook of Kazenas et al. [25].

The investigation of the evaporation process provided the rich information about the composition of the vapour, stability of the gas compounds and equilibrium processes in the gas phase. The most of studies were carried out by means of mass spectrometry using effusion Knudsen cell method. The composition of vapour of individual oxides is not simple and contains monomer and oligomer molecules. The composition of the vapour of ternary oxides is even more complicated. The composition of oxide ternary systems in the gas phase differs from the composition of condense state. Some compounds of oxide system exist in both gas and condense state; other compounds of the same oxide system exist only in the gas or condense state.

Mass spectrometric experiment gives the possibility to determine the partial pressures of gaseous species and consequently the equilibrium constant of gas reactions.

The dependence of the recorded ion currents on the partial pressure of the particular ion is described by the following equation:

$$p_i = c \cdot \frac{\sum I_i \cdot T}{\sigma_i \cdot S}$$ (1.1)

where p_i = the partial pressure of component i, c = the proportionality factor, $\sum I_i$ = the intensity of all of the ions formed by the ionisation and fragmentation of a gaseous molecule of i, T = temperature, σ_i = the ionisation cross section and S_i = the electron multiplier efficiency. The approximated eq. 1.2 can be used in most cases (the procedure of simplification is described elsewhere [26]):

$$p_i = c \cdot \sum I_i \cdot T$$ (1.2)

The proportionality factor c is determined by a calibration experiment.

The mass spectrometric study of the gaseous oxide systems which presented in that work is limited by the narrow temperature range. Therefore the obtaining of the reaction enthalpy $\Delta_r H^0_T$ by means of second law of thermodynamics, where temperature dependence of equilibrium constants has to be determined (eq. 1.3), is not possible.

$$\mathrm{d} \ln K_{p,T} / \mathrm{d}\, T = \Delta_r H^0_T / RT^2$$ (1.3)

The third law of thermodynamic (eq. 1.4) can be applied. The difficulty of that approach is determination of the reaction entropy $\Delta_R S^0_T$.

$$\Delta_r H^0_T = -R \cdot T \cdot \ln K_{p,T} + T \cdot \Delta_R S^0_T$$ (1.4)

Usually the calculation of entropies based on "rigid rotor-harmonic oscillator" approximation, with using data on molecular structures and normal mode frequencies. Except the mentioned method of statistical thermodynamics quantum chemical calculations can be applied for the determination of reaction entropy. Additionally quantum chemical calculation give the possibility determine the reactions enthalpy of the equilibrium processes at standard and experimental temperatures, the structure of the gaseous components in oxide system and IR spectra of the molecules. Thus the two main methods applied in the present study are mass spectrometry and quantum chemical calculations.

2 Objects of the investigation.

In the present work hitherto unknown ternary gaseous oxides have been investigated. Following systems are in the centre of interest: $MoO_3 - TeO_2$, $PbO - MoO_3$, $PbO - TeO_2$, $PbO - X_2O_3$ (where X = As, Sb), $Sb_2O_3 - MO_3$ (M = Mo, W) and $Sb_2O_3 - TeO_2$. The individual oxides MoO_3, WO_3, TeO_2, PbO, As_2O_3 and Sb_2O_3 are widely used in the industry.

Transition metal oxides such as MoO_3 and WO_3 are n-type semiconductors and have unique gas sensing properties for a series of target gases. Tellurium dioxide TeO_2 is p-type semiconductor and it is also important gas sensing material. These three oxides are suitable for the detection of oxidizing and reducing gases.

The mechanism of gas detection is following. The target gas interacts with the surface of the metal oxide film, which results in a change in charge carrier concentration of the material. This change in charge carrier concentration serves to alter the conductivity (or resistivity) of the material. An n-type semiconductor upon interaction with a reducing gas an increase in conductivity occurs. Conversely, an oxidising gas serves to deplete the sensing layer of charge carrying electrons, resulting in a decrease in conductivity. A p-type semiconductor is a material that conducts with positive holes being the majority charge carriers; hence, the opposite effects are observed with the material and showing an increase in conductivity in the presence of an oxidising gas (where the gas has increased the number of positive holes). A resistance increase with a reducing gas is observed, where the negative charge introduced in to the material reduces the positive (hole) charge carrier concentration [27]. Band gap theory is also applied in studying of gas sensors.

It was reported that MoO_3 and WO_3 with band gap 3.2 and 2.7 eV [28 -29] respectively are sensitive to NO [30-31], NO_2 [30-31], NH_3 [32, 31], H_2S [33-34], H_2 [32, 35], CO [36-37], CH_3CH_2OH [36, 38] and volatile organic compounds (VOC) [39-40]. MoO_3 is also sensitive to CH_4 [30] and WO_3 is sensitive to O_3 [37], Cl_2 [41] and SO_2 [42]. Molybdenum and tungsten oxides exhibit other interesting properties such as electrochromism [43-44], photocromism [45-46], photoluminescence [47-48], luminescence [49] and used in catalyst [50-52]. Gas sensors and other devices are produced as nanostructure and thin films by different techniques, including CVD, PVD, sol-gel process and sputtering.

Tellurium dioxide used for detection of NO_2 [53-54], NH_3 [53, 55], H_2S [53] and Cl_2 [56]. In addition TeO_2 thin films is a sensitive material for γ-radiation and were suggested as an effective material for room temperature real time radiation dosimetry due to observed changes in both the optical and the electrical properties [57]. TeO2 is important acousto-optical and electro-optical material with a variety of desirable characteristics [58]. Band gaps of TeO_2 are 3.41 eV for annealed TeO_2 crystalline film, 3.5 eV for single-crystal TeO_2 and increased band gap 3.73-4.2 eV for amorphous TeO_2 [59-60].

Sb_2O_3 and As_2O_3 oxides are important materials because of their unique properties and applications in optics and electronics. These trioxides can serve as glass former when mixed with other oxides [61]. The $Sb_2O_3 – As_2O_3$ based glasses (for example $PbO-Sb_2O_3-As_2O_3$) can

be used in non-linear optical devices and as thermoluminescent material [62]. This alkali free glass systems, is expected to be relatively moisture resistant and possess low rates of crystallization [63]. Many of Sb_2O_3 or As_2O_3 based glass systems with optical and electrical properties are known: V_2O_5-As_2O_3 [64], Sb_2O_3-B_2O_3 [65], Li_2O–Sb_2O_3–GeO_2 glasses mixed with different modifiers (viz., PbO, ZnO, BaO, SrO and CaO) [66], ZnO–Sb_2O_3–As_2O_3 [67], PbO-P_2O_5-As_2O_3 [68], Sb_2O_3–Na_2O–WO_3–PbO [69], CaO–Sb_2O_3–B_2O_3 [70], PbO–Sb_2O_3–B_2O_3 [71] etc.

Lead oxide, which is one of these semiconductor nanostructures, has important applications in storage batteries, the glass industry, and pigments. Various forms of lead oxide and their nanostructure compositions are known, including nanoplates, nanostars, nanorods, nanopowders, nanosheets and nanotubes. PbO is an indirect band gap semiconductor with tetragonal and orthorhombic phases. The tetragonal and orthorhombic phases of PbO have band gaps of 1.9–2.2 eV and 2.6 eV, respectively [72].

Over past decades the development of nanotechnology was very intensive. Science and industry focused their interest on this class of materials. Optics and electronics were in the centre of interests too. As was shown above the MoO_3, WO_3, TeO_2, PbO, As_2O_3 and Sb_2O_3 oxides are widely applied in the mentioned fields. Therefore ternary oxides with their unique properties, which can combine the properties of the individual oxides, have a big potential for the industry.

3 Investigation of gaseous ternary oxides

3.1 Formation and stability of molybdenum-tellurium oxides MoTeO$_5$, Mo$_2$TeO$_8$, Mo$_3$TeO$_{11}$ and MoTe$_2$O7 in the gas phase. Quantum chemical and mass spectrometry determination of standard enthalpy of formation.

E. Berezovskaya, E. Milke, M. Binnewies

Dalton Transactions

PAPER

Formation and stability of molybdenum-tellurium oxides MoTeO₅, Mo₂TeO₈, Mo₃TeO₁₁ and MoTe₂O₇ in the gas phase. Quantum chemical and mass spectrometry determination of standard enthalpy of formation

E. Berezovskaya,* E. Milke and M. Binnewies

The formation of mixed molybdenum-tellurium oxides MoTeO₅, Mo₂TeO₈, Mo₃TeO₁₁, MoTe₂O₇ in the gas phase has been studied by mass spectrometry (MS) experiments at temperatures of about 938 K and studied theoretically by quantum chemical (QC) methods. Structural and thermodynamic data for the molecules was calculated. The mixed oxides MoTeO₅, Mo₂TeO₈, Mo₃TeO₁₁ and MoTe₂O₇ in the gas phase have been reported for the first time. Experimental thermodynamic data have been determined by means of MS and confirmed theoretically by DFT and *ab initio* (MP2) calculations. Adiabatic ionisation potentials (IPs) were obtained experimentally and compared with theoretical vertical ionisation potentials. The following values are given:

$\Delta_f H^0{}_{298}$ (MoTeO₅) = −730.2 kJ mol⁻¹ (MS),
$\Delta_f H^0{}_{298}$ (MoTeO₅) = −735.4 kJ mol⁻¹ (DFT), −717.3 kJ mol⁻¹ (MP2),
$S^0{}_{298}$ (MoTeO₅) = 389.5 J mol⁻¹ K⁻¹ (DFT),
$c_p{}^0{}_T$(MoTeO₅) = 141.71 + 13.54 × 10⁻³ T − 2.53 × 10⁶ T^{-2} J mol⁻¹ K⁻¹ (298 < T < 940 K) (DFT),

$\Delta_f H^0{}_{298}$ (Mo₂TeO₈) = −1436.3 kJ mol⁻¹ (MS),
$\Delta_f H^0{}_{298}$ (Mo₂TeO₈) = −1436.1 kJ mol⁻¹ (DFT), −1455.9 kJ mol⁻¹ (MP2),
$S^0{}_{298}$ (Mo₂TeO₈) = 517.1 J mol⁻¹ K⁻¹ (DFT),
$c_p{}^0{}_T$(Mo₂TeO₈) = 228.64 + 24.15 × 10⁻³ T − 4.09 × 10⁶ T^{-2} J mol⁻¹ K⁻¹ (298 < T < 940 K) (DFT),

$\Delta_f H^0{}_{298}$ (Mo₃TeO₁₁) = −2132.7 kJ mol⁻¹ (MS),
$\Delta_f H^0{}_{298}$ (Mo₃TeO₁₁) = −2110.7 kJ mol⁻¹ (DFT), −2163.2 kJ mol⁻¹ (MP2),
$S^0{}_{298}$ (Mo₃TeO₁₁) = 629.3 J mol⁻¹ K⁻¹ (DFT),
$c_p{}^0{}_T$(Mo₃TeO₁₁) = 316.40 + 34.10 × 10⁻³ T − 5.74 × 10⁶ T^{-2} J mol⁻¹ K⁻¹ (298 < T < 940 K) (DFT),

$\Delta_f H^0{}_{298}$ (MoTe₂O₇) = −999.7 kJ mol⁻¹ (MS),
$\Delta_f H^0{}_{298}$ (MoTe₂O₇) = −1002.7 kJ mol⁻¹ (DFT), −1000.9 kJ mol⁻¹ (MP2),
$S^0{}_{298}$ (MoTe₂O₇) = 504.8 J mol⁻¹ K⁻¹ (DFT),
$c_p{}^0{}_T$(MoTe₂O₇) = 211.19 + 18.02 × 10⁻³ T − 3.53 × 10⁶ T^{-2} J mol⁻¹ K⁻¹ (298 < T < 940 K) (DFT),

IP(MoTeO₅) = 10.68 eV (DFT),
IP(Mo₂TeO₈) = 10.4 ± 0.5 eV (MS), IP(Mo₂TeO₈) = 10.41 eV (DFT),
IP(Mo₃TeO₁₁) = 10.7 ± 0.5 eV (MS), IP(Mo₃TeO₁₁) = 10.18 eV (DFT),
IP(MoTe₂O₇) = 9.91 eV (DFT).

1 Introduction

A number of experimental investigations have been carried out on the structure and properties of mixed molybdenum-tellurium

Institut für Anorganische Chemie, Callinstr. 9, 30167, Hannover. E-mail: katja.berezovskaya@aca.uni-hannover.de; Fax: 0511-762-2254

oxides in the crystal and glass state.[1–4] The molybdate–tellurite glass network has been modelled in a quantum chemical study.[5] Lattices of MoO₃ and TeO₂ have very different crystal structures with many modifications;[6–9] they are able to combine, giving rise to a new crystal structure. MoTe₂O₇ is the only stoichiometric compound in the phase diagram of the system MoO₃–TeO₂.[10] Its structure is also specified. The molybdenum atom Mo⁶⁺ is sixfold

coordinated[2] and the tellurium atoms are fourfold coordinated to oxygen in two different configurations.[3] In both configurations tellurium is in the Te^{4+} valence state. The coordination numbers and valence states of Mo and Te in the mixed oxide are the same as in pure oxides.

The gas phase of pure tellurium[11–13] and molybdenum oxides[14,15] has also been the subject of some studies. These compounds are two examples of metal oxides which evaporate congruently without decomposition. The gas phase contains monomer and oligomer molecules: $(MoO_3)_x$, $(x = 1–5)$,[14] $(TeO_2)_y$, $(y = 1–4)$.[11,12] Structures of these oxides and their oligomers have been described by quantum chemical calculations.[14,16]

Among many publications, devoted to molybdenum and tellurium oxides, there are no publications on the properties of mixed molybdenum-tellurium oxides in the gas phase. In present work we concentrate on gaseous molybdenum-tellurium oxides. Structure chemistry of these compounds in a vapour is quite rich. We have observed $MoTeO_5$, Mo_2TeO_8, Mo_3TeO_{11} and $MoTe_2O_7$ in the gas phase during evaporation of a mixture of MoO_3 and TeO_2. The formation and stability of mixed molybdenum-tellurium oxides in the gas phase has been investigated. Structures of mixed compounds were characterised by quantum chemical calculations.

2 Experimental

Mass spectrometric measurements were carried out by using an ion trap mass spectrometer Finigan type 212 with electron impact at 70 eV. A mixture of the solid oxides MoO_3 (extra pure grade) and TeO_2 (grade purum) in a ratio of 1:2 was heated in a Knudsen cell to 938 K, ionised gas was registered and the spectrum was analysed. Ionisation potentials (IPs) for mixed molybdenum-tellurium oxides were obtained by varying the energy of the electron impact source and determination of onset of the ions. Argon was applied as the calibration gas to transform the voltage scale into electron energy.

Quantum chemical calculations were performed using the TURBOMOLE program package.[17] All the structures of the molecules were fully optimised by using the density functional theory (DFT) with the BP86 functional, which incorporates the exchange functional of Becke and correlation functional of Perdew.[18,19] The def2-TZVP triple split valence basis set with a polarisation function and small core ECP functions for Mo and Te atoms was employed for computation. RI-treatment, which was also applied, allows to speed up computation by a factor of 10 at least without sacrificing accuracy.[20,21] Stationary points of the molecules were characterised by harmonic frequency computations at the same theoretical level. Module AOFORCE performed vibration frequencies and IR intensities. Thermodynamic characteristics were determined with the help of the module FREEH, the procedure of statistical thermodynamics. The highest possible molecular symmetry for each compound is given. The structures with higher symmetries correspond to the transition state and have imaginary frequencies. Additionally computations on the RI-MP2 level with the def2-TZVP basis set were performed. The geometries were also optimised. Vibration frequency calculations for molybdenum-tellurium oxides using the RI-MP2/def2-TZVP method require enormous computer resources. Therefore thermodynamic characteristics such as heat

capacity, entropy and thermal energy of molecules were taken from the RI-BP86/def2-TZVP calculation. First vertical ionisation potentials of the investigated systems were obtained by the RI-BP86/def2-TZVP method. Ionisation potentials were taken as the difference between the energy of the neutral molecule and the corresponding cation at the same geometry according to the Franck–Condon principle. The singlet spin state was taken as the electronic ground state for all neutral molecules. The open-shell method was applied for computation of molecular ions in doublet spin states.

3 Results and discussion

3.1. Mass Spectrometry

The original mass spectrum with characteristic isotopic patterns according to mass numbers of ions is shown in Fig. 1. Several peaks corresponding to different ions overlap with each other and give additive intensity in the mass spectrum. However, it is possible to distinguish individual ions in the mass spectrum and to calculate their relative intensity. Relative intensities of the main gas compounds are presented below in parenthesis:
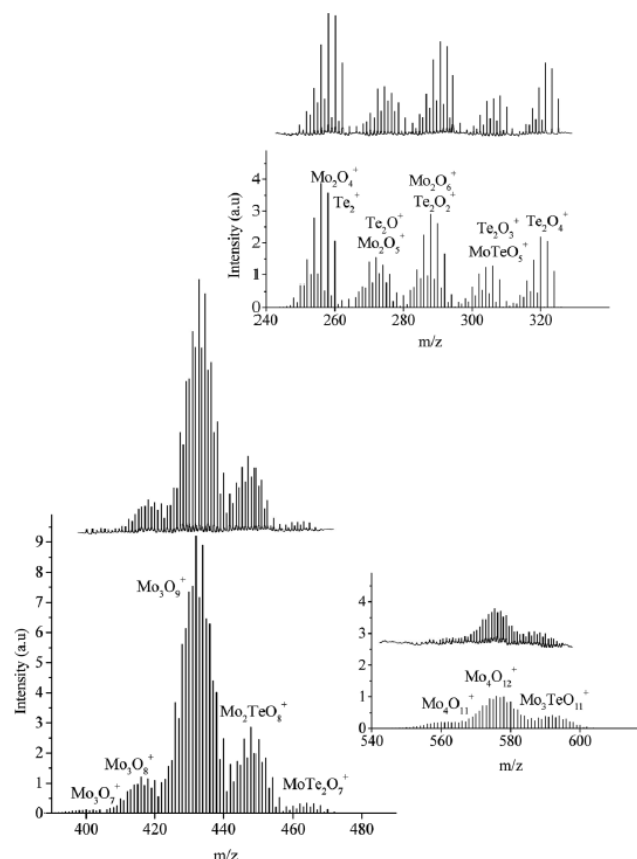
Fig. 1 Experimental and simulated mass spectra of MoO_3-TeO_2 (1:2) mixture, 938 K, 70 eV.

MoO^+ (1.6), MoO_2^+ (5.4), Te^+ (14.9), TeO^+ (37.0), TeO_2^+ (100), Mo_2O^+ (0.3), $Mo_2O_4^+$ (1.6), Te_2^+ (4.8), Te_2O^+ (0.4), $Mo_2O_5^+$ (3.3), $Te_2O_2^+$ (2.8), $Mo_2O_6^+$ (2.7), $Te_2O_3^+$ (0.8), $MoTeO_5^+$ (1.6), $Te_2O_4^+$ (3.2), $Mo_3O_7^+$ (0.4), $Mo_3O_8^+$ (3.8), $Mo_3O_9^+$ (30.0), $Mo_2TeO_8^+$ (8.6), $MoTe_2O_7^+$ (0.9), $Mo_4O_{11}^+$ (0.7), $Mo_4O_{12}^+$ (4.1), $Mo_3TeO_{11}^+$ (2.0).

These relative intensities and values of natural abundances of Mo, Te, O isotopes were used to perform a mathematical simulation of the mass spectrum (Fig. 1). Experimental and simulated spectra show very good agreement. This indicates that the calculated relative intensities given in parenthesis are correct.

Detection of $MoTeO_5^+$, $Mo_2TeO_8^+$, $Mo_3TeO_{11}^+$ and $MoTe_2O_7^+$ ions could mean the existance of mixed oxides: $MoTeO_5$, Mo_2TeO_8, Mo_3TeO_{11}, $MoTe_2O_7$ in the gas phase. Ionisation potentials for two molecules Mo_2TeO_8, Mo_3TeO_{11} were determined experimentally with the help of appearance potential. Ionisation efficiency curves for these compounds are presented in Fig. 2. Extrapolation of appearance potentials give values of adiabatic ionisation potentials: $IP(Mo_2TeO_8) = 10.4 \pm 0.5$ eV, $IP(Mo_3TeO_{11}) = 10.7 \pm 0.5$ eV. Quantum chemical values of vertical ionisation potentials, which are given later, are consistent with experimental values. This proves that $Mo_2TeO_8^+$ and $Mo_3TeO_{11}^+$ ions were obtained by ionisation rather than by fragmentation. In the case of the formation of ions by fragmentation, appearance potential is expected to be several eV higher. Intensities of $MoTeO_5^+$ and $MoTe_2O_7^+$ ions were too small at low electron impact energy to determine reliable ionisation potentials.
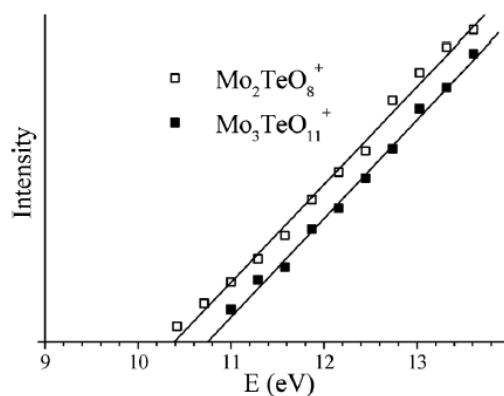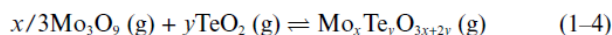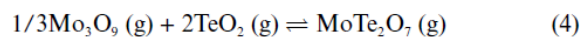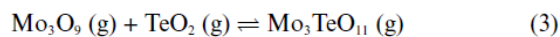

Fig. 2 Ionisation efficiency curves of $Mo_2TeO_8^+$ and $Mo_3TeO_{11}^+$.

Trioxide Mo_3O_9 and monoxide TeO_2 are the main gas components in the gas phase of pure molybdenum und tellurium oxides at a wide temperature range, including 938 K. In the mass spectra of the pure oxides MoO_3 and TeO_2 the biggest relative intensities belong to the ions $Mo_3O_9^+$ and TeO_2^+, correspondingly.[11,12,14] In our experiment the two highest relative intensities in the mass spectra belong to the parent ions TeO_2^+ and $Mo_3O_9^+$. Therefore the relative intensities of these ions and $Mo_xTe_yO_{3x+2y}^+$ ions were used to evaluate the experimental data. The ions $Mo_3O_8^+$, $Mo_3O_7^+$, Te^+ and TeO^+ formed by fragmentations have also been taken into account; their intensities were added to the intensities of the parent ions $Mo_3O_9^+$ and TeO_2^+, correspondingly.

The following reactions (1–4) were considered for the calculation of the equilibrium constant K_p and the standard enthalpy of formation $\Delta_f H^0_{298}$ of the mixed oxides:

$$1/3Mo_3O_9 \text{ (g)} + TeO_2 \text{ (g)} \rightleftharpoons MoTeO_5 \text{ (g)} \quad (1)$$

$$2/3Mo_3O_9 \text{ (g)} + TeO_2 \text{ (g)} \rightleftharpoons Mo_2TeO_8 \text{ (g)} \quad (2)$$

$$Mo_3O_9 \text{ (g)} + TeO_2 \text{ (g)} \rightleftharpoons Mo_3TeO_{11} \text{ (g)} \quad (3)$$

$$1/3Mo_3O_9 \text{ (g)} + 2TeO_2 \text{ (g)} \rightleftharpoons MoTe_2O_7 \text{ (g)} \quad (4)$$

$$x/3Mo_3O_9 \text{ (g)} + yTeO_2 \text{ (g)} \rightleftharpoons Mo_xTe_yO_{3x+2y} \text{ (g)} \quad (1–4)$$
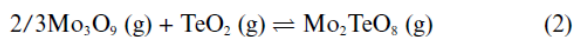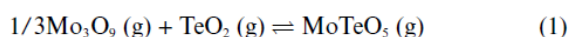
The equilibrium constant of the reaction, K_p, represents the ratio of the partial pressures of the gas components:

$$K_p = \frac{p(Mo_xTe_yO_{3x+2y})}{p(Mo_3O_9)^{x/3}p(TeO_2)^y} \quad (5)$$

Firstly, it is necessary to determine the partial pressures of molybdenum, tellurium and mixed oxides in order to obtain the constant of the reaction K_p. The intensities of the ions in the mass spectra depend on the partial pressures of the gas component, which produced these ions and could be approximated by eqn (6):

$$p_i = c\sum I_i T \quad (6)$$

where p_i is the partial pressure of the ion, T is the equilibrium temperature, $\sum I_i$ is the sum of the intensities parent ion and fragments from that ion, c is the proportionality factor.

The proportionality factor c is unknown and has to be determined. We apply two equations, describing the total pressures of pure molybdenum and tellurium oxides in the liquid state: $\lg(p(MoO_3)/bar) = -16.83 \times 10^3 T^{-1} - 14.23\lg(T) + 56.89$ $(1074\ldots1378\ K)^{22}$ and $\ln(p(TeO_2)/Pa) = -25.84 \times 10^3 T^{-1} + 28.38$ $(1006\ldots1075\ K)^{23}$. The ratio of tellurium oxide to molybdenum oxide $TeO_2 : MoO_3$ within the Knudsen cell was $2 : 1$ mol. It corresponds to the liquid state in the phase diagram[10] at 938 K. Therefore we have to use $p - T$ relations for liquid MoO_3 and liquid TeO_2. The $p - T$ equations give the following values of total pressures at 938 K for the pure oxides : $p(TeO_2) = 2.3 \times 10^{-5}$ bar and $p(MoO_3) = 4.5 \times 10^{-4}$ bar. The contribution from molybdenum and tellurium oxides to total pressure in our investigating system according to Raoult's law for ideal mixtures can be approximated by the following equation:

$$p(MoO_3, TeO_2) = 2/3p(TeO_2) + 1/3p(MoO_3) = 1.7 \times 10^{-4} \text{ bar.}$$

By using eqn (6), the proportionality factor c can be calculated:

$$c = p(MoO_3, TeO_2)/\sum I(MoO_3, TeO_2)T = 8.6 \times 10^{-10} \text{ bar K}^{-1}$$

where $\sum I(MoO_3, TeO_2)$ is the total sum of the relative intensities of $(MoO_3)_x^+$ and $(TeO_2)_y^+$ at a temperature of 938 K.

The partial pressures of the gaseous species are also calculated from eqn (6):

$$p(Mo_3O_9) = 2.8 \times 10^{-5} \text{ bar}$$

$$p(TeO_2) = 1.2 \times 10^{-4} \text{ bar}$$

$$p(MoTeO_5) = 1.3 \times 10^{-6} \text{ bar}$$

$$p(Mo_2TeO_8) = 6.9 \times 10^{-6} \text{ bar}$$

$$p(Mo_3TeO_{11}) = 1.6 \times 10^{-7} \text{ bar}$$

$$p(MoTe_2O_7) = 7.3 \times 10^{-7} \text{ bar}$$

15

Equilibrium constants K_p of reactions 1–4 at 938 K have been calculated from eqn (5):

$$K_p(1) = 0.34, K_p(2) = 62, K_p(3) = 467, K_p(4) = 1610.$$

The equilibrium constant K_p is related to the reaction enthalpy, reaction entropy and temperature by the van't Hoff-eqn (7).

$$\ln K_p = -\frac{\Delta_R H^0{}_T}{RT} + \frac{\Delta_R S^0{}_T}{R} \qquad (7)$$

$$\Delta_R H^0{}_T = -RT\ln K_p + T\Delta_R S^0{}_T$$

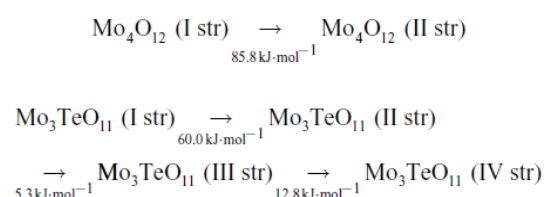We will use this equation below to calculate the reaction enthalpies (1–4).

3.2 Density functional theory and *ab initio* computation

Calculations were carried out for the following oxides of molybdenum and tellurium: MoO_3, Mo_2O_6, Mo_3O_9, Mo_4O_{12}, TeO_2, Te_2O_4, $MoTeO_5$, Mo_2TeO_8, Mo_3TeO_{11} and $MoTe_2O_7$. The optimal geometry configuration, which corresponds to the lowest energy on the potential energy surface, was calculated for every oxide. As stated above, molybdenum and tellurium atoms in pure and mixed oxides in a crystal structure have valence state +6 and +4, correspondingly, and are bound to oxygen atoms. By a search for the optimal geometry of the above mentioned gas oxides we limit the enormous number of possible structures of those oxides, where the valence state of the Te atom is +4, the valence state of Mo atom is +6 and the metal atoms are bound to oxygen atoms. Thus several isomers are possible for Mo_4O_{12} and Mo_3TeO_{11}, smaller oxides have only one structure. Structures of all the calculated compounds with bond lengths and symmetries of molecular geometries are presented in Fig. 3. There is a clear influence of a nonbonding valence electron pair from the tellurium atom on the stereochemistry of the compounds. The presence of the tellurium atom leads to a lowering of the symmetry of the structure. Total energies, calculated by *ab initio* MP2 and DFT methods, thermal energies and entropies of the molecules are presented in Table 1.

Two isomers of Mo_4O_{12} and four isomers of Mo_3TeO_{11} are considered. It was found that the structures of the compound with one ring of alternating metal atoms and oxygen atoms (*i.e.*

structures with four-coordinated Mo^{6+}) have a lower total energy than the others.

The standard enthalpies of isomer transition for Mo_4O_{12} and Mo_3TeO_{11} (RI-BP86/def2-TZVP method) are given:

$$Mo_4O_{12} \text{ (I str)} \xrightarrow[85.8\,kJ\cdot mol^{-1}]{} Mo_4O_{12} \text{ (II str)}$$

$$Mo_3TeO_{11} \text{ (I str)} \xrightarrow[60.0\,kJ\cdot mol^{-1}]{} Mo_3TeO_{11} \text{ (II str)}$$

$$\xrightarrow[5.3\,kJ\cdot mol^{-1}]{} Mo_3TeO_{11} \text{ (III str)} \xrightarrow[12.8\,kJ\cdot mol^{-1}]{} Mo_3TeO_{11} \text{ (IV str)}$$

Structures (I str) with the lowest total energy are preferable and used further for calculation of the thermodynamic values.

The thermodynamic values for all the compounds were obtained with the help of the module FREEH in a range from standard temperature to temperature of the mass spectrometric experiment 298–940 K. The heat capacity $c_p^0{}_T$ can be approximated as a polynomial function of temperature (8). Coefficients a, b and c were calculated mathematically by fitting ten points $c_p^0{}_T(T)$.

$$c_p^0{}_T = a + b10^{-3}T + c10^6T^{-2} \qquad (8)$$

To demonstrate the adequacy of the chosen RI-BP86/def2-TZVP method of calculations, experimental thermodynamic data were compared with our calculations. Experimental[22] and calculated thermodynamic values for molybdenum and tellurium oxides are presented in Table 2. Experimental standard heat capacities $c_p^0{}_{289}$ for MoO_3, Mo_2O_6, Mo_3O_9, TeO_2 and Te_2O_4 were calculated using the literature values for the coefficient a, b and c and eqn (8). The values of $c_p^0{}_{289}$ were compared with quantum chemical calculated values (Table 2). Agreement between heat capacities is quite satisfactory. Fig. 4 demonstrates experimental and calculated entropies $S^0{}_T$ at different temperatures for MoO_3, Mo_2O_6, Mo_3O_9, TeO_2 and Te_2O_4 molecules. Experimental values of the entropy $S^0{}_T$ are given as function (9), theoretical values were calculated at ten different temperatures. Both curves are in good agreement with each other.

$$S^0{}_T = S^0{}_{298} + \int_{298}^{T} c_p^0 \frac{dT}{T} \qquad (9)$$

Table 1 Total energies, thermal energies and entropies calculated for oxides of molybdenum and tellurium (DFT, RI-BP86/def2-TZVP; MP2, RI-MP2/def2-TZVP)

Molecule	E_{tot} (a.u.) (DFT)	E_{tot} (a.u) (MP2)	$E^{therm}{}_{298}$ (kJ mol^{-1}) (DFT)	$S^0{}_{298}$ (J mol^{-1} K^{-1}) (DFT)
MoO_3	−294.201556	−293.5157057	33.81	284.31
TeO_2	−418.646847	−417.7736934	20.54	273.72
Mo_2O_6	−588.567760	−587.1955501	76.06	391.73
Te_2O_4	−837.371218	−835.6233962	48.78	378.43
Mo_3O_9	−882.913202	−880.8663883	118.15	525.52
Mo_4O_{12} (I)	−1177.237313	−1174.5089716	160.27	639.41
Mo_4O_{12} (II)	−1177.204197	not calc.[a]	159.15	633.23
$MoTeO_5$	−712.970035	−711.4077195	62.05	389.52
Mo_2TeO_8	−1007.303581	−1005.0734200	104.23	517.06
Mo_3TeO_{11} (I)	−1301.627133	−1298.7271779	146.19	629.29
Mo_3TeO_{11} (II)	−1301.604017	not calc.[a]	145.47	629.58
Mo_3TeO_{11} (III)	−1301.601851	not calc.[a]	145.08	623.94
Mo_3TeO_{11} (IV)	−1301.597061	not calc.[a]	145.29	632.74
$MoTe_2O_7$	−1131.697447	−1129.2681826	90.63	504.81

[a] Total energy is not calculated for unstable isomers at the MP2 level.

Table 2 Experimental[22] and calculated thermodynamic characteristics of molybdenum and tellurium oxides (DFT, RI-BP86/def2-TZVP)

| Molecule	$\Delta_f H^0_{298}$ (kJ mol^{-1}) (exp)	S^0_{298} (J mol^{-1} K^{-1}) (exp//DFT)	$c_p^0{}_T$ (J mol^{-1} K^{-1}) (exp//DFT)	$c_p^0{}_T = a + b10^{-3}T + c10^6 T^{-2}$ (exp//DFT)		
				a	b	c
MoO$_3$(g)	−346.4	283.9//284.3	59.4//59.2	74.5//70.6	5.1//10.4	−1.5//−1.3
Mo$_2$O$_6$(g)	−984.9	407.4//391.7	152.8//129.8	181.2//159.1	0.4//19.8	−2.5//−3.2
Mo$_3$O$_9$(g)	−1878.3	526.7//525.5	221.6//203.3	274.5//245.9	4.2//30.5	−4.8//−4.7
Mo$_4$O$_{12}$(g)	−2570.1	654//639.4	299.8//277.9	371.4//331.8	5.7//41.8	−6.5//−6.1
TeO$_2$(g)	−61.3	275.4//273.7	42.2//45.5	54.8//52.5	2.4//4.8	−1.2//−0.8
Te$_2$O$_4$(g)	−347.3	376.7//378.4	112.6//104.2	131.8//123.8	0.7//7.8	−1.7//−2.0
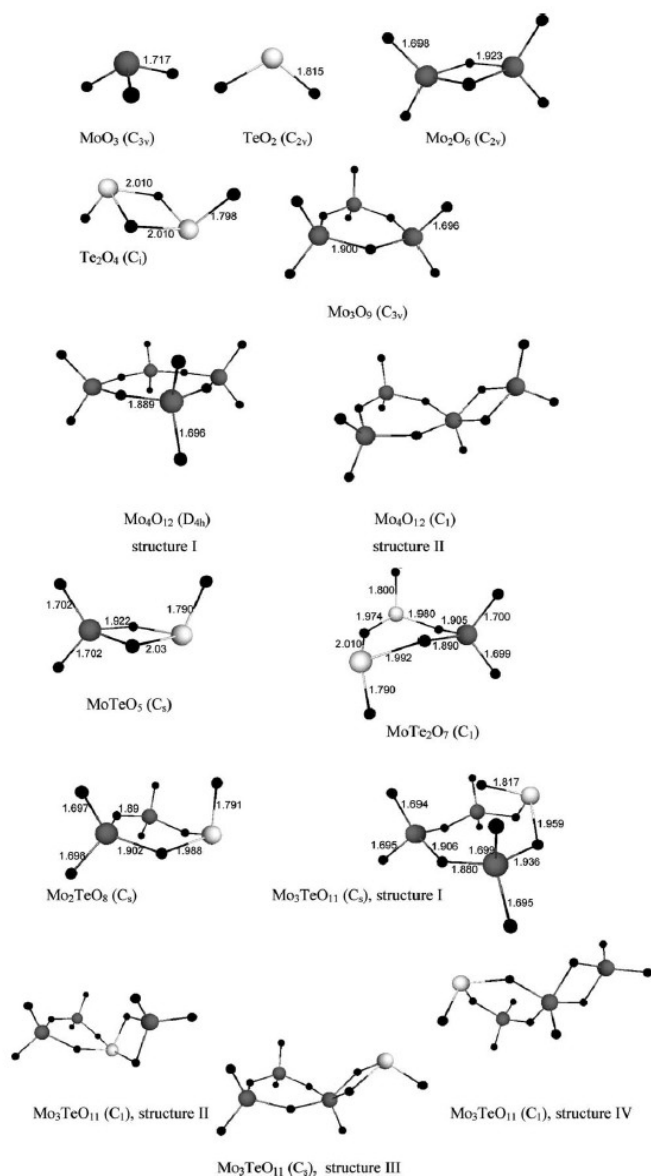
Fig. 3 Structures of molybdenum and tellurium oxides with bond lengths in Å and group of symmetry, calculated using the RI-BP86/def2-TZVP method (bond lengths are given for the stable isomers).

Thermodynamic data (standard entropies S^0_{298}, function of heat capacities $c_p^0{}_T$ and coefficient a, b, c of approximated $c_p^0{}_T$-function) for four mixed oxides MoTeO$_5$, Mo$_2$TeO$_8$, Mo$_3$TeO$_{11}$ and MoTe$_2$O$_7$ are presented in Table 3.
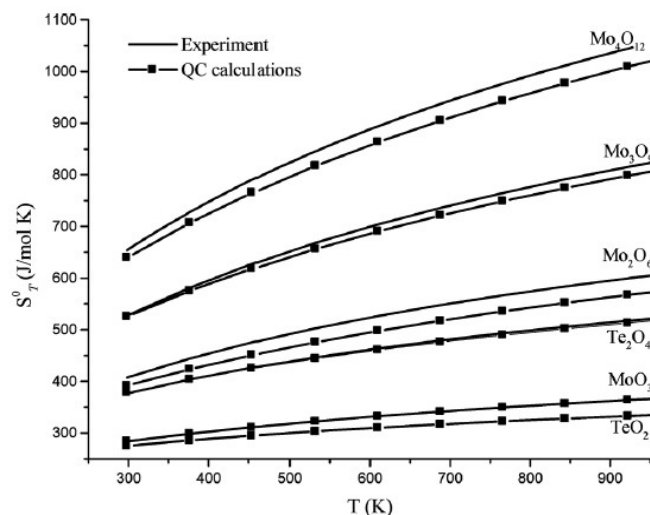
Fig. 4 Comparison of quantum chemical calculated and experimental entropies S^0_T.

Standard enthalpies of formation $\Delta_f H^0_{298}$ of Mo$_x$Te$_y$O$_{3x+2y}$ oxides can be obtained with help of the following equation:

$$\Delta_f H^0_{298}(\text{Mo}_x\text{Te}_y\text{O}_{3x+2y},\text{QC}) = \Delta_R H_{298}(\text{QC}) + x/3\Delta_f H^0_{298}(\text{Mo}_3\text{O}_9,\text{exp}) + y\Delta_f H^0_{298}(\text{TeO}_2, \text{exp}).$$

Quantum chemical calculated reaction enthalpies $\Delta_R H^0_{298}$ (1–4) and standard enthalpies of formation $\Delta_f H^0_{298}$ are presented in Table 4.

We have determined known standard enthalpies of formation of Mo$_4$O$_{12}$ and Te$_2$O$_4$ by using the RI-BP86/def2-TZVP and RI-MP2/def2-TZVP methods and known experimental values of $\Delta_f H^0_{298}(\text{Mo}_3\text{O}_9)$ and $\Delta_f H^0_{298}(\text{TeO}_2)$ to prove reasonableness of our approach:

$$\Delta_f H^0_{298}(\text{Mo}_4\text{O}_{12},\text{QC}) = \Delta_R H_{298}(\text{QC}) + 4/3\Delta_f H^0_{298}(\text{Mo}_3\text{O}_9, \text{exp})$$

$$\Delta_f H^0_{298}(\text{Te}_2\text{O}_4,\text{QC}) = \Delta_R H_{298}(\text{QC}) + 2\Delta_f H^0_{298}(\text{TeO}_2, \text{exp}).$$

The following theoretical values were obtained:

$$\Delta_f H^0_{298}(\text{Mo}_4\text{O}_{12}, \text{DFT}) = -2554.2 \text{ kJ mol}^{-1},$$

$$\Delta_f H^0_{298}(\text{Mo}_4\text{O}_{12}, \text{MP2}) = -2562.8 \text{ kJ mol}^{-1},$$

$$\Delta_f H^0_{298}(\text{Te}_2\text{O}_4, \text{DFT}) = -320.9 \text{ kJ mol}^{-1},$$

$$\Delta_f H^0_{298}(\text{Te}_2\text{O}_4, \text{MP2}) = -316.9 \text{ kJ mol}^{-1}.$$

17

Table 3 Calculated thermodynamic characteristics of mixed molybdenum-tellurium oxides (DFT, RI-BP86/def2-TZVP)

Molecule	S^0_{298} (J mol^{-1} K^{-1}) (DFT)	$c_p{}^0{}_T = a + b10^{-3}T + c10^6T^{-2}$ (DFT)		
		a	b	c
MoTeO$_5$ (g)	389.5	141.71	13.54	−2.53
Mo$_2$TeO$_8$ (g)	517.1	228.64	24.15	−4.09
Mo$_3$TeO$_{11}$ (g)	629.3	316.40	34.10	−5.74
MoTe$_2$O$_7$ (g)	504.8	211.19	18.02	−3.53

Table 4 Calculated enthalpies of reaction and standard enthalpy of formation for product of corresponding reaction (DFT, RI-BP86/def2-TZVP; MP2, RI-MP2/def2-TZVP)

Reaction	$\Delta_R H^0_{298}$ (kJ mol^{-1}) (DFT)	$\Delta_R H^0_{298}$ (kJ mol^{-1}) (MP2)	$\Delta_f H^0_{298}$ (kJ mol^{-1}) (DFT)	$\Delta_f H^0_{298}$ (kJ mol^{-1}) (MP2)
1/3 Mo$_3$O$_9$ (g) + TeO$_2$ (g) $\rightleftharpoons$ MoTeO$_5$ (g)	−48.0	−29.9	−735.4	−717.3
2/3 Mo$_3$O$_9$ (g) + TeO$_2$ (g) $\rightleftharpoons$ Mo$_2$TeO$_8$ (g)	−122.6	−142.4	−1436.1	−1455.9
Mo$_3$O$_9$ (g) + TeO$_2$ (g) $\rightleftharpoons$ Mo$_3$TeO$_{11}$ (g)	−171.1	−223.6	−2110.7	−2163.2
1/3 Mo$_3$O$_9$ (g) + 2 TeO$_2$ (g) $\rightleftharpoons$ MoTe$_2$O$_7$ (g)	−254.0	−252.2	−1002.7	−1000.9

Table 5 Calculated enthalpies and entropies of reaction at 938 K (DFT, RI-BP86/def2-TZVP; MP2,– RI-MP2/def2-TZVP)

Reaction	$\Delta_R H^0_{938}$ (kJ mol^{-1}) (DFT)	$\Delta_R H^0_{938}$ (kJ mol^{-1}) (MP2)	ΔS^0_{938} (J mol^{-1} K^{-1}) (DFT)	$\ln K_{p938}$ (DFT)	(MP2)
1/3 Mo$_3$O$_9$ (g) + TeO$_2$ (g) $\rightleftharpoons$ MoTeO$_5$ (g)	−44.4	−26.3	−52.9	−0.7	−3.0
2/3 Mo$_3$O$_9$ (g) + TeO$_2$ (g) $\rightleftharpoons$ Mo$_2$TeO$_8$ (g)	−115.5	−135.3	−94.5	3.5	6.0
Mo$_3$O$_9$ (g) + TeO$_2$ (g) $\rightleftharpoons$ Mo$_3$TeO$_{11}$ (g)	−160.6	−213.2	−151.3	2.4	9.0
1/3 Mo$_3$O$_9$ (g) + 2 TeO$_2$ (g) $\rightleftharpoons$ MoTe$_2$O$_7$ (g)	−240.3	−238.3	−193.3	8.1	7.3

Experimental values of the standard enthalpy of formation $\Delta_f H^0_{298}$(Mo$_4$O$_{12}$) and $\Delta_f H^0_{298}$ (Te$_2$O$_4$) are given in Table 2. The difference between experimental and quantum chemical calculated enthalpies are satisfactory: 15.9 and 7.3 kJ mol^{-1} for DFT and MP2 levels of theory correspondingly for Mo$_4$O$_{12}$ and 26.4 and 30.4 kJ mol^{-1} for DFT and MP2 levels of theory correspondingly for Te$_2$O$_4$.

Enthalpies $\Delta_R H^0$, entropies $\Delta_R S^0$ and natural logarithm of the equilibrium constant $\ln K_p$ for the reaction (1–4) were calculated at the temperature of the experiment (Table 5). Further we have compared these calculated values with the experimental values at the temperature of the experiment.

Total energies of cations MoO$_3{}^+$, Mo$_2$O$_6{}^+$, Mo$_3$O$_9{}^+$, TeO$_2{}^+$, MoTeO$_5{}^+$, Mo$_2$TeO$_8{}^+$, Mo$_3$TeO$_{11}{}^+$ and MoTe$_2$O$_7{}^+$ were computed in the doublet spin state to determine the ionisation potentials of the corresponding molecules (Table 6). All the cations in the low spin state have a lower energy E_{tot} than in the high spin state. Therefore the first IP was determined as the difference between the total energy of the cation in the doublet state and the energy of the neutral molecule. Experimental IP values from literature for MoO$_3$, TeO$_2$, Mo$_2$O$_6$, Mo$_3$O$_9$[24] and our experimental adiabatic IP values for Mo$_2$TeO$_8$, Mo$_3$TeO$_{11}$ were compared with calculated vertical IPs (Table 7). As we mentioned already that confirms that Mo$_2$TeO$_8{}^+$, Mo$_3$TeO$_{11}{}^+$ ions were formed by ionisation, not by fragmentation of the parent ions. The values are comparable and show small deviations. The comparison of experimental adiabatic and theoretical vertical values of ionisation potential is adequate,

Table 6 Total energies of molecular ions in geometries of corresponding neutral molecule in the doublet spin state (DFT, RI-BP86/def2-TZVP)

Molecular ion	E_{tot} (a.u.) (DFT)
MoO$_3{}^+$	−293.765448
TeO$_2{}^+$	−418.249529
Mo$_2$O$_6{}^+$	−588.158418
Mo$_3$O$_9{}^+$	−882.516290
MoTeO$_5{}^+$	−712.577586
Mo$_2$TeO$_8{}^+$	−1006.921106
Mo$_3$TeO$_{11}{}^+$	−1301.253166
MoTe$_2$O$_7{}^+$	−1131.333410

since the geometries of the molecules and their cations are very close.

3.3 Determination of standard enthalpy of formation of $\Delta_f H^0_{298}$

It was not possible to obtain the second-law (10) of enthalpy of reaction in our experiment because the temperature range of the experiment was too narrow.

$$\Delta_R H^0_T = -R \left[\partial \ln K_p(T)/(\partial(1/T)) \right] \quad (10)$$

The third law of enthalpy can be calculated in that case. The rigid rotor harmonic oscillator (RRHO) approximation has to be used to obtain thermodynamic functions. For this purpose, the structure parameter and the vibration wavenumbers of the investigated molecules have to be determined. Usually these parameters are

18

Table 7 Experimental and calculated first ionisation potentials (IP), (DFT – RI-BP86/def2-TZVP)

Compound	IP (eV)	
	(exp)	(DFT)
MoO_3 (g)	11.8 ± 0.5[24]	11.87
TeO_2 (g)	11.3 ± 0.5[24]	10.81
Mo_2O_6 (g)	12.1 ± 0.6[24]	11.14
Mo_3O_9 (g)	12.0 ± 1.0[24]	10.80
$MoTeO_5$ (g)	—	10.68
Mo_2TeO_8 (g)	10.4 ± 0.5[a]	10.41
Mo_3TeO_{11} (g)	10.7 ± 0.5[a]	10.18
$MoTe_2O_7$ (g)	—	9.91

[a] This work.

taken from quantum chemical computation or approximated from known experimental values of related compounds.[25,26] We have obtained thermodynamic functions (entropies and heat capacities) with the procedure of statistical thermodynamics in the FREEH module of the Turbomole program package.

Enthalpies of reactions at temperature 938 K $\Delta_R H^0_{938}$ can be calculated using the van't Hoff eqn (7). We have obtained equilibrium constants K_{P938} (1–4) of the formation reaction of mixed molybdenum-tellurium oxides by mass spectrometry. The experimental values of K_{P938} are in good agreement with theoretical values (Table 5, 8). The experimental entropies of reaction (1–4) $\Delta_R S^0_T$ are unknown. We have used calculated values of entropies of reaction (Table 5) to calculate $\Delta_R H^0_{938}$(exp) from eqn (7):

$$\Delta_R H^0_{938}(\text{exp}, 1\text{–}4) = -RT\ln K_p + T\Delta_R S^0_{938}(\text{QC}, 1\text{–}4)\ (T = 938\ K)$$

Experimental values of enthalpy of reaction (1–4) $\Delta_R H^0_{938}$, given in Table 8, are also in good agreement with the calculations.

Now enthalpies of formation $\Delta_f H^0_{938}$ for mixed oxides can be also calculated:

$$\Delta_f H^0_{938}(Mo_xTe_yO_{3x+2y}, \text{exp}) = \Delta_R H^0_{938}(\text{exp}) + x/3\Delta_f H^0_{938}(Mo_3O_9, \text{exp}) + y\Delta_f H^0_{938}(TeO_2, \text{exp})$$

and converted to standard enthalpies of formation $\Delta_f H^0_{298}$ with the help of eqn (11):

$$\Delta_f H^0_{298} = \Delta_f H^0_T + \int_T^{298} c_p^0 dT \qquad (11)$$

Coefficients of c_p^0-function for $Mo_xTe_yO_{3x+2y}$ oxides have been taken from quantum chemical calculations. Enthalpies of formation $\Delta_f H^0_{938}$ for Mo_3O_9 (g) and TeO_2 (g) have also been calculated from experimental values with the help of eqn (11).

All experimental and theoretical values of standard enthalpies of formation for mixed oxides as well as differences between them are presented in Table 9. Calculated and experimental enthalpies of formation perfectly agree with each other for smaller molecules $MoTeO_5$, Mo_2TeO_8 and $MoTe_2O_7$. For the Mo_3TeO_{11} molecule the difference between the calculated and experimental enthalpies is also satisfactory and does not exceed 30.5 kJ mol^{-1}.

3.4 Conclusion

Mixed molybdenum-tellurium oxides $MoTeO_5$, Mo_2TeO_8, Mo_3TeO_{11} and $MoTe_2O_7$ in the gas phase have been observed for the first time. The enthalpies of formation in the gas phase for the oxides were determined with help of mass spectrometry and compared with the quantum chemical calculations. First ionisation potentials have been experimentally obtained for Mo_2TeO_8 and Mo_3TeO_{11} and confirmed by calculated values. Agreement between experimental and calculated values of ionisation potentials and enthalpies of formation proves the existence of gaseous Mo_2TeO_8 and Mo_3TeO_{11} molecules. The most probable other two oxides $MoTeO_5$ and $MoTe_2O_7$ are also present in the gas phase, since their enthalpies of formation, which are obtained by mass spectrometric experiment and quantum chemical calculation are in very good agreement.

Acknowledgements

Table 8 Experimental standard enthalpies of formation for molybdenum-tellurium oxides

Reaction	$\ln K_{P938}$ (exp)	$\Delta_R H^0_{938}$ (kJ mol^{-1}) (exp)	$\Delta_f H^0_{938}$ (kJ mol^{-1}) (exp)	$\Delta_f H^0_{298}$ (kJ mol^{-1}) (exp)
$1/3\ Mo_3O_9$ (g) + TeO_2 (g) $\rightleftharpoons$ $MoTeO_5$ (g)	−1.1	−41.3	−639.9	−730.2
$2/3\ Mo_3O_9$ (g) + TeO_2 (g) $\rightleftharpoons$ Mo_2TeO_8 (g)	4.1	−120.8	−1290.1	−1436.3
Mo_3O_9 (g) + TeO_2 (g) $\rightleftharpoons$ Mo_3TeO_{11} (g)	6.2	−189.9	−1929.9	−2132.7
$1/3\ Mo_3O_9$ (g) + $2\ TeO_2$ (g) $\rightleftharpoons$ $MoTe_2O_7$ (g)	7.4	−238.9	−865.5	−999.7

Table 9 Comparison of calculated and experimental standard enthalpies of formation for molybdenum-tellurium oxides (DFT, RI-BP86/def2-TZVP; MP2, RI-MP2/def2-TZVP)

Compound	$\Delta_f H^0_{298}$ (kJ mol^{-1}) (exp)	$\Delta_f H^0_{298}$ (kJ mol^{-1}) (DFT)	$\Delta_f H^0_{298}$ (kJ mol^{-1}) (MP2)	$\Delta_f H^0_{298}$(exp) − $\Delta_f H^0_{298}$(QC) (kJ mol^{-1}) (DFT//MP2)
$MoTeO_5$ (g)	−730.2	−735.4	−717.3	5.2//−12.9
Mo_2TeO_8 (g)	−1436.3	−1436.1	−1455.9	−0.2//19.6
Mo_3TeO_{11} (g)	−2132.7	−2110.7	−2163.2	−22.0//30.5
$MoTe_2O_7$ (g)	−999.7	−1002.7	−1000.9	3.0//1.2

19

References

1 A. Mekki, G. D. Khattak and L. E. Wenger, *J. Non-Cryst. Solids*, 2005, **351**, 2493.
2 T. Sekiya, N. Mochida and S. Ogawa, *J. Non-Cryst. Solids*, 1995, **185**, 135.
3 S. Neov, I. Gerasimova, B. Sidzimov, V. Kozhukharov and P. Mikula, *J. Mater. Sci.*, 1988, **23**, 347.
4 P. Y. Arnaud, M. T. Averbuch-Pouchot, A. Durif and J. Guidot, *Acta Crystallogr., Sect. B: Struct. Crystallogr. Cryst. Chem.*, 1976, **32**, 1417.
5 O. Sokolov, V. G. Plotnichenko, V. V. Koltashev and I. A. Grishin, *J. Non-Cryst. Solids*, 2009, **355**, 239.
6 O. Noguera, T. Merle-Mejean, A. P. Mirgorodsky, M. B. Smirnov, P. Thomas and J.-C. Champarnaud-Mesjard, *J. Non-Cryst. Solids*, 2003, **330**, 50.
7 J. C. Champarnaud-Mesjard, S. Blanchandin, P. Thomas, A. Mirgorodsky, T. Merle-Mejean and B. Frit, *J. Phys. Chem. Solids*, 2000, **61**, 1499.
8 V. V. Atuchin, T. A. Gavrilova, T. I. Grigorieva, N. V. Kuratieva, K. A. Okotrub, N. V. Pervukhina and N. V. Surovtsev, *J. Cryst. Growth*, 2011, **318**, 987.
9 H. Negishi, S. Negishi, Y. Kuroiwa, N. Sato and S. Aoyagi, *Phys. Rev. B: Condens. Matter Mater. Phys.*, 2004, **69**.
10 G. Petrini and J. C. J. Bart, *Z. Anorg. Allg. Chem.*, 1981, **474**, 229.
11 D. W. Muenow, J. W. Hastie, R. Hauge, R. Bautista and J. L. Margrave, *Trans. Faraday Soc.*, 1969, **65**, 3210.
12 T. S. Lakshmi Narasimhan, R. Balasubramanian, S. Nalini and M. Sai Baba, *J. Nucl. Mater.*, 1997, **247**, 28.
13 R. J. M. Konings, A. S. Booij and A. Kovács, *Chem. Phys. Lett.*, 1998, **292**, 447.
14 V. B. Goncharov and E. F. Fialko, *J. Struct. Chem.*, 2002, **43**(5), 777.
15 D. L. Neikirk, J. C. Fagerli, M. L. Smith, D. Mosman and T. C. Devore, *J. Mol. Struct.*, 1991, **244**, 165.
16 O. Noguera, M. Smirnov, A. P. Mirgorodsky, T. Merle-Mejean, P. Thomas and J.-C. Champarnaud-Mesjard, *J. Non-Cryst. Solids*, 2004, **345–346**, 734.
17 R. Ahlrichs, M. Bär, H.-P. Baron, R. Bauernschmitt, S. Böcker, P. Deglmann, M. Ehrig, K. Eichkorn, S. Elliott, F. Furche, F. Haase, M. Häser, C. Hättig, H. Horn, C. Huber, U. Huniar, M. Kattannek, A. Köhn, C. Kölmel, M. Kollwitz, K. May, C. Ochsenfeld, H. Öhm, A. Schäfer, U. Schneider, M. Sierka, O. Treutler, B. Unterreiner, M. von Arnim, F. Weigend, P. Weis, H. Weiss, *Turbomole* (vers. 5.9.1), Universität Karlsruhe (2007).
18 A. D. Becke, *Phys. Rev. A: At., Mol., Opt. Phys.*, 1988, **38**, 3098.
19 J. P. Perdew, *Phys. Rev. B*, 1986, **33**, 8822.
20 K. Eichkorn, F. Weigend, O. Treutler and R. Ahlrichs, *Theor. Chem. Acc.*, 1997, **97**, 119.
21 K. Eichkorn, O. Treutler, H. Ohm, M. Haser and R. Ahlrichs, *Chem. Phys. Lett.*, 1995, **242**, 652.
22 M. Binnewies, E. Milke, *Thermochemical data of Elements and Compounds*, 2nd ed., Wiley-VCH, 2002.
23 M. S. Samant, A. S. Kerkar, S. N. Tripathi, S. R. Dharwadkar, *Proc. Natl. Symp. Therm. Anal.*, 9th, 1993, 576.
24 NIST Chemistry WebBook, http://webbook.nist.gov/.
25 R. Viswanathan, R. W. Schmude and K. A. Gingerich, *J. Chem. Thermodyn.*, 1995, **27**, 1303.
26 O. Kaposi, L. Lelik, G. A. Semenov and E. N. Nikolaev, *Acta Chim. Hung.*, 1985, **120**, 79.

20

3.2 The formation and stability of molybdenum-antimony and tungsten-antimony ternary oxides Sb_2MO_6, $Sb_2M_2O_9$, $Sb_2Mo_3O_{12}$ and Sb_4MO_9 in the gas phase (M = Mo, W). Quantum chemical and mass spectrometric studies

E. Berezovskaya, E. Milke, M. Binnewies

Dalton Transactions

PAPER

The formation and stability of molybdenum–antimony and tungsten–antimony ternary oxides Sb_2MO_6, $Sb_2M_2O_9$, $Sb_2Mo_3O_{12}$ and Sb_4MO_9 in the gas phase (M = Mo, W). Quantum chemical and mass spectrometric studies†

E. Berezovskaya,* E. Milke and M. Binnewies

The ternary oxides Sb_2MO_6, $Sb_2M_2O_9$, Sb_4MO_9 (M = Mo, W) and $Sb_2Mo_3O_{12}$ were detected in the gas phase by means of mass spectrometry (MS). These gaseous oxides are reported for the first time. Thermodynamic data was obtained experimentally and confirmed by quantum chemical (QC) calculations. In addition, structural data on these molecules was obtained. The ionisation potentials (IP) were also determined both experimentally and theoretically.

1 Introduction

Metal halide chemistry has been widely investigated over the last few decades.[1,2] It is well known that the volatility of metal halides is enhanced by several orders of magnitude when in the presence of other metal halides, *e.g.*, $AlCl_3$. The reaction of two different halides leads to so-called gas complexes, *e.g.*, $CoCl_2(s)$ + $Al_2Cl_6(g) \rightleftharpoons CoAl_2Cl_8(g)$.[2] Such reactions may be important for high-temperature industrial processes. We are investigating similar reactions using metal oxide systems. Enhancement of the volatility of metal oxides in the presence of another oxide, the volatility of which is usually very low, may play a role in the thermal processes used to recycle rare metals in the future. We recently reported one such reaction between different oxides in the gas phase and we characterised the reaction products:[3] the TeO_2 and MoO_3 oxides react in the gas phase to form the gaseous ternary oxides $MoTeO_5$, Mo_2TeO_8, Mo_3TeO_{11} and $MoTe_2O_7$. Herein, we describe further examples of reactions between oxides in the gas phase, namely the reactions between MoO_3 or WO_3 and Sb_2O_3. The gas phase of the pure molybdenum, tungsten and antimony oxides has been the subject of several mass spectrometric studies.[4–8] It has been shown that the molybdenum and tungsten oxides, MoO_3 and WO_3, evaporate congruently without decomposition as the gas phase contains monomer and oligomer molecules $(MO_3)_x$, (M = Mo, W; $x = 1–5$).[4,6] The antimony oxide, Sb_2O_3, also evaporates congruently and the gas phase primarily contains antimony oxide in the dimeric form, Sb_4O_6. In the present article, we report the results of mass spectrometric and theoretical investigations of the formation and stability of the gaseous ternary molybdenum–

antimony and tungsten–antimony oxides Sb_2MO_6, $Sb_2M_2O_9$, Sb_4MO_9, (M = Mo, W) and $Sb_2Mo_3O_{12}$ (Scheme 1). The structures of these complexes are also discussed in the present work.

2 Experimental

2.1 Mass spectrometry

Mass spectrometric measurements were carried out using a modified Finigan type 212 mass spectrometer with electron impact ionisation (70 eV). The experimental setup is described elsewhere.[9]

According to the phase diagram of the Sb_2O_3–MoO_3 system,[10] there are two ternary stoichiometric compounds in the solid state: Sb_2MoO_6 and $Sb_2Mo_3O_{12}$. These two compounds were prepared and subjected to a mass spectrometric investigation. Mixtures of MoO_3 and Sb_2O_3 (3 : 1 and 1 : 1 mol) were heated in sealed silica ampoules *in vacuo* at 830 K for ten days. The obtained samples were characterised using X-ray diffraction (XRD) techniques. Comparison of the XRD patterns of the synthesised samples with the literature data confirms the crystal structures of the obtained Sb_2MoO_6 and $Sb_2Mo_3O_{12}$ compounds. Vaporisation of the two Sb_2MoO_6 and $Sb_2Mo_3O_{12}$ solid oxides using a conventional Knudsen cell was studied at 840 and 893 K, respectively.

The tungsten–antimony ternary oxide was not observed in an analogous experiment using the Knudsen cell due to the very different partial pressures of the antimony and tungsten oxides. As a result, the mass spectra show the antimony oxide vapour but no tungsten-containing species. Therefore, a double Knudsen cell (described elsewhere[9]) was employed in the investigation of the Sb_2O_3–WO_3 system in the gas phase. Antimony oxide was continuously evaporated at 646 K and flowed through solid tungsten oxide, which was heated at 1080 K. The reaction products leaving the Knudsen cell were analysed by mass spectrometry.

Institut für Anorganische Chemie, Leibniz Universität Hannover, Callinstr. 9, 30167 Hannover, Germany.
E-mail: katja.berezovskaya@aca.uni-hannover.de;
Fax: +49-0511-762-2254

$Sb_2O_3^+(13.4)$, $Sb_2O_2^+(6.6)$, $SbO^+(9.8)$, $SbMoO_4^+(2.9)$

$Sb_3O_4^+$
(0.3)

parent ions
$Mo_3O_9^+$ $Sb_4O_6^+$
(30.6)   (1.4)

$Sb_2MoO_6^+$ $Sb_2Mo_2O_9^+$ $Sb_2Mo_3O_{12}^+$
(9.4)   (100)   (6.9)

$Mo_3O_8^+$
(3.8)

$Sb_2MoO_5^+$ $Sb_2Mo_2O_8^+$ $SbMo_2O_7^+$
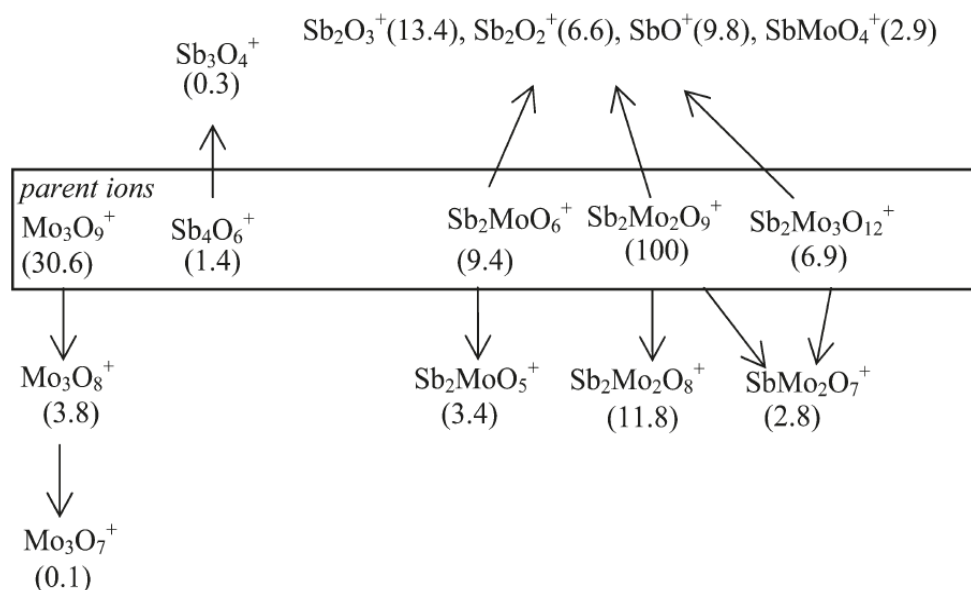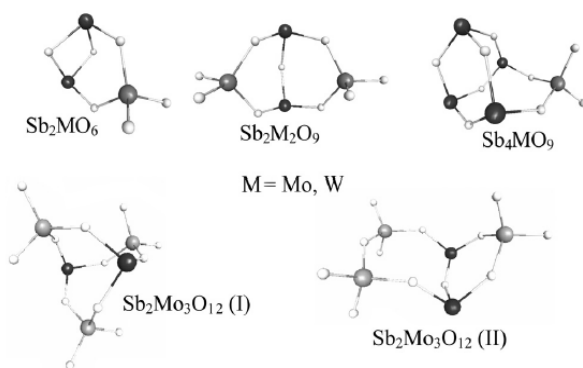(3.4)   (11.8)   (2.8)

$Mo_3O_7^+$
(0.1)

Fig. 1 Scheme of the fragmentation pathways of the gas molecules in the vapour above $Sb_2Mo_3O_{12}$, 893 K, 70 eV. The relative intensities are given in parentheses.

Sb_2MO_6 $Sb_2M_2O_9$ Sb_4MO_9

M = Mo, W

$Sb_2Mo_3O_{12}$ (I)

$Sb_2Mo_3O_{12}$ (II)

Scheme 1 Structures of antimony–molybdenum and antimony–tungsten ternary oxides in the gas phase.

Appearance potentials (APs) of the ions of the ternary molybdenum–antimony and tungsten–antimony oxides were obtained by varying the electron energy to determine the onset of the ions. Argon was applied as a calibration gas.

2.2 Quantum chemical calculations

Quantum chemical calculations were performed using the TURBOMOLE program package.[11] All molecular structures were fully optimised using density functional theory (DFT) with the BP86 functional, which incorporates the Becke exchange functional and the Perdew correlation functional.[12,13] The def2-TZVP triple split valence basis set with a polarisation function and small core ECP functions was employed during the computation for the Mo, W and Sb atoms. RI treatment, which was also applied, sped up the computation by a factor of at least 10 without sacrificing the accuracy.[14,15] Stationary points of the molecules were characterised by harmonic frequency

computations at the same theoretical level. The AOFORCE module was used to calculate the vibrational frequencies and IR intensities. The vibrational wave numbers were not calibrated with a scaling factor (scaling factor = 1.0). Thermodynamic characteristics were obtained using the FREEH module, which is based on statistical thermodynamics. The highest possible molecular symmetry for each compound was considered. The structures with higher molecular symmetries correspond to transition states and have imaginary frequencies. The first vertical ionisation potentials of the investigated systems were obtained using the def2-TZVP/RI-BP86 method. Ionisation potentials were taken as the difference between the energy of the neutral molecule and the corresponding cation in the same molecular geometry. The singlet spin state was taken as the electronic ground state for all neutral molecules. The open-shell method was applied for the computation of molecular ions in doublet spin states.

3 Results and discussion

3.1 Evaluation of the experimental data

The dependence of the recorded ion currents on the partial pressure is described by the following equation:

$$p_i = c \frac{\Sigma I_i T}{\sigma_i S} \qquad (1)$$

where p_i = the partial pressure of component i, c = the proportionality factor, $\sum I_i$ = the intensity of all the ions formed by the ionisation and fragmentation of a gaseous molecule i, T = the temperature, σ_i = the ionisation cross section and S_i = the electron multiplier efficiency. The approximated eqn (2) can be used in most cases (the simplification procedure is described

23

elsewhere[16]):

$$p_i = c \sum I_i T \qquad (2)$$

The proportionality factor c was determined by a calibration experiment using antimony oxide. Additionally, we obtained the necessary information about the fragmentation pathways of pure antimony oxide under our experimental conditions. The mass spectrum of antimony oxide at 673 K is presented in Table 1. Eqn (3)[7] was used to calculate the partial pressure of antimony oxide:

$$\lg(p/\text{bar}) = -(10\ 066 \pm 203)\text{K}/T + (9.390 \pm 0.297) \quad (3)$$

By applying eqn (2), the proportionality factors c_1 and c_2 were obtained: $c_1 = 1.7 \times 10^{-11}$ and $c_2 = 7.2 \times 10^{-12}$ bar K^{-1} (c_1 corresponds to the experiments with Sb_2MoO_6 and $Sb_2Mo_3O_{12}$ evaporation and c_2 corresponds to the Sb_2O_3–WO_3 system). Using the c_1 and c_2 values and the relative intensities $\sum I_i$, the partial pressures of the gaseous molecules in the equilibrium system can be calculated.

Mass spectrometric investigation of the vapour above solid $Sb_2Mo_3O_{12}$ and Sb_2MoO_6. The vaporisation of solid $Sb_2Mo_3O_{12}$ and Sb_2MoO_6 samples was studied by mass spectrometry. The characteristic isotopic patterns of some of the ions from these samples are shown in Fig. S1 and S2 (ESI†). The relative intensities of the ions in the mass spectra of $Sb_2Mo_3O_{12}$ and Sb_2MoO_6 are presented in Table 1. Using these relative

intensities and the values of the natural abundance of the Mo, Sb and O isotopes, mathematically simulated mass spectra were calculated. This procedure was performed to validate the interpretation of the $Sb_2Mo_3O_{12}$ and Sb_2MoO_6 mass spectra because several peaks (m/z) correspond to between one and five ions and these ions contribute additively to the observed intensity. Both the experimental and simulated spectra correlate perfectly (Fig. S1 and S2, ESI†).

The following ions are considered to be parent ions: $Sb_4MoO_9^+$, $Sb_2M_3O_{12}^+$, $Sb_2M_2O_9^+$, $Sb_2MoO_6^+$, $Sb_4O_6^+$, $M_3O_9^+$ and are marked as M$^+$ in Table 1. The detection of the $Sb_2MoO_5^+$, $Sb_2MoO_6^+$, $Sb_2Mo_2O_8^+$, $Sb_2Mo_2O_9^+$, $Sb_2Mo_3O_{12}^+$ and $Sb_4MoO_9^+$ ions indicates the existence of the ternary oxides Sb_2MoO_6, $Sb_2Mo_2O_9$, $Sb_2Mo_3O_{12}$ and Sb_4MoO_9 in the gas phase. The appearance potentials of the $Sb_2Mo_2O_9^+$, $Sb_2Mo_3O_{12}^+$ and $Sb_4MoO_9^+$ ions were determined experimentally using ionisation efficiency curves. Extrapolation of the linear part of the ionisation efficiency curves to an intensity of zero gave the following values for the appearance potentials: AP($Sb_2Mo_2O_9^+$) = 10.0 ± 0.5 eV, AP($Sb_2Mo_3O_{12}^+$) = 9.7 ± 0.5 eV and AP($Sb_4MoO_9^+$) = 9.9 ± 0.5 eV. The quantum chemical values of the ionisation potentials, presented below, are consistent with these experimental values. These values prove that the $Sb_2Mo_2O_9^+$, $Sb_2Mo_3O_{12}^+$ and $Sb_4MoO_9^+$ ions are formed by ionisation and not by fragmentation. If these ions were formed by fragmentation, the appearance potentials would be expected to be several eV higher. It was not possible to determine a reliable appearance potential of the $Sb_2MoO_6^+$ ion because the

Table 1 Mass spectra of the Sb_2O_3, Sb_2MoO_6, $Sb_2Mo_3O_{12}$, MoO_3 and WO_3 oxides and the Sb_2O_3–WO_3 mixture

Ion	Relative intensity					
	Sb_2O_3, 673 K	Sb_2MoO_6, 840 K	$Sb_2Mo_3O_{12}$, 893 K	Sb_2O_3–WO_3, 1080 K	MoO_3, 873 K	WO_3,[5] 1460 K 64 eV
$Sb_4MoO_9^+$ (M$^+$)	—	5.9	<0.5	1.8	—	—
$Sb_2M_3O_{12}^+$ (M$^+$)	—	—	6.9	—	—	—
$Sb_2M_2O_9^+$ (M$^+$)	—	5.7	100	11.8	—	—
$Sb_2M_2O_8^+$	—	0.4	11.8	2.0	—	—
$Sb_3MO_7^+$	—	5.1	—	5.2	—	—
$SbM_2O_7^+$	—	—	2.8	—	—	—
$Sb_2MO_6^+$ (M$^+$)	—	2.2	9.4	69.1	—	—
$Sb_2MO_5^+$	—	0.4	3.4	18.8	—	—
$SbMO_4^+$	—	0.2	2.9	1.5	—	—
$Sb_4O_6^+$ (M$^+$)	100	100	1.4	100	—	—
$Sb_4O_5^+$	0.6	0.7	—	0.8	—	—
$Sb_3O_4^+$	24.2	32.9	0.3	30.7	—	—
$Sb_3O_3^+$	0.3	0.4	—	—	—	—
$Sb_2O_3^+$	0.3	1.2	13.4	1.4	—	—
$Sb_2O_2^+$	2.7	4.4	6.6	5.5	—	—
Sb_2O^+	0.1	0.3	0.3	0.5	—	—
SbO^+	5.1	7.7	9.8	17.6	—	—
Sb^+	0.1	0.1	0.8	2.2	—	—
$M_5O_{15}^+$ (M$^+$)	—	—	—	—	1.9	—
$M_4O_{12}^+$ (M$^+$)	—	—	10.7	—	45.3	13.6
$M_4O_{11}^+$	—	—	0.6	—	6.3	4.8
$M_3O_9^+$ (M$^+$)	—	—	30.6	—	100	100
$M_3O_8^+$	—	—	3.8	—	18.4	34
$M_3O_7^+$	—	—	0.1	—	2.7	—
$M_2O_6^+$	—	—	1.1	—	8.1	14.4
$M_2O_5^+$	—	—	1.8	—	13.6	20.4
$M_2O_4^+$	—	—	1.1	—	9.5	—
MO_3^+	—	—	0.9	—	7.5	32
MO_2^+	—	—	3.0	—	29.7	172

M$^+$ = parent ion, M = Mo, W.

24

intensities of the $Sb_2MoO_6^+$ and $Mo_3O_9^+$ ions overlap and the ionisation efficiency curve belongs to both ions.

The ternary oxides Sb_2MoO_6, $Sb_2Mo_2O_9$, $Sb_2Mo_3O_{12}$ and Sb_4MoO_9, as well as the antimony oxide Sb_4O_6, have Sb atoms in the 3+ oxidation state and Mo atoms in the 6+ oxidation state. The $SbMoO_4^+$, $SbMo_2O_7^+$ and $Sb_3MoO_7^+$ ions are fragments of these ternary oxides rather than ionised individual oxides with a reduced oxidation state of the metallic atoms. The appearance potentials of $SbMoO_4^+$ and $Sb_3MoO_7^+$ were experimentally obtained. Both values exceed 18 eV, indicating that $SbMoO_4^+$ and $Sb_3MoO_7^+$ are fragments. The appearance potential of $SbMo_2O_7^+$ was not determined because the $Mo_3O_8^+$, $Sb_2MoO_5^+$, $Sb_2MoO_6^+$, $Mo_3O_9^+$ and $Sb_3O_4^+$ ion peaks overlap. It is prob-able that the $SbMo_2O_7^+$ ion (as well as $SbMoO_4^+$ and $Sb_3MoO_7^+$) is also a fragment, likely arising from the $Sb_2Mo_2O_9$ and $Sb_2Mo_3O_{12}$ molecules.

By comparing the Sb_2MoO_6, $Sb_4Mo_3O_{12}$, MoO_3 and Sb_2O_3 compound mass spectra, we are able to propose the nature of the main fragmentation pathways of the gaseous ternary molyb-denum–antimony oxides in the mass spectrometric experiment (Fig. 1 and 2). The relative intensities of the $Sb_2O_3^+$, $Sb_2O_2^+$, Sb_2O^+, SbO^+ and Sb^+ ions are comparable in the Sb_2O_3 and Sb_2MoO_6 mass spectra. The intensities of these ions are signifi-cantly higher relative to the $Sb_4O_6^+$ intensity in the mass spec-trum of $Sb_2Mo_3O_{12}$. This difference indicates that the $Sb_2O_3^+$, $Sb_2O_2^+$, Sb_2O^+, SbO^+ and Sb^+ ions mainly result from the gaseous ternary oxides Sb_2MoO_6, $Sb_2Mo_2O_9$ and $Sb_2Mo_3O_{12}$ rather than from Sb_4O_6. It is likely that $Sb_2O_3^+$ and $Sb_2O_2^+$ have different formation sources because the $I(Sb_2O_3^+)/I(Sb_2O_2^+)$ ratio is very different in all of the experiments.

Mass spectrometric investigation of the Sb_4O_6–WO_3 system. The evaporation of solid tungsten oxide in a stream of gaseous antimony oxide was studied. The following ions, which indicate the presence of the ternary tungsten–antimony oxides in the gas phase, were detected: $Sb_2WO_6^+$, $Sb_2W_2O_9^+$ and $Sb_4WO_9^+$. Two appearance potentials could be obtained experimentally: $AP(Sb_2WO_6^+) = 9.9 \pm 0.5$ eV and $AP(Sb_2W_2O_9^+) = 9.8 \pm 0.5$ eV. The intensity of $Sb_4WO_9^+$ was too small to permit the determi-nation of $AP(Sb_4WO_9^+)$. The mass spectrum of the system is presented in Table 1 and Fig. S3 (ESI†) and the mathematically

simulated mass spectrum is also provided. The $Sb_2WO_6^+$, $Sb_2W_2O_9^+$ and $Sb_4WO_9^+$ ions are marked as parent ion by M^+ in Table 1. The proposed fragmentation pathways in the tungsten-containing system (Fig. 3) are similar to the fragmentation scheme of the molybdenum-containing system (Fig. 2). In both experiments (Fig. 2 and 3), $Sb_4O_6^+$ is the most abundant ion, the same types of $Sb_yM_xO_z^+$ ions are detected and no $M_3O_z^+$ or $Sb_2M_3O_z^+$ ions are observed (M = Mo, W; $x = 1$–2, $y = 1$–4, $z = 4$–9). However, there is a large difference in the relative intensity of the $Sb_2MO_6^+$ and $Sb_2MO_5^+$ ions: $I(Sb_2WO_6^+) \gg I(Sb_2MoO_6^+)$, and $I(Sb_2WO_5^+) \gg I(Sb_2MoO_5^+)$. In other words, the gaseous ternary oxides are mainly present as Sb_2WO_6 in the tungsten-containing system.

Calculation of the partial pressures in the Sb_4O_6–MO_3 systems (M = Mo, W). The partial pressures of the gaseous com-ponents in all of the experiments can be obtained by applying eqn (2). It must be taken into account that the antimony oxide in the WO_3–Sb_4O_6 system was constantly evaporating from the double Knudsen cell at 646 K and that the mass spectrum was obtained at 1080 K.

Table 2 presents the parent ions and their fragments, the attri-buted gas molecules and the partial pressures of these molecules. The $SbMo_2O_7^+$ ion is related to the $Sb_2Mo_2O_9(g)$ and $Sb_2Mo_3O_{12}(g)$ oxides and therefore, the intensity $I(SbMo_2O_7^+)$ was distributed between these two ternary oxides, according to the contributions of the $Sb_2Mo_2O_9^+$, $Sb_2Mo_2O_8^+$ and $Sb_2Mo_3O_{12}^+$ ions in the mass spectrum of $Sb_2Mo_3O_{12}$. The $SbMoO_4^+$, $Sb_2O_3^+$, $Sb_2O_2^+$, Sb_2O^+, SbO^+ and Sb^+ fragments are not attributed to any specific molecule because their origins are not distinct but they likely result from the ternary oxides in the experiment with $Sb_2Mo_3O_{12}$, as discussed above.

Using the partial pressures, we determined the equilibrium constants for the formation of the molybdenum–antimony and tungsten–antimony ternary oxides.

3.2 Density functional theory computation

The def2-TZVP/RI-BP86 method is very suitable for the quantum chemical calculation of ternary oxides and gives a good correlation between the experimental and theoretical values, as

$Sb_4O_5^+$ $Sb_3O_4^+$
(0.7) (32.9)

$Sb_2O_3^+$(1.2), $Sb_2O_2^+$(4.4), SbO^+(7.7), $SbMoO_4^+$ (0.2)

parent ions

$Sb_4O_6^+$ (100) $MoSb_2O_6^+$ (2.2) $Mo_2Sb_2O_9^+$ (5.7) $MoSb_4O_9^+$(5.9)

$Sb_2MoO_5^+$ (0.4) $Sb_2Mo_2O_8^+$(0.4) $Sb_3MoO_7^+$(5.1)

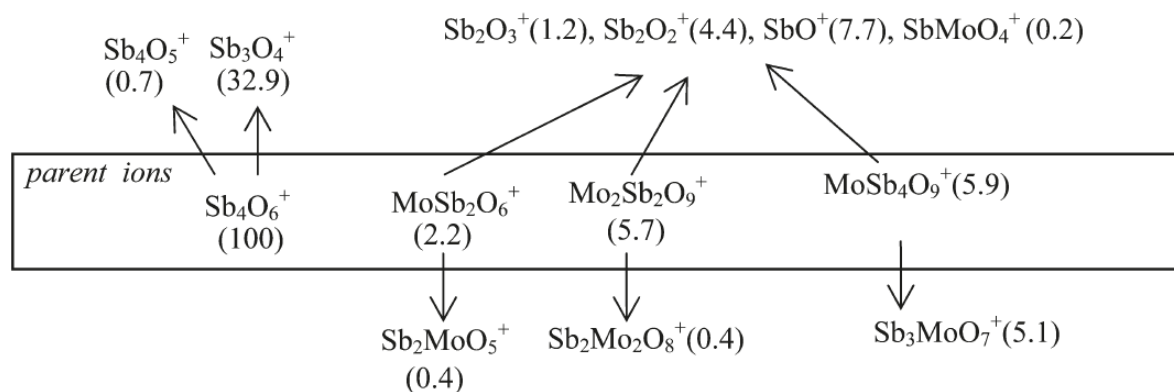**Fig. 2** Scheme of the fragmentation pathways of the gas molecules in the vapour above Sb_2MoO_6, 840 K, 70 eV. The relative intensities are given in parentheses.
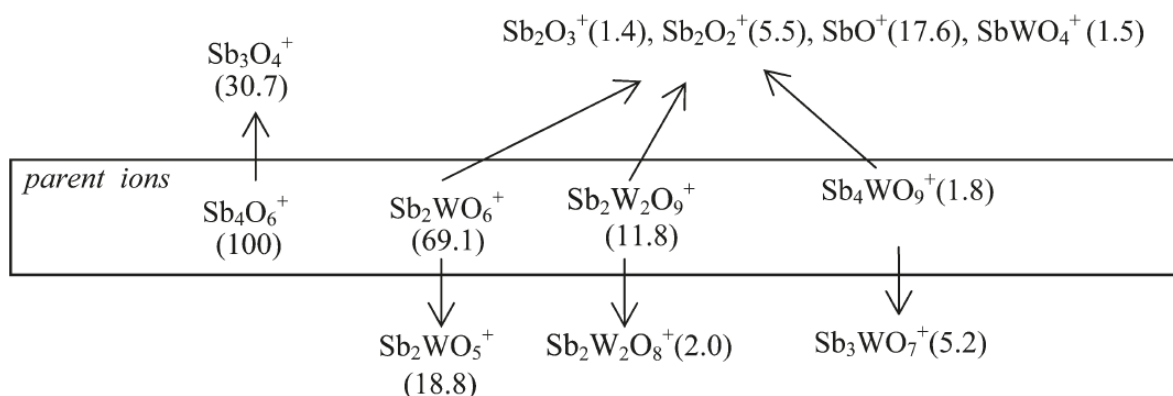
25

$Sb_2O_3^+$ (1.4), $Sb_2O_2^+$ (5.5), SbO^+ (17.6), $SbWO_4^+$ (1.5)

$Sb_3O_4^+$
(30.7)

parent ions

$Sb_4O_6^+$
(100)

$Sb_2WO_6^+$
(69.1)

$Sb_2W_2O_9^+$
(11.8)

$Sb_4WO_9^+$ (1.8)

$Sb_2WO_5^+$
(18.8)

$Sb_2W_2O_8^+$ (2.0)

$Sb_3WO_7^+$ (5.2)

Fig. 3 Scheme of the fragmentation pathways of the gas molecules in the vapour above solid WO_3 with Sb_4O_6, 1080 K, 70 eV. The relative intensities are given in parentheses.

Table 2 Gaseous molecules, their fragments and partial pressures (M = Mo, W)

		Partial pressure, p (bar)		
Molecule	Attributed ions	Vapour above $Sb_2Mo_3O_{12}$ 893 K	Vapour above Sb_2MoO_6 840 K	Vapour in Sb_2O_3–WO_3 1080 K
M_3O_9	$M_3O_9^+$, $M_3O_8^+$, $M_3O_7^+$	5.1×10^{-7}	Not detectable	Not detectable
Sb_4O_6	$Sb_4O_6^+$, $Sb_3O_4^+$, $Sb_3O_3^+$	2.5×10^{-8}	3.6×10^{-6}	6.1×10^{-7}
Sb_2MoO_6	$Sb_2MoO_6^+$, $Sb_2MoO_5^+$	1.9×10^{-7}	7.0×10^{-8}	6.8×10^{-7}
$Sb_2M_2O_9$	$Sb_2M_2O_9^+$, $Sb_2M_2O_8^+$, $SbM_2O_7^+$	1.7×10^{-6}	1.6×10^{-7}	1.1×10^{-7}
$Sb_2M_3O_{12}$	$Sb_2M_3O_{12}^+$, $SbM_2O_7^+$	1.1×10^{-7}	Not detectable	Not detectable
Sb_4MoO_9	$Sb_4MoO_9^+$, $Sb_3MoO_7^+$	$<7.8 \times 10^{-9}$	2.9×10^{-7}	5.5×10^{-8}

demonstrated with the oligomers of the molybdenum and tellurium oxides.[3] Here, we additionally compare the experimental and calculated vibration spectra of the gaseous Sb_4O_6 and Mo_3O_9 and the structural parameters of the gaseous Sb_4O_6. The experimental (176.2 cm^{-1}, 292.4 cm^{-1}, 415.6 cm^{-1}, 785.0 cm^{-1})[17] frequencies and our calculated (165.2 cm^{-1}, 270.7 cm^{-1}, 401.53 cm^{-1}, 741.4 cm^{-1}) frequencies are in good agreement. The geometric parameters for gaseous Sb_4O_6 were obtained by electron diffraction, as reported elsewhere:[18] r(Sb–O) = 2.00 ± 0.02 Å, ∠(O–Sb–O) = 98°, ∠(Sb–O–Sb) = 129.0 ± 2.5°. Our quantum chemical calculated bond distances and angles for Sb_4O_6 are as follows: r(Sb–O) = 1.986 Å, ∠(O–Sb–O) = 98.6° and ∠(Sb–O–Sb) = 128.3°. These results are in very good agreement with the previous experiment.[18] The IR spectra have been reported for gas phase molybdenum trioxide.[19] Two clear bands at 974.7 cm^{-1} and 838.0 cm^{-1} were observed in the 1050–750 cm^{-1} range of wave numbers. These frequencies are in good agreement with our calculated values of 992.4 cm^{-1} and 839.8 cm^{-1}.

The following oxides of molybdenum, tungsten and antimony were experimentally detected in the gas phase and computed quantum chemically: M_5O_{15}, M_4O_{12}, M_3O_9, Sb_4O_6, Sb_2MoO_6, $Sb_2M_2O_9$, Sb_4MoO_9 (M = Mo, W) and $Sb_2Mo_3O_{12}$. Several isomeric structures were considered for each molecule. The structures were chosen in such a way that the Sb^{3+}- and M^{6+}-atoms are bonded to oxygen atoms and could have different coordination numbers. The optimal geometry configuration corresponding to the lowest energy on the potential energy surface was found for all the structures including any isomers. Their total energies, thermal energies and molecular symmetries are given in Tables S1 and S2 (ESI†). The calculated structures are presented in Fig. S4 and S5 (ESI†), which depict the isomer transitions. These transitions are characterised by the Gibbs free energy. The most stable structures are located on a "zero level" such that the Gibbs free energy (Δ_iG_T) at the experimental temperature is positive for all the isomer transitions. The presented structures contain fragments of ten-, eight-, six- and four-membered rings and antimony has a three-coordinate structure, whereas molybdenum and tungsten are four- or five-coordinate structures (Fig. S5†). It is clear that the most stable isomeric structures for molybdenum, tungsten, antimony and their ternary oxides have some common characteristics. In particular, all of the structures contain four-coordinate Mo^{6+} or W^{6+} and three-coordinate Sb^{3+}, favour the formation of ten-, eight- or six-membered rings and disfavour the formation of four-membered rings. The formation of one four-membered ring or the presence of five-coordinate Mo^{6+} or W^{6+} destabilises the molecules. Two isomers of $Sb_2Mo_3O_{12}$ have a small difference in total energy (9.3 kJ mol^{-1}) and the Gibbs free energy of the isomer transition is 1.5 kJ mol^{-1} at 893 K (Fig. S5, ESI†). Both of these oxides contain four-coordinate Mo^{6+} and three-coordinate Sb^{3+} and have no four-membered rings.

From this point on, we consider only one structure for Sb_2MoO_6, $Sb_2M_2O_9$ and Sb_4MoO_9 (M = Mo, W) and two isomers for $Sb_2Mo_3O_{12}$. Because the calculated Gibbs free energy of the isomer transition, Δ_iG_{893}(II → I), for $Sb_2Mo_3O_{12}$ is small, it is possible that both isomers could exist in the gas phase at the experimental temperature.

26

Table 3 Total energies of the molecular ions in the geometries of the neutral molecule, calculated and experimental vertical first ionisation potentials (IP) (def2-TZVP/RI-BP86)

Molecular ion	E_{tot} (a.u.)	IP (eV)	
		QC	Exp.
$Sb_4O_6^+$	−1413.122828	8.93	9.31[20]
$Mo_3O_9^+$	−882.516290	10.80	12.0 ± 1.0[21]
$Sb_2MoO_6^+$	−1000.652141	9.90	—
$Sb_2Mo_2O_9^+$	−1294.984879	10.01	9.9 ± 0.5[a]
$Sb_4MoO_9^+$	−1707.441280	9.05	9.9 ± 0.5[a]
$Sb_2Mo_3O_{12}^+$ (I)	−1589.313125	9.76	9.8 ± 0.5[a]
$Sb_2Mo_3O_{12}^+$ (II)	−1589.309951	9.75	9.8 ± 0.5[a]
$W_3O_9^+$	−879.266761	11.44	12.0 ± 0.2[22]
$W_4O_{12}^+$	−1172.557923	10.41	12.0 ± 0.2[22]
$W_5O_{15}^+$	−1465.808767	10.24	12.1 ± 0.2[22]
$Sb_2WO_6^+$	−999.578821	9.89	9.9 ± 0.5[a]
$Sb_2W_2O_9^+$	−1292.836905	10.01	9.8 ± 0.5[a]
$Sb_4WO_9^+$	−1706.370681	9.01	—

[a] This work.

Here, we briefly describe the structural characteristics of the most stable isomers presented in Fig. S4 and S5.† The bond lengths of the same bond type (single M–O, Sb–O and double M=O, where M = Mo, W) are very similar in all the structures: r(Mo–O) = 1.89 ± 0.01 Å, r(W–O) = 1.90 ± 0.01 Å, r(Mo=O) = 1.70 ± 0.01 Å, r(W=O) = 1.73 ± 0.01 Å and r(Sb–O) = 1.99 ± 0.02 Å. The angles, centred on the molybdenum or tungsten atoms, are ∠(O–M–O) = 107.5 ± 2.5° and ∠(O=M=O) = 107.5 ± 0.5°. The angles, centred on the antimony atoms belonging to six- or eight-membered rings, are ∠(O–Sb–O) = 98.5 ± 2.5° for all of the structures. In the Sb_2MO_6 structures with four-membered rings, the angles ∠(O–Sb–O) are equal to 82°.

The total energies of the $Sb_4O_6^+$, $Mo_3O_9^+$, $W_3O_9^+$, $W_4O_{12}^+$, $W_5O_{15}^+$, $Sb_2MO_6^+$, $Sb_2M_2O_9^+$, $Sb_4MO_9^+$ (M = Mo, W) and $Sb_2Mo_3O_{12}^+$ cations were computed in a doublet spin state in the geometry of a neutral molecule to determine the vertical ionisation potentials (IP) of the corresponding molecules (Table 3). The first IP was determined as the difference between the total energy of the cation in a doublet state and the energy of the neutral molecule. The known experimental values of the IP for the antimony, molybdenum and tungsten oxide from the literature and our experimental AP values were compared with theoretical IPs (Table 3) and all of the data is in good agreement. This agreement between the values confirms that these ions were formed by the ionisation of ternary oxides rather than by a fragmentation processes.

Thermodynamic values for all the compounds were obtained using the FREEH module, with a range from the standard temperature to the temperature of the mass spectrometric experiments at 298–1000 K. The entropy, S_T^0, can be approximated as a function of temperature:

$$S_T^0 = S_{298}^0 + \int_{298}^{T} c_{p,T}^0 \frac{dT}{T} \tag{4}$$

$$\text{where } c_{p,T}^0 = a + b \times 10^{-3} \times T + c \times 10^6 \times T^{-2}$$

The a, b and c coefficients of the heat capacity function, $c_{p,T}^0$, were calculated mathematically by fitting ten values of S_T^0 in the temperature range of 298–1000 K. The calculated entropies for

gaseous Sb_4O_6, Mo_3O_9, Mo_4O_{12}, Mo_5O_{12}, W_3O_9 and W_4O_{12} were compared with experimental literature values to demonstrate the adequacy of the chosen calculation method (Table S3, ESI†). The calculated and experimental values of S_{298}^0 and S_T are in good agreement for the antimony, molybdenum and tungsten oxides. The experimental and calculated coefficients, b, of the $c_{p,T}^0$ function differ from each other but yield correct entropy values. Therefore, the calculated coefficients, a, b and c, for the ternary oxides are acceptable and can be used in the calculations. The calculated entropies and coefficients, a, b and c, for the ternary oxides are presented in Table S4 (ESI†).

The enthalpies and entropies of the main equilibrium reaction with participation of the ternary oxides were calculated at the standard conditions and temperature of the mass spectrometry experiment. These values are presented in Table 4 and the natural logarithms of the equilibrium constants, $K_{p,T}$, for these reactions are also listed.

The calculated standard enthalpies of formation ($\Delta_f H_{298}^0$) of the ternary oxides were obtained using the reaction enthalpies, $\Delta_r H_{298}^0$, of processes 1–4 and 7–9 from Table 4 and the known experimental values[23] of $\Delta_f H_{298}^0$(Mo_3O_9) = −1878.3 kJ mol^{-1}, $\Delta_f H_{298}^0$(W_3O_9) = −2023.4 kJ mol^{-1} and $\Delta_f H_{298}^0$(Sb_4O_6) = −1215.5 kJ mol^{-1}. These quantum chemically calculated (QC) values are as follows:

$$\Delta_f H_{298}^0(Sb_2MoO_6, QC) = -1197.9 \text{ kJ mol}^{-1}$$

$$\Delta_f H_{298}^0(Sb_2Mo_2O_9, QC) = -1907.8 \text{ kJ mol}^{-1}$$

$$\Delta_f H_{298}^0(Sb_2Mo_3O_{12}(I), QC) = -2570.2 \text{ kJ mol}^{-1}$$

$$\Delta_f H_{298}^0(Sb_2Mo_3O_{12}(II), QC) = -2560.8 \text{ kJ mol}^{-1}$$

$$\Delta_f H_{298}^0(Sb_4MoO_9, QC) = -1888.9 \text{ kJ mol}^{-1}$$

$$\Delta_f H_{298}^0(Sb_2WO_6, QC) = -1251.1 \text{ kJ mol}^{-1}$$

$$\Delta_f H_{298}^0(Sb_2W_2O_9, QC) = -2012.1 \text{ kJ mol}^{-1}$$

$$\Delta_f H_{298}^0(Sb_4WO_9, QC) = -1945.5 \text{ kJ mol}^{-1}.$$

3.3 Experimental determination of the standard enthalpies of formation of $\Delta_f H_{298}^0$

Because the entropies of all the gaseous molecules presented here could be well defined using quantum chemical calculations, we selected the third law method to evaluate the reaction enthalpies. The reaction enthalpies were calculated for reactions 1–3 and 5–9 (Table 5) using eqn (5). The equilibrium constant, $K_{p,T}$, related to the reaction enthalpy, reaction entropy and temperature by the van't Hoff equation, was obtained experimentally from the partial pressures of the gaseous components. The reaction entropy values, $\Delta_R S_T^0$ (QC), were determined using quantum chemical calculations.

$$\Delta_r H_T^0(\text{exp.}) = -RT \ln K_{p,T}(\text{exp.}) + T\Delta_r S_T^0(QC) \tag{5}$$

27

Table 4 Calculated standard enthalpies and entropies of the reaction and equilibrium constants for the equilibrium processes with participation of the molybdenum–antimony oxides (def2-TZVP/RI-BP86)

	Reaction	$\Delta_r H^0{}_T$ (kJ mol^{-1}) 298 K//T^a	$\Delta S^0{}_T$ (J mol^{-1} K^{-1}) 298 K//T^a	$\ln K_{p,T}$ 298 K//T^a
1	$1/3\ Mo_3O_9 + 1/2\ Sb_4O_6 \rightleftharpoons Sb_2MoO_6{}^b$	35.9//34.2	34.9//31.5	−10.3//−0.8
2	$2/3\ Mo_3O_9 + 1/2\ Sb_4O_6 \rightleftharpoons Sb_2Mo_2O_9{}^b$	−47.8//−46.3	−14.8//−12.1	17.5//4.8
3.I	$Mo_3O_9 + 1/2Sb_4O_6 \rightleftharpoons Sb_2Mo_3O_{12}(I)^b$	−84.2//−79.3	−65.4//−56.4	26.1//3.9
3.II	$Mo_3O_9 + 1/2Sb_4O_6 \rightleftharpoons Sb_2Mo_3O_{12}(II)^b$	−74.8//−69.9	−56.6//−47.7	23.4//3.7
4	$1/3\ Mo_3O_9 + Sb_4O_6 \rightleftharpoons Sb_4MoO_9{}^b$	−47.3//−43.9	−10.7//−4.4	17.8//5.4
5	$1/2\ Mo_2Sb_2O_9 + 3/4\ Sb_4O_6 \rightleftharpoons Sb_4MoO_9{}^c$	−23.4//−21.1	−3.3//1.3	9.0//3.2
6	$Sb_2MoO_6 + 1/2\ Sb_4O_6 \rightleftharpoons Sb_4MoO_9{}^c$	−83.3//−78.5	−45.6//−36.4	28.1//6.6
7	$1/3\ W_3O_9 + 1/2\ Sb_4O_6 \rightleftharpoons Sb_2WO_6{}^d$	31.2//25.7	37.2//33.2	−8.1//1.2
8	$2/3\ W_3O_9 + 1/2\ Sb_4O_6 \rightleftharpoons Sb_2W_2O_9{}^d$	−55.4//−50.2	0.4//3.8	22.4//5.9
9	$1/3\ W_3O_9 + Sb_4O_6 \rightleftharpoons Sb_4WO_9{}^d$	−55.5//−51.0	−1.5//6.0	22.2//6.3

^{a} T = temperature of the mass spectrometric experiment, ^{b} T = 893 K. ^{c} T = 840 K. ^{d} T = 1080 K.

Table 5 Experimental equilibrium constants and enthalpies of reaction

	Reaction	$\ln K_{p,T}$	$\Delta_r H^0{}_T$ (kJ mol^{-1})
1	$1/3\ Mo_3O_{9(g)} + 1/2\ Sb_4O_{6(g)} \rightleftharpoons Sb_2MoO_{6(g)}{}^a$	−1.9	42.1
2	$2/3\ Mo_3O_{9(g)} + 1/2\ Sb_4O_{6(g)} \rightleftharpoons Sb_2Mo_2O_{9(g)}{}^a$	5.1	−48.9
3.I	$Mo_3O_{9(g)} + 1/2\ Sb_4O_{6(g)} \rightleftharpoons Sb_2Mo_3O_{12}(I)_{(g)}{}^a$	6.6	−99.2
3.II	$Mo_3O_{9(g)} + 1/2\ Sb_4O_{6(g)} \rightleftharpoons Sb_2Mo_3O_{12}(II)_{(g)}{}^a$	6.4	−89.9
5	$1/2\ Mo_2Sb_2O_{9(g)} + 3/4\ Sb_4O_{6(g)} \rightleftharpoons Sb_4MoO_{9(g)}{}^b$	2.2	−14.1
6	$Sb_2MoO_{6(g)} + 1/2\ Sb_4O_{6(g)} \rightleftharpoons Sb_4MoO_{9(g)}{}^b$	7.7	−82.8
7	$WO_{3(s)} + 1/2\ Sb_4O_{6(g)} \rightleftharpoons Sb_2WO_{6(g)}{}^c$	−7.0	200.9
8	$2\ WO_{3(s)} + 1/2\ Sb_4O_{6(g)} \rightleftharpoons Sb_2W_2O_{9(g)}{}^c$	−8.9	287.4
9	$WO_{3(s)} + Sb_4O_{6(g)} \rightleftharpoons Sb_4WO_{9(g)}{}^c$	−2.4	129.6

^{a} T = 893 K. ^{b} T = 840 K. ^{c} T = 1080 K.

For the experimental determination of the standard enthalpy of formation of Sb_2MoO_6, $Sb_2Mo_2O_9$ and $Sb_2Mo_3O_{12}$, equilibrium processes 1–3 (Table 5) were selected. The standard enthalpy of formation of Sb_4MoO_9 can be defined from reaction 5. Reaction 6 was additionally considered to confirm the standard enthalpy of formation of Sb_2MoO_6, calculated from reaction 1. Because gaseous tungsten oxide was not detected in the mass spectrometry experiment, equilibrium reactions 7–9 between solid WO_3 and gaseous Sb_4O_6 were employed for the determination of the standard enthalpies of formation for Sb_2WO_6, $Sb_2W_2O_9$ and Sb_4WO_9.

The equilibrium constants, $K_{p,T}$, representing the ratio of partial pressures of the gas species, were calculated (Table 5) using the partial pressures from Table 2. As discussed above, $Sb_2Mo_3O_{12}$ is present in the gas phase at 893 K in two isomeric forms (Fig. S5, ESI†). The Gibbs free energy of the isomer transition, $\Delta_i G^0{}_T(QC)$, is theoretically calculated to be 1.5 kJ mol^{-1}. Using this value, we calculated the ratio of the partial pressures of the two isomers $p(Sb_2Mo_3O_{12}$ (I)): $p(Sb_2Mo_3O_{12}$ (II)) and obtained $\ln K_{p,T}$ for the reactions 3.I and 3.II. The experimental values of $\ln K_{p,T}$ for reactions 1–3 and 5 and 6 (Table 5) and the quantum chemically calculated values of $\ln K_{p,T}$ (Table 4) are in very good agreement. Using the determined equilibrium constants, $K_{p,T}$, for reactions 1–3 and 5–9, the enthalpies of formation ($\Delta_f H^0{}_T$) of the ternary oxides can been obtained. The following values were used for these calculations: $\Delta_f H^0{}_{893}$-(Mo_3O_9), $\Delta_f H^0{}_{893}(Sb_4O_6)$, $\Delta_f H^0{}_{840}(Sb_4O_6)$, $\Delta_f H^0{}_{840}(Sb_2Mo_2O_9)$ and $\Delta_f H^0{}_{1080}(WO_{3(s)})$, which were obtained using eqn (6). The values of $\Delta_f H^0{}_T(Mo_3O_9)$, $\Delta_f H^0{}_T(Sb_4O_6)$ and $\Delta_f H^0{}_T(WO_{3(s)})$ were

calculated from the standard enthalpies of formation[23] and $\Delta_f H^0{}_{840}(Sb_2Mo_2O_9)$ was calculated from $\Delta_f H^0{}_{893}(Sb_2Mo_2O_9)$ using eqn (6). All the calculated enthalpies of formation for the ternary oxides, $\Delta_f H^0{}_T$, were converted into the standard enthalpies of formation, $\Delta_f H^0{}_{298}$, using eqn (6) and the calculated a, b and c coefficients of the $c^0{}_{p,T}$ function. The $\Delta_f H^0{}_T$ and $\Delta_f H^0{}_{298}$ enthalpies of the ternary oxides are presented in Table 6.

$$\Delta_f H^0_{T'} = \Delta_f H^0_T + \int_T^{T'} c^0_{p,T}\ dT \qquad (6)$$

Finally we compared the quantum chemically calculated and experimental values of the standard enthalpies of formation for the ternary oxides (Table 6). The differences between the calculated and experimental enthalpies of formation are not high and do not exceed 20 kJ mol^{-1}. The standard enthalpies of formation for Sb_2MoO_6, obtained from reactions 1 and 6, are very close to each other.

4 Conclusions

A series of mass spectrometry studies on the reactions of gaseous molybdenum, tungsten and antimony oxides were carried out. It was shown that seven novel ternary molybdenum–antimony and tungsten–antimony oxides exist in the gas phase: Sb_2MO_6, $Sb_2M_2O_9$, Sb_4MO_9 (M = Mo, W) and $Sb_2Mo_3O_{12}$. The maximum number of metallic atoms in the gaseous ternary compounds, as well as in the gaseous molybdenum and tungsten oxide species, is 5. The vapour over solid $Sb_2Mo_3O_{12}$ primarily

Table 6 Experimental and calculated standard enthalpies of formation for the gaseous ternary oxides

Compound	$\Delta_f H^0{}_T$ (exp.) (kJ mol^{-1})	$\Delta_f H^0{}_{298}$ (exp.) (kJ mol^{-1})	$\Delta_f H^0{}_{298}$ (QC) (kJ mol^{-1})	$\Delta_f H^0{}_{298}$ (QC)–$\Delta_f H^0{}_{298}$ (exp.) (kJ mol^{-1})
Sb_2MoO_6 (from reaction 1)	-1077.0^a	-1187.9	-1197.9	-10.0
$Sb_2Mo_2O_9$	-1742.8^a	-1905.9	-1907.8	-1.9
$Sb_2Mo_3O_{12}$ (I)	-2367.8^a	-2583.1	-2570.2	12.9
$Sb_2Mo_3O_{12}$ (II)	-2358.5^a	-2573.7	-2560.8	12.9
Sb_4MoO_9	-1718.7^b	-1881.6	-1888.9	-7.3
Sb_2MoO_6 (from reaction 6)	-1087.5^b	-1187.8	-1197.9	-10.1
Sb_2WO_6	-1092.1^c	-1240.7	-1251.1	-10.4
$Sb_2W_2O_9$	-1775.4^c	-1994.3	-2012.1	-17.8
Sb_4WO_9	-1686.2^c	-1926.8	-1945.5	-18.7

^{a} $T = 893$ K. ^{b} $T = 840$ K. ^{c} $T = 1080$ K.

contains of three gaseous oxides: Sb_2MoO_6, $Sb_2Mo_2O_9$ and two isomers of $Sb_2Mo_3O_{12}$. The largest antimony oxide is bound in the gaseous ternary oxide $Sb_2Mo_2O_9$, which has a partial pressure that exceeds five times the sum of the partial pressures of the antimony-containing oxides Sb_2MoO_6, $Sb_2Mo_3O_{12}$ and Sb_4O_6. The evaporation of solid Sb_2MoO_6 and the mixture of the gaseous WO_3 and Sb_2O_3 yields primarily three oxides in the gas phase: Sb_2MO_6, $Sb_2M_2O_9$ and Sb_4MO_9, (M = Mo, W). There are no binary gaseous molybdenum or tungsten oxides in these systems because the molybdenum and tungsten oxides are exclusively present as ternary oxides. This reflects a significant enhancement of the volatility of MO_3 and Sb_2O_3 in the ternary system relative to the binary system.

The isostructural molybdenum and tungsten ternary oxides differ from each other in terms of their stability in the gas phase. The gaseous Sb_2MO_6 is the most abundant ternary oxide in the Sb_2O_3–WO_3 system, unlike in the Sb_2O_3–MoO_3 system, where the presence of Sb_2MoO_6 is much lower. The $Sb_2M_2O_9$ oxide has the highest partial pressure in the Sb_2O_3–MoO_3 system with an excess of molybdenum oxide. In other systems, the presence of that oxide is also considerable but not dominant. On increasing of partial pressure of Sb_4O_6, the partial pressure of Sb_4MoO_9 grows and the partial pressures of the other ternary oxides Sb_2MoO_6, $Sb_2Mo_2O_9$ and $Sb_2Mo_3O_{12}$ decreases.

The structures of all the ternary molybdenum–antimony and tungsten–antimony oxides have common characteristics. All the ternary oxides tend to form structures of six- or eight-membered rings of alternating oxygen and metallic atoms, whereas four-membered rings are disfavoured. The only exception is the structure of Sb_2MO_6 because it is not possible to avoid the formation of four-membered rings. All of the structures contain four-coordinate M^{6+} and three-coordinate Sb^{3+} ions.

The enthalpies of formation of the oxides in the gas phase were determined using mass spectrometry and compared with quantum chemical calculations. The experimental and calculated standard enthalpies of formation are in very good agreement. The first ionisation potentials were experimentally obtained for Sb_2WO_6, $Sb_2M_2O_9$ (M = Mo, W), $Sb_2Mo_3O_{12}$ and Sb_4MoO_9 and were confirmed by theoretical values, thus proving the existence of these oxides in the gas phase. In addition, we propose that Sb_2MoO_6 and Sb_4WO_9 are also present in the gas phase because the experimental standard enthalpy of formation of these oxides was confirmed by quantum chemical calculations.

Acknowledgements

References

1 H. Schäfer and U. Flörke, *Z. Anorg. Allg. Chem.*, 1980, **469**, 172.
2 H. Schäfer, *Angew. Chem., Int. Ed. Engl.*, 1976, **15**, 713.
3 E. Berezovskaya, E. Milke and M. Binnewies, *Dalton Trans.*, 2012, **41**(8), 2464.
4 V. B. Goncharov and E. F. Fialko, *J. Struct. Chem.*, 2002, **43**, 777.
5 K. N. Marushkin, A. S. Alikhanyan, J. H. Greenberg, V. B. Lazarev, V. A. Malyusov, O. N. Rozanova, B. T. Melekh and V. I. Gorgoraki, *J. Chem. Thermodyn.*, 1985, **17**, 245.
6 J. Berkowitz, W. A. Chupka and M. G. Inghram, *J. Chem. Phys.*, 1957, **26**, 842.
7 R. G. Behrens and G. M. Rosenblatt, *J. Chem. Thermodyn.*, 1973, **5**, 173.
8 N. A. Asryan, A. S. Alikhanian and G. D. Nipan, *Dokl. Phys. Chem.*, 2003, **392**, 221.
9 M. Binnewies, *Z. Anorg. Allg. Chem.*, 1977, **435**, 156.
10 M. Parmentier, A. Courtois and Ch. Gleitzer, *Bull. Soc. Chim. Fr.*, 1974, **19**, 75.
11 R. Ahlrichs, M. Bär, H.-P. Baron, R. Bauernschmitt, S. Böcker, P. Deglmann, M. Ehrig, K. Eichkorn, S. Elliott, F. Furche, F. Haase, M. Häser, C. Hättig, H. Horn, C. Huber, U. Huniar, M. Kattannek, A. Köhn, C. Kölmel, M. Kollwitz, K. May, C. Ochsenfeld, H. Öhm, A. Schäfer, U. Schneider, M. Sierka, O. Treutler, B. Unterreiner, M. von Arnim, F. Weigend, P. Weis and H. Weiss, *TURBOMOLE, version 5.9.1*, Universität Karlsruhe, Karlsruhe, Germany, 2007.
12 A. D. Becke, *Phys. Rev. A: At., Mol., Opt. Phys.*, 1988, **38**, 3098.
13 J. P. Perdew, *Phys. Rev. B*, 1986, **33**, 8822.
14 K. Eichkorn, F. Weigend, O. Treutler and R. Ahlrichs, *Theor. Chem. Acc.*, 1997, **97**, 119.
15 K. Eichkorn, O. Treutler, H. Ohm, M. Haser and R. Ahlrichs, *Chem. Phys. Lett.*, 1995, **242**, 652.
16 M. Binnewies, K. Rinke and H. Schäfer, *Z. Anorg. Allg. Chem.*, 1973, **395**, 50.
17 R. J. M. Konings, A. S. Booij and E. H. P. Cordfunke, *Chem. Phys. Lett.*, 1993, **210**, 380.
18 P. A. Akishin and V. P. Spiridonov, *J. Struct. Chem.*, 1961, **2**, 502.
19 D. L. Neikirk, J. C. Fagerli, M. L. Smith, D. Mosman and T. C. Devore, *J. Mol. Struct.*, 1991, **244**, 165.
20 R. G. Egdell, M. H. Palmer and R. H. Findlay, *Inorg. Chem.*, 1980, **19**, 1314.
21 R. P. Burns, G. De Maria, J. Drowart and R. T. Grimley, *J. Chem. Phys.*, 1960, **32**, 1363.
22 S. T. Bennett, S.-S. Lin and P. W. Gilles, *J. Phys. Chem.*, 1974, **78**, 266.
23 M. Binnewies and E. Milke, *Thermochemical Data of Elements and Compounds*, Wiley-VCH, Weinheim, Germany, 2nd edn, 2002.

29

The formation and stability of molybdenum-antimony and tungsten-antimony ternary oxides Sb_2MO_6, $Sb_2M_2O_9$, $Sb_2Mo_3O_{12}$ and Sb_4MO_9 in the gas phase (M = Mo, W). Quantum chemical and mass spectrometric studies.

E. Berezovskaya*, E. Milke and M. Binnewies

Supplementary Materials

Table S1 Molecular symmetries, total energies and thermal energies of the antimony, molybdenum and tungsten oxides and their isomers (def2-TZVP/RI-BP86).

molecule	molecular symmetry	E_{tot} (a.u.)	$E_{therm\ 298}$ (kJ·mol^{-1})
Sb_4O_6 (I)	T_d	-1413.450842	84.18
Sb_4O_6 (II)	D_{2h}	-1413.408816	84.13
Mo_3O_9 (I)	C_{3v}	-882.913202	118.15
Mo_3O_9 (II)	C_{2v}	-882.874712	117.55
Mo_4O_{12} (I)	D_{4h}	-1177.237313	160.27
Mo_4O_{12} (II)	C_1	-1177.204197	159.15
Mo_5O_{15} (I)	C_s	-1471.553735	201.98
Mo_5O_{15} (II)	C_{2v}	-1471.530664	200.63
W_3O_9 (I)	D_{3h}	-879.687121	117.18
W_3O_9 (II)	C_1	-879.651945	116.62
W_4O_{12} (I)	C_{4v}	-1172.940438	159.00
W_4O_{12} (II)	C_1	-1172.914854	158.31
W_5O_{15} (I)	C_s	-1466.184910	200.43
W_5O_{15} (II)	C_{2v}	-1466.173493	199.75

Table S2 Molecular symmetries, total energies and thermal energies of the antimony,
molybdenum and tungsten ternary oxides and their isomers (def2-TZVP/RI-BP86).

molecule	molecular symmetry	E_{tot} (a.u.)	$E_{therm\,298}$ (kJ·mol^{-1})
Sb_2MoO_6 (I)	C_{2v}	-1001.015868	80.37
Sb_2MoO_6 (II)	C_s	-1000.964235	78.00
$Sb_2Mo_2O_9$ (I)	C_s	-1295.352819	122.25
$Sb_2Mo_2O_9$ (II)	C_1	-1295.331719	122.14
$Sb_2Mo_2O_9$ (III)	C_1	-1295.324831	121.21
$Sb_2Mo_2O_9$ (IV)	C_1	-1295.323287	121.18
$Sb_2Mo_2O_9$ (V)	C_1	-1295.313122	120.61
Sb_4MoO_9 (I)	C_s	-1707.773869	125.97
Sb_4MoO_9 (II)	C_4	-1707.765030	125.07
Sb_4MoO_9 (III)	C_s	-1707.753925	125.08
Sb_4MoO_9 (IV)	C_s	-1707.749597	126.03
Sb_4MoO_9 (V)	C_s	-1707.725305	126.41
Sb_4MoO_9 (VI)	C_{2v}	-1707.718893	125.12
$Sb_2Mo_3O_{12}$ (I)	C_s	-1589.671665	164.08
$Sb_2Mo_3O_{12}$ (II)	C_1	-1589.668129	164.18
$Sb_2Mo_3O_{12}$ (III)	C_1	-1589.647773	164.22
$Sb_2Mo_3O_{12}$ (IV)	C_1	-1589.637061	161.81
Sb_2WO_6 (I)	C_{2v}	-999.942317	80.01
Sb_2WO_6 (II)	C_{2v}	-999.902957	78.15
$Sb_2W_2O_9$ (I)	C_s	-1293.204927	121.50
$Sb_2W_2O_9$ (II)	C_1	-1293.186000	121.53
$Sb_2W_2O_9$ (III)	C_1	-1293.182354	120.67
$Sb_2W_2O_9$ (IV)	C_1	-1.293.186766	120.82
$Sb_2W_2O_9$ (V)	C_1	-1.293.181353	120.12
Sb_4WO_9 (I)	C_s	-1706.701626	125.62
Sb_4WO_9 (II)	C_4	-1706.705806	125.13
Sb_4WO_9 (III)	C_s	-1706.695186	125.09
Sb_4WO_9 (IV)	C_1	-1706.677443	125.75
Sb_4WO_9 (V)	C_s	-1706.653897	126.11
Sb_4WO_9 (VI)	C_{2v}	-1706.662854	125.26

Table S3 Experimental[23] and calculated thermodynamic characteristics of the molybdenum and antimony oxides (def2-TZVP/RI-BP86).

Molecule	S^0_{298} $(J \cdot mol^{-1} \cdot K^{-1})$ (exp. // QC)	S^0_{1000} $(J \cdot mol^{-1} \cdot K^{-1})$ (exp. // QC)	$c^0_{p,T} = a + b \cdot 10^{-3} \cdot T + c \cdot 10^6 \cdot T^2$ (exp. // QC)		
			a	b	c
Sb_4O_6	444.2 // 461.8	699.8 // 719.1	217.6 // 222.6	14.1 // 9.0	-3.5 // -3.6
Mo_3O_9	526.7 // 525.5	837.3 // 820.0	274.5 // 246.8	4.2 // 30.7	-4.8 // -5.1
Mo_4O_{12}	654.0 // 639.4	1074.2 // 1038.8	371.4 // 333.1	5.7 // 42.3	-6.5 // -6.5
Mo_5O_{15}	771.5 // 798.1	1301.3 // 1302.7	468.2 // 420.4	7.2 // 52.9	-8.2 // -8.0
W_3O_9	504.7 // 542.5	845.3 // 838.2	274.5 // 247.7	4.2 // 30.1	-4.8 // -4.9
W_4O_{12}	605.3 // 668.1	1028.9 // 1069.2	372.0 // 334.1	5.0 // 41.4	-5.9 // -6.3

Table S4 Calculated thermodynamic characteristics of the molybdenum and antimony oxides (def2-TZVP/RI-BP86).

Molecule	S^0_{298} $(J \cdot mol^{-1} \cdot K^{-1})$	$c^0_{p,T} = a + b \cdot 10^{-3} \cdot T + c \cdot 10^6 \cdot T^2$		
		a	b	c
Sb_2MoO_6	440.9	188.9	16.8	-3.3
$Sb_2Mo_2O_9$	566.4	273.3	31.0	-4.7
$Sb_2Mo_3O_{12}$ (I)	691.0	360.2	41.4	-6.1
$Sb_2Mo_3O_{12}$ (II)	699.9	360.3	41.4	-6.2
Sb_4MoO_9	626.3	306.6	23.0	-4.8
Sb_2WO_6	448.9	192.8	11.8	-3.5
$Sb_2W_2O_9$	593.0	281.4	20.5	-5.0
Sb_4WO_9	569.2	311.7	16.4	-5.0

exp.

$Sb_2Mo_3O_{12}^+$

$Sb_4MoO_9^+$

sim.

exp.

$Sb_2Mo_2O_9^+$

$Sb_3MoO_7^+$

$Sb_4O_6^+$

$Mo_4O_{12}^+$

$Sb_2Mo_2O_8^+$

$Mo_4O_{11}^+$

sim.

exp.

$Mo_3O_9^+$

$Sb_3O_4^+$

$SbMo_2O_7^+$

$Sb_2MoO_6^+$

$SbMo_2O_5^+$

$Mo_3O_8^+$

sim.

m/z
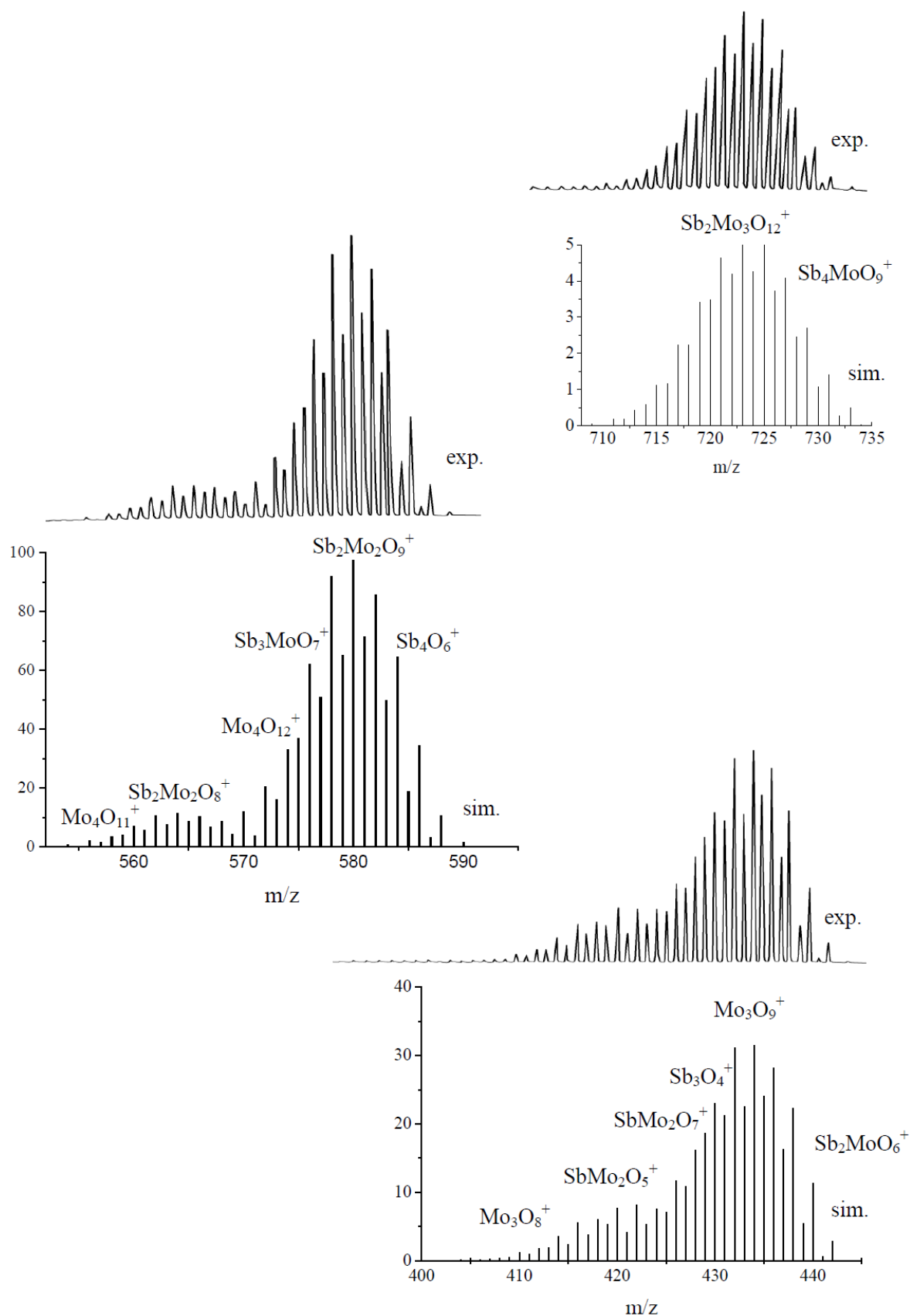
Fig. S1 Experimental and simulated mass spectra of $Sb_2Mo_3O_{12}$, 893 K, 70 eV.
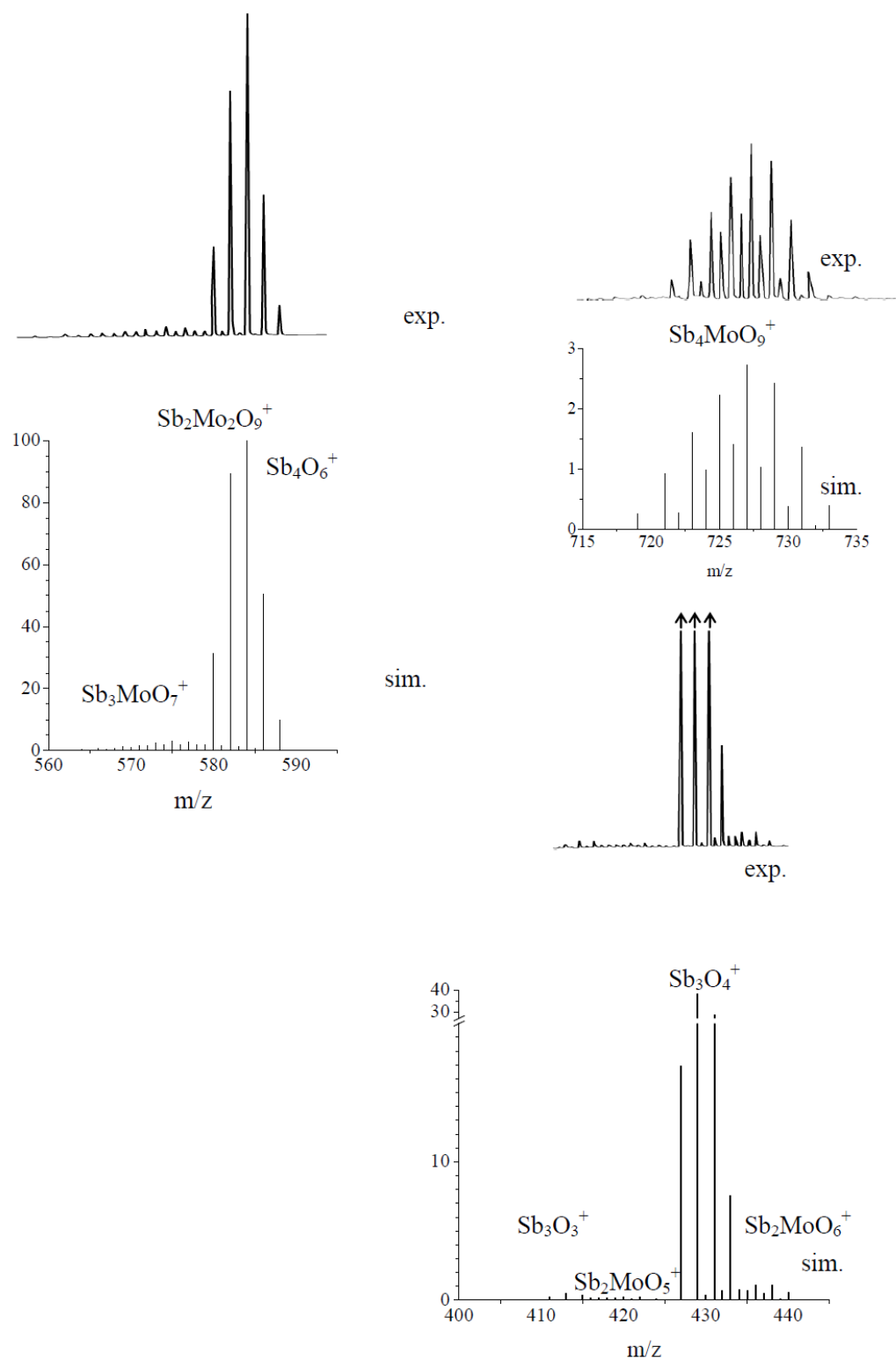
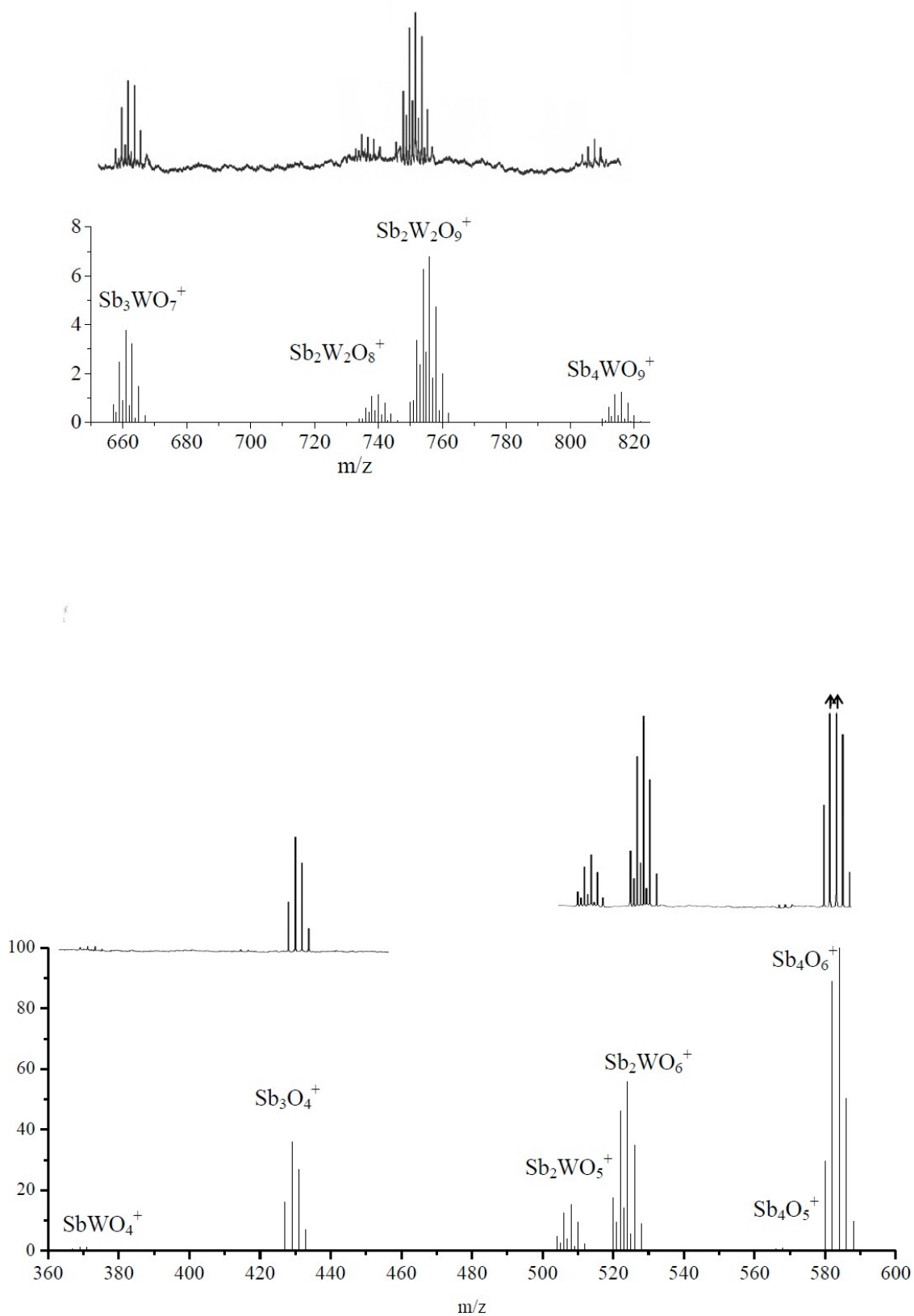**Fig. S2** Experimental and simulated mass spectra of Sb_2MoO_6, 840 K, 70 eV.

Fig. S3 Experimental and simulated mass spectra of gaseous Sb_2O_3 above solid WO_3, 1080 K, 70 eV.
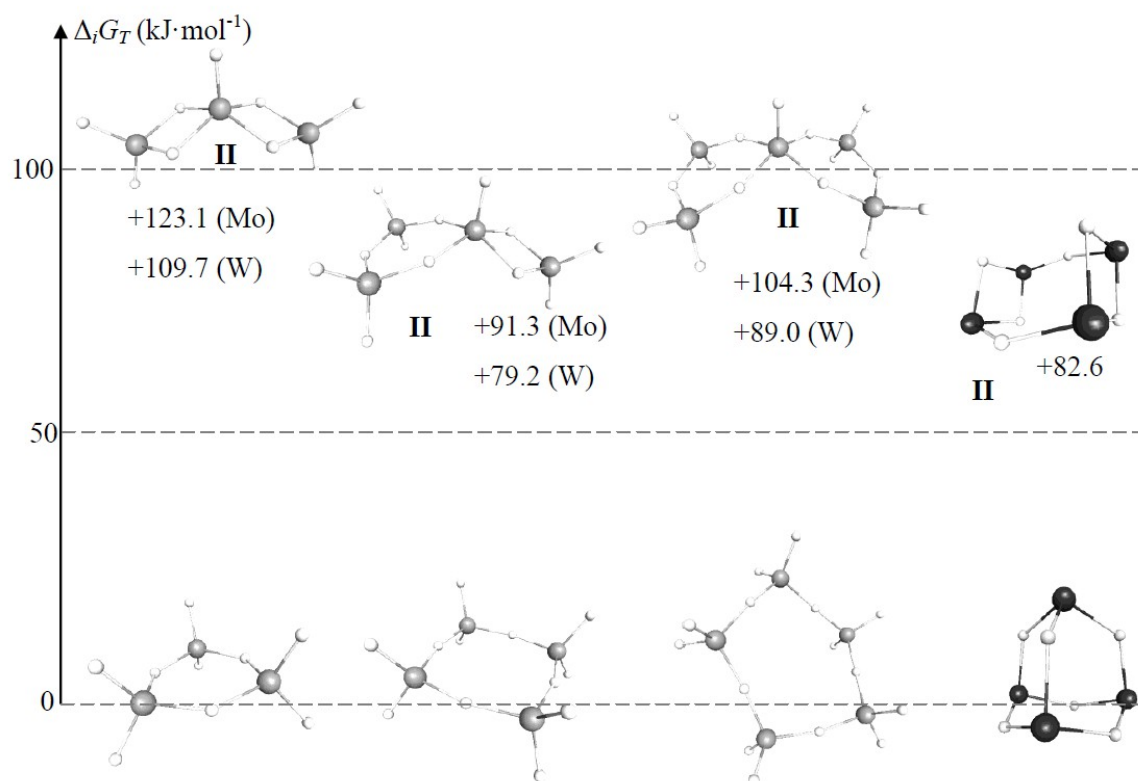
Fig. S4 Gibbs free energy of the isomer transition of $(MO_3)_x$ (x = 3-5, M = Mo, W) and Sb_4O_6 (def2-TZVP/RI-BP86) at the experimental temperatures.

$\Delta_i G_T \ (\text{kJ·mol}^{-1})$

VI
+151.1 (Mo)
+127.4 (W)

IV
+148.6 (Mo)

V
+150.8 (Mo)
+134.9 (W)

II
+134.5 (Mo)
+117.1 (W)

V
+111.1 (Mo)
+115.9 (W)

IV
+103.8 (Mo)
+95.2 (W)

III
+89.7 (Mo)
+97.8 (W)

IV
+65.7 (Mo)
+89.2 (W)

III
+85.0 (Mo)
+71.1 (W)

II
+74.4 (Mo)
+66.4 (W)

III
+30.4 (Mo)

II
+23.2 (Mo)
+33.0 (W)

II
+1.5 (Mo)

I

0
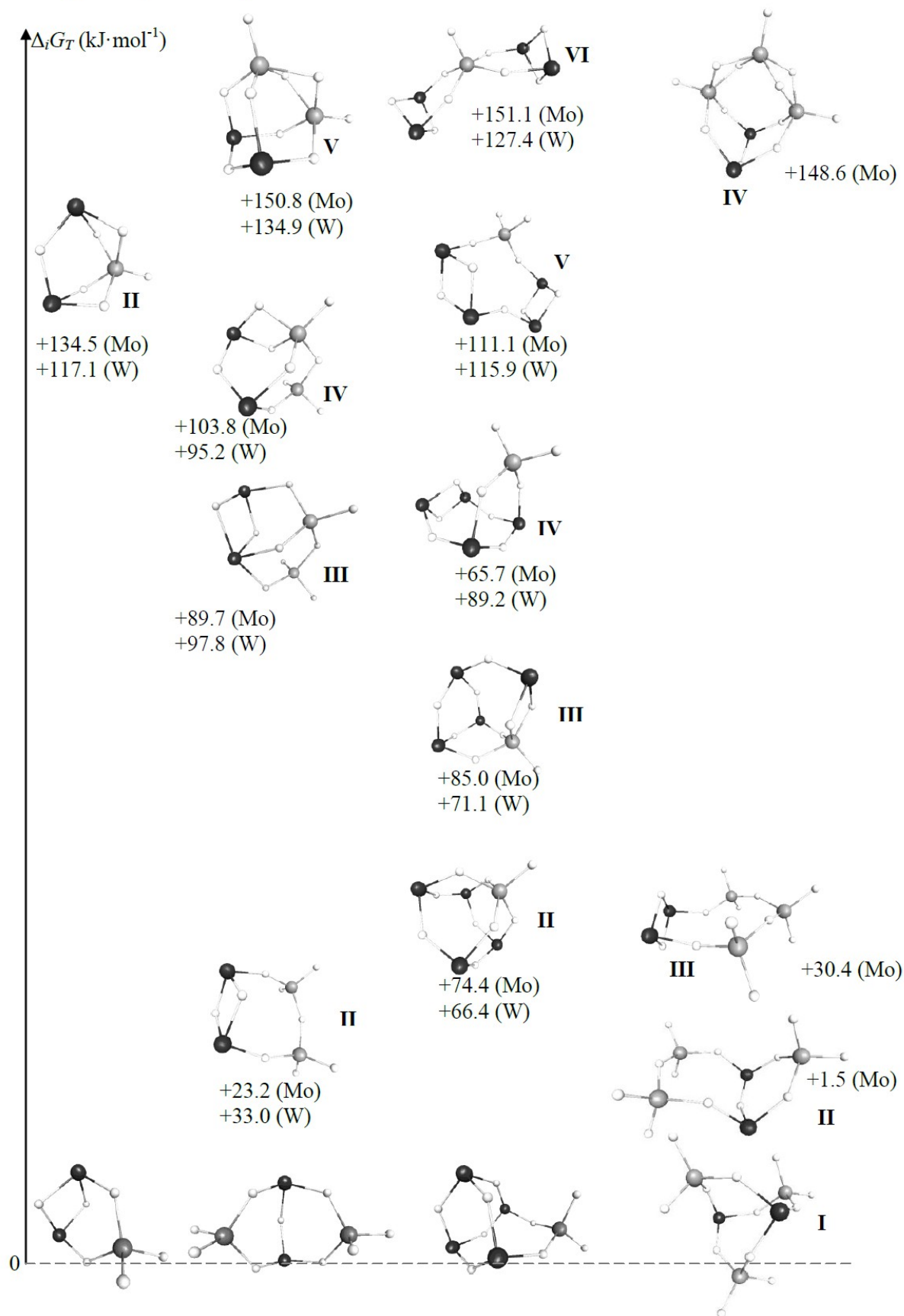
Fig. S5 Gibbs free energy of the isomer transition of Sb_2MO_6, $Sb_2M_2O_9$, Sb_4MO_9 (M = Mo, W)
and $Sb_2Mo_3O_{12}$ oxides (def2-TZVP/RI-BP86) at the experimental temperatures.

3.3 A mass spectrometric and quantum chemical study of the vaporisation of lead monoxide in a flow of gaseous arsenic and antimony trioxides.

K. Kunkel, E. Milke, M. Binnewies

PAPER

A mass spectrometric and quantum chemical study of the vaporisation of lead monoxide in a flow of gaseous arsenic and antimony trioxides†

K. Kunkel,* E. Milke and M. Binnewies

Mass spectrometric studies of the vapours over solid lead oxide in a flow of gaseous arsenic and antimony trioxides were conducted. The following ions of the ternary oxides were detected: $Pb_3As_2O_6^+$, $Pb_3AsO_4^+$, $PbAs_2O_4^+$, $PbAsO_2^+$, $PbSb_2O_4^+$, and $PbSbO_2^+$. The origin of these species produced by the ionisation and/or fragmentation of ternary gaseous oxides is discussed. The $PbAs_2O_4$ species was undoubtedly identified by the determination of the appearance energy. Presumably, the $Pb_3As_2O_6$ and $PbSb_2O_4$ species also existed in the gas phase. Thermodynamic data for the ternary oxides were obtained experimentally by means of a mass spectrometric Knudsen-cell method and were confirmed by quantum chemical calculations.

1. Introduction

Previously, we reported the following gaseous ternary oxides built from a transition metal and a main group metal or metalloid: $Sb_2Mo_3O_{12}$, $Sb_2M_2O_9$, Sb_4MO_9, Sb_2MO_6 (where M = Mo or W), Mo_3TeO_{11}, Mo_2TeO_8, $MoTe_2O_7$ and $MoTeO_{15}$.[1,2] We continue our investigation of gaseous ternary oxides with a system consisting of a volatile metalloid oxide X_2O_3 (where X = As or Sb) and the PbO metal oxide, which has a lower volatility. Several studies of the vaporisation of the pure oxides of PbO,[3–5] As_2O_3[6,7] and Sb_2O_3[8,9] using mass spectrometric methods have been reported by several authors. In the gas phase over solid lead monoxide at a temperature of approximately 1000 K, PbO, Pb_2O_2 and Pb_4O_4 were found to be the main compounds. Very low concentrations of Pb_3O_3, Pb_5O_5 and Pb_6O_6 were also detected.[3–5] Mass spectrometric studies of the vaporisation of As_2O_3 have shown that the gas phase of the As–O system is highly complex.[6] Besides gaseous As_4O_6 and AsO species, which were previously known to exist in the gas phase, other stable species including As_4O_5, As_4O_4, As_4O_3, As_3O_4, As_2O_3 and AsO_2 were detected in the gas phase.[6] The studies of the Sb–O system showed incongruent evaporation of Sb_2O_3 trioxide and revealed errors in previous studies on the congruent evaporation of Sb_2O_3.[8,9] Analogous to the As–O system, the gas phase over antimony trioxide primarily consisted of Sb_4O_6 molecules. The formation and thermodynamic stability of antimony monoxide SbO have been previously

investigated by mass spectrometry.[10] The authors observed the formation of SbO species by the oxidation of atomic Sb at temperatures of approximately 1880 K.

There are several gaseous ternary oxides such as $SnPO_2$, $SnPO_3$[11] and $GePO_3$,[12] which are related to the lead–arsenic and lead–antimony oxides, which have been detected using mass spectrometry. To the best of our knowledge, no other experimental and quantum chemical studies of gaseous ternary molecular oxides of groups 14 and 15 elements have been reported. Two relative solid compounds $PbAs_2O_4$ and $Pb_2As_2O_5$ were reported and their structures were investigated elsewhere.[13] In the present work, with the help of mass spectrometry and quantum chemical calculations, we discuss the formation and stability of ternary oxides over two gaseous mixtures, PbO–As_2O_3 and PbO–Sb_2O_3. The structures of the gaseous ternary oxides $PbAs_2O_4$, $Pb_3As_2O_6$ and $PbSb_2O_4$ are also reported and discussed.
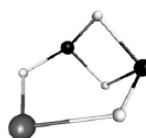
$PbAs_2O_4$

$PbSb_2O_4$
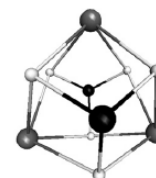
$Pb_3As_2O_6$

2. Results and discussion

2.1. Mass spectrometric study

The As_2O_3, Sb_2O_3 and PbO oxides have very different volatilities. The melting points of the oxides are 585 K, 929 K and

Institut für Anorganische Chemie, Callinstr. 9, 30167 Hannover, Germany.
E-mail: katja.kunkel@aca.uni-hannover.de; Fax: +49 511-762-2254

1161 K, respectively, and the equations describing the partial pressures as a function of temperature are as follows:

$$\text{for As}_2\text{O}_3 \quad \lg(p/\text{atm}) = -(6067 \pm 125)/T + (9.905 \pm 0.319) \quad (367–429\ \text{K}) \tag{1}$$

14

$$\text{for Sb}_2\text{O}_3 \quad \lg(p/\text{atm}) = -(10\ 066 \pm 203)/T + (9.390 \pm 0.297) \quad (627–723\ \text{K}) \tag{2}$$

15

$$\text{for PbO} \quad \lg(p/\text{bar}) = -32\ 032/T + 1915 \quad (850–1100\ \text{K}) \tag{3}$$

3

$$\text{or} \quad \lg(p/\text{Pa}) = -13\ 345/T + 11.9 \quad (900–1150\ \text{K}) \tag{4}$$

16

Therefore, a double Knudsen cell was used in the mass spectrometric experiment. In the first experiment, solid As_2O_3 was continuously evaporated at 423 K and flowed through the solid PbO at 900 K. Analogously, in the second experiment, Sb_2O_3 was evaporated at 673 K and flowed through the solid PbO at 1110 K. The reaction products leaving the Knudsen cell were analysed by mass spectrometry.

The relative intensities of the ions in the mass spectra are presented in Table 1. Additionally, mass spectrometric measurements of the vaporisation of pure oxides were conducted for comparison, and those results are also presented in Table 1. The highest relative intensities were observed for the $X_4O_6^+$ ions, and the second highest relative intensities

Table 1 Relative intensities of ionic species over PbO–X_2O_3 systems and the pure oxides X_2O_3 (X = As or Sb) and PbO at 70 eV

| | Relative intensity | | | | |
| | X_2O_3–PbO | | X_2O_3 | | PbO |
Ion	X = As 900 K	X = Sb 1100 K	X = As 423 K	X = Sb 673 K	1002 K
$Pb_4O_4^+$ (M$^+$)	—	6.0	—	—	100
$Pb_3X_2O_6^+$ (M$^+$)	3.6	—	—	—	—
$Pb_3XO_4^+$	2.8	—	—	—	—
$Pb_3O_3^+$ (M$^+$)	—	—	—	—	10.5
$Pb_3O_2^+$	—	—	—	—	6.0
$Pb_2O_2^+$	—	2.9	—	—	59.7
Pb_2O^+	—	—	—	—	15.1
$PbX_2O_4^+$ (M$^+$)	37.5	7.9	—	—	—
$PbXO_2^+$	37.3	1.6	—	—	—
$X_4O_6^+$ (M$^+$)	100	100	100	100	—
$X_4O_5^+$	0.8	—	0.7	0.6	—
X_4^+	22.7	—	0.8	—	—
$X_3O_4^+$	74.8	20.3	66.2	24.2	—
X_3^+	1.8	—	1.6	—	—
PbO^+ (M$^+$)	—	2.7	—	—	44.2
Pb^+	18.7	11.6	—	—	45.1
$X_2O_3^+$	1.6	—	0.7	0.3	—
$X_2O_2^+$	5.7	—	0.7	2.7	—
X_2^+	14.0	—	4.4	—	—
XO^+	37.5	0.7	14.1	5.1	—
X^+	3.9	0.1	0.5	0.1	—

belonged to the $X_3O_4^+$ ions in the mass spectra of the ternary oxides as well as the pure arsenic and antimony trioxides. The $Pb_4O_4^+$, $Pb_2O_2^+$ and PbO^+ ions were detected in the mass spectrometric experiment with antimony oxide (PbO–Sb_2O_3 system), in which PbO was heated to 1110 K. In the experiment with arsenic oxide (PbO–As_2O_3 system), the partial pressure of PbO at 900 K was too low ($\sim 10^{-8}$ bar) for the detection of the PbO^+ signal in the mass spectra. Three parent ions of ternary oxides were detected: $Pb_3As_2O_6^+$ (M$^+$), $PbAs_2O_4^+$ (M$^+$) and $PbSb_2O_4^+$ (M$^+$) (where M$^+$ is the parent ion), which indicated the existence of gaseous $Pb_3As_2O_6$, $PbAs_2O_4$ and $PbSb_2O_4$. The $Pb_2As_2O_5^+$ ion was not detected. The appearance energy was obtained only for the $PbAs_2O_4^+$ ion because the intensities of the $Pb_3As_2O_6^+$ and $PbSb_2O_4^+$ ions were too small. Extrapolation of the linear portion of the ionisation efficiency curves to an intensity of zero gave the following value for the appearance energy: AE($PbAs_2O_4^+$) = 9.7 ± 0.5 eV.

The following species, which can have two formation sources, were also observed: $Pb_3AsO_4^+$, $PbAsO_2^+$ and $PbSbO_2^+$. The first way in which these ions could have been formed was by the splitting of [AsO_2] from the $Pb_3As_2O_6^+$ and $PbAs_2O_4^+$ parent ions and the splitting of [SbO_2] from $PbSb_2O_4^+$, i.e., by the fragmentation process

$$Pb_nX_2O_{n+3}^+ \rightarrow Pb_nXO_{n+1}^+ + [XO_2] \text{ (where X = As or Sb,}$$
$$n = 1 \text{ or } 3).$$
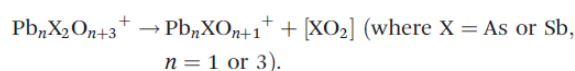
Under the designation [XO_2], neutral species were united to give a total of one X atom and two O atoms: XO_2, $XO + O$, $X + O_2$ and $X + 2O$.

The second way in which the $Pb_3AsO_4^+$, $PbAsO_2^+$ and $PbSbO_2^+$ ions could have been formed was as products of the ionisation of molecules with X^{2+}. As mentioned above, gaseous AsO species, where the oxidation state of As is 2+, are thermodynamically stable. Brittain et al.[6] have shown that AsO$^+$ formed primarily by the ionisation of AsO(g) in unsaturated vapour over As_2O_3(s) at 1160 K. In our experiment, the relative intensities of AsO$^+$ and $PbAsO_2^+$ in the mass spectra of the As_2O_3–PbO gaseous mixture were quite high. The appearance energies for these two ions were determined to be AE($PbAsO_2^+$) = 10.0 ± 0.5 eV and AE(AsO$^+$) = 15.7 ± 0.5 eV. The quantum chemical calculated ionisation energies for the individual molecules are IE($PbAsO_2$) = 6.74 eV and IE(AsO) = 8.48 eV, and the experimental value of Brittain et al.[6] was AE(AsO$^+$) = 9.0 ± 0.3 eV. Thus, under the conditions of our experiment, AsO$^+$ and $PbAsO_2^+$ ions were the fragmented species but were not the parent ions as was originally believed. The intensities of the $Pb_3AsO_4^+$ and $PbSbO_2^+$ ions were too small to determine their appearance energies, but presumably, these ions were also fragments.

The dependence of the recorded ion currents on the partial pressure of the particular ion is described by the following equation:

$$p_i = c \frac{\sum I_i T}{\sigma_i S_i} \tag{5}$$

Table 2 Molecules and their ions in the gas phase of the PbO–As_2O_3 system

Molecule	Attributed ions	Partial pressure, p (bar) (900 K)
As_4O_6	$As_4O_6^+$, $As_4O_5^+$, As_4^+, $As_3O_4^+$, As_3^+	3.1×10^{-5}
$PbAs_2O_4$	$PbAs_2O_4^+$, $PbAsO_2^+$	2.5×10^{-5}
$Pb_3As_2O_6$	$Pb_3As_2O_6^+$, $Pb_3AsO_4^+$	2.1×10^{-6}

Table 3 Molecules and their ions in the gas phase of the PbO–Sb_2O_3 system

Molecule	Attributed ions	Partial pressure, p (bar) (1100 K)
PbO	PbO^+	1.0×10^{-7}
Sb_4O_6	$Sb_4O_6^+$, $Sb_3O_4^+$, SbO^+, Sb^+	2.8×10^{-6}
$PbSb_2O_4$	$Sb_2PbO_4^+$, $SbPbO_2^+$	3.6×10^{-7}

where p_i = the partial pressure of component i, c = the proportionality factor, $\sum I_i$ = the intensity of all of the ions formed by the ionisation and fragmentation of a gaseous molecule of i, T = the temperature, σ_i = the ionisation cross section and S_i = the electron multiplier efficiency. The approximated eqn (6) can be used in most cases (the procedure of simplification is described elsewhere[17]):

$$p_i = c \sum I_i T \qquad (6)$$

The proportionality factors c_1 and c_2 were determined by a calibration experiment for both systems and were found to be $c_1 = 3.6 \times 10^{-10}$ and $c_2 = 3.4 \times 10^{-11}$ bar K^{-1}.

The mass spectrometric measurements of pure oxides As_2O_3 and Sb_2O_3 were used for the calibration. The proportional factors c_1 and c_2 were determined within the error of a factor of 8 and 7 respectively.

Using the c_1 and c_2 values, the relative intensities $\sum I_i$, and applying eqn (6), the partial pressures of the gaseous molecules in the two equilibrium gaseous mixtures PbO–As_2O_3 and PbO–Sb_2O_3 can be calculated (Table 2). It was taken into account that arsenic and antimony oxides were constantly evaporating at lower temperatures (423 K and 673 K, respectively) and when they passed by lead oxide at higher temperatures (900 K and 1110 K, respectively). Tables 2 and 3 present the parent ions, their fragments, which contributed to the gaseous molecules, and the partial pressures of these molecules. We assumed equilibrium inside the Knudsen cell in the systems under consideration. The equilibrium in the Knudsen cell was confirmed by vaporisation of As_2O_3 oxide.[14] The equilibrium in the gas phase was investigated in the Knudsen cell over Sb_2O_3 and PbO oxides too.[3–5,8,9,15]

Using the partial pressures, we determined the equilibrium constants of the formation of the arsenic–lead and antimony–lead ternary oxides, which will be given later in this paper.

2.2. Density functional theory computations

The def2-TZVP/RI-BP86 method allows a good correlation between the calculated values and the experimental data for many oxides to be obtained. We successfully used the method employed previously for studying oxide systems containing molybdenum, tungsten, tellurium and antimony oxides.[1,2] We also used the def2-TZVP/RI-BP86 method in the current study and showed the correlation between the experimental and calculated data for arsenic, antimony and lead oxides.

First, the oxides PbO, Pb_2O_2, Pb_3O_3, Pb_4O_4, and X_4O_6 (where X = As or Sb) were quantum chemically investigated. Total energies, thermal energies, point groups of the molecules and geometrical structures of pure lead, arsenic and antimony oxides are given in Table 4.

Monomers and oligomers of lead oxide, arsenic oxide and antimony oxide have also been theoretically studied elsewhere.[18–20] The calculated geometrical structures with their point groups, bond lengths and angles in that study agree well with our calculations. Table 5 presents a comparison of the experimental structural data from the literature and our calculated structural data for lead, arsenic and antimony oxides. The geometric parameters for gaseous As_4O_6 and Sb_4O_6 obtained by electron diffraction agree well with the calculated values. The experimental data are also in good agreement.

The experimental and calculated vibration spectra of gaseous As_4O_6, Sb_4O_6, Pb_2O_2 and Pb_4O_4 are presented in Table 6. The experimental frequencies and our calculated frequencies for As_4O_6, Sb_4O_6, Pb_4O_4, Pb_2O_2 and PbO are in

Table 4 Symmetries, total energies and thermal energies of the molecules (def2-TZVP/RI-BP86, scaling factor = 1.053)
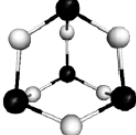
Molecule	Point group	Structure	E_{tot} (a.u.)	E_{298}^{therm} (kJ mol^{-1})
PbO	$C_{\infty v}$		−267.940878	10.99
Pb_2O_2	D_{2h}		−536.690429	26.83
Pb_3O_3	D_{3h}		−805.068223	44.09
Pb_4O_4	T_d		−1073.497158	60.50
As_4O_6	T_d		−9396.461653	89.58
Sb_4O_6	T_d		−1413.450842	85.86
AsO	$C_{\infty v}$		−2311.386123	12.42

42

Table 5 Experimental and calculated geometric parameters of gaseous molecules

		r(M–O) Å	<(O–M–O)	<(M–O–M)
Pb_4O_4	Exp.[21]	—	86°	94°
	Calc.	2.265	81.7°	97.8°
Pb_2O_2	Exp.[21]	—	80°	
	Calc.	2.138	83.3°	
As_4O_6	Exp.[22]	1.80 ± 0.02	100 ± 1.5°	126 ± 3°
	Calc.	1.817	100.2°	125.8°
Sb_4O_6	Exp.[23]	2.00 ± 0.02	98°	129.0 ± 2.5
	Calc.	1.986	98.6°	128.3°

Table 6 Observed and calculated vibrational frequencies for gaseous As_4O_6, Sb_4O_6, Pb_4O_4, Pb_2O_2 and PbO (scaling factor = 1)

		Vibrational frequencies (cm^{-1})			
As_4O_6	Exp.[24]	255.0	372.9	495.6	833.2
	Calc.	239.3	350.3	470.0	779.1
Sb_4O_6	Exp.[25]	172.2	292.4	415.6	785.0
	Calc.	165.2	270.7	401.5	741.4
Pb_4O_4	Exp.[21]	—	372	464	
	Calc.	113.3	353.3	451.8	
Pb_2O_2	Exp.[21]	—	463	558	
	Calc.	86.6	455.2	542.7	
PbO	Exp.[21]	714			
	Calc.	724.0			

Table 7 Symmetries, total energies and thermal energies of the molecules (def2-TZVP/RI-BP86, scaling factor = 1.053)
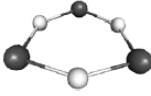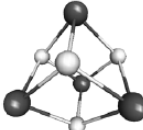
Molecule		E_{tot} (a.u.)	E_{298}^{therm} (kJ mol^{-1})
$PbAs_2O_4$	C_s	−4966.580578	58.57
$PbAsO_2$	C_1	−2579.790596	28.36
$Pb_3As_2O_6$(I)	D_{3h}	−5503.395177	92.3
$Pb_3As_2O_6$(II)	C_{3v}	−5503.369471	90.72
$Pb_3As_2O_6$(III)	C_s	−5503.364595	91.88
$PbSb_2O_4$	C_s	−975.065646	56.49
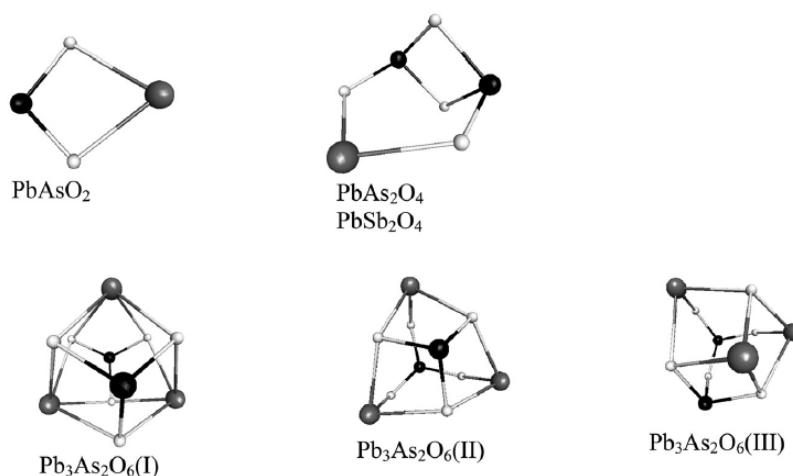
good agreement but almost all of the experimental frequencies (except PbO) insignificantly (5–6%) exceed the calculated values. Therefore vibrational wave numbers were calibrated using scaling factor = 1.053.

Total energies, thermal energies and point groups for the ternary oxides $PbAs_2O_4$, $Pb_3As_2O_6$, $PbSb_2O_4$ and the hypothetical molecule $PbAsO_2$ are presented in Table 7, and the structures are shown in Fig. 1. For $Pb_3As_2O_6$, several structural isomers were found, and the optimised geometries and total energies of the isomers were also calculated and are presented in Table 7 (E_{tot}(I) < E_{tot}(II) < E_{tot}(III)) and in Fig. 1.

Transitions between the isomers of $Pb_3As_2O_6$ at the experimental temperature of 900 K can be characterised by Gibbs free energy: $\Delta_i G_{900}$(II→I) = −51.9 kJ mol^{-1} and $\Delta_i G_{900}$(III→I) = −66.1 kJ mol^{-1}. According to the values of $\Delta_i G_{900}$, the ratio of the partial pressures of the isomers can be calculated at a temperature of 900 K: $p(Pb_3As_2O_6$(I)) : $p(Pb_3As_2O_6$(II)) : $p(Pb_3As_2O_6$(III)) = 6843 : 7 : 1. Because the partial pressures of $Pb_3As_2O_6$(II) and $Pb_3As_2O_6$(III) are insignificant in the gas phase, we will not consider them further.

The total energies of the cations $X_4O_6^+$, PbO$^+$, $PbX_2O_4^+$, $PbAsO_2^+$ and $Pb_3As_2O_6^+$ (X = As or Sb) were computed in a doublet spin state in the geometry of a neutral molecule to determine the vertical ionisation energies (IE) of the corresponding molecules (Table 15 ESI†). The first IE was determined as the difference between the total energy of the cation in a doublet state and the energy of the neutral molecule. Known experimental IE and AE values for the lead, arsenic and antimony oxides and AE values for $PbAs_2O_4^+$ and $PbAsO_2^+$ from the present study were compared with computed theoretical IE values (Table 8). The experimental AE values are in good agreement with theoretical IE values for all molecules except $PbAsO_2$. This agreement confirms that the $PbAs_2O_4^+$ ion was formed by ionisation of ternary oxides rather than by fragmentation processes. If $PbAs_2O_4^+$ is a fragment of $Pb_3As_2O_6^+$, the AE($PbAs_2O_4^+$) is expected to be much higher. Our measured AE values for $PbAsO_2^+$ and AsO$^+$ greatly exceeded the

Fig. 1 Structures of the ternary oxides $PbAs_2O_4$, $PbAsO_2$, $Pb_3As_2O_6$, $PbSb_2O_4$ and Pb_3AsO_4.

Table 8 The calculated vertical first ionisation energies (IE) (def2-TZVP/RI-BP86) and experimental appearance energies (AE)

Molecule	IE (eV) QC	AE, IE (eV) Exp.
PbO	9.65	9.4 ± 0.3 (EI, AE)[26] 9.0 ± 0.5 (EI, AE)[5]
Pb$_2$O$_2$	8.41	8.8 ± 0.5 (EI, AE)[5]
As$_4$O$_6$	9.60	10.05 ± 0.05 (PE, IE)[27]
Sb$_4$O$_6$	8.92	9.31 ± 0.05 (PE, IE)[27]
AsO	8.48	9.0 ± 0.3 (EI, AE)[6]
PbAs$_2$O$_4$	9.07	9.7 ± 0.5 (EI)[a]
PbAsO$_2$	6.74	10.0 ± 0.5 (EI)[a]
Pb$_3$As$_2$O$_6$(I)	8.47	—
PbSb$_2$O$_4$	8.49	—

[a] This work; EI – electron ionisation, PE – photoelectron ionisation.

calculated values, which means that these ions were formed by fragmentation.

Thermodynamic values for all of the compounds were obtained using the FREEH module and a scaling factor of 1.053 with a temperature range from the standard temperature to the temperature of the mass spectrometric experiments of 298–1000 K. The entropy, S_T^0, can be approximated as a function of temperature:

$$S_T^0 = S_{298}^0 + \int_{298}^{T} c_{p,T}^0 \frac{dT}{T} \tag{7}$$

$$\text{where } c_{p,T}^0 = a + b \times 10^{-3} \times T + c \times 10^6 \times T^{-2}$$

The a, b and c coefficients of the heat capacity function $c_{p,T}^0$ were calculated mathematically by fitting ten values of S_T^0 in the temperature range of 298–1100 K. Calculated entropies for gaseous PbO, As$_4$O$_6$, and Sb$_4$O$_6$ were compared with the experimental literature values to demonstrate the adequacy of the calculation method chosen (Table 9) for the study of thermodynamics. The calculated and experimental values of S_{298}^0 and S_{1000}^0 are in good agreement. The experimental and calculated values of coefficient b of the $c_{p,T}^0$ function differ from each other but yield correct entropy values. Therefore, the calculated coefficients a, b and c for the ternary oxides are acceptable and can be used in the calculations. The calculated entropy values and the values of coefficients a, b and c for the ternary oxides are presented in Table 10.

The thermodynamics of gaseous monomer and oligomer molecules of lead oxides have been studied elsewhere.[3–5] The enthalpies of oligomerisation for the lead oxides from the literature and our calculated values are compared in Table 11.

The calculated standard enthalpies of dimerisation and tetra-merisation are in very good agreement with the literature values. The literature values of the enthalpy of the trimerisation process differ from each other and had an error of ±25 kJ mol^{-1}; our standard enthalpy value falls between the experimentally obtained ones. Thus, our method gives satisfactory results for the calculations of the enthalpies of reactions and can be used to investigate the thermodynamic characteristics of the ternary oxides.

Table 12 presents the reactions for the formation of the ternary lead–arsenic and lead–antimony oxides as well as the calculated enthalpies, entropies and equilibrium constants at standard and experimental temperatures for these reactions.

The calculated standard enthalpies of formation $\Delta_f H_{298}^0$ of the ternary oxides have been obtained with the help of the reaction enthalpies $\Delta_r H_{298}^0$ of the processes from Table 12 and the experimental values of $\Delta_f H_{298}^0$(PbO) = 70.3 kJ mol^{-1},[28] $\Delta_f H_{298}^0$(As$_4$O$_6$) = −1196.1 kJ mol^{-1},[28] and $\Delta_f H_{298}^0$(Sb$_4$O$_6$) = −1215.5 kJ mol^{-1} [28] and are as follows:

$$\Delta_f H_{298}^0(\text{PbAs}_2\text{O}_4, \text{QC}) = -668.5 \text{ kJ mol}^{-1},$$

$$\Delta_f H_{298}^0(\text{PbSb}_2\text{O}_4, \text{QC}) = -653.4 \text{ kJ mol}^{-1}, \text{and}$$

$$\Delta_f H_{298}^0(\text{Pb}_3\text{As}_2\text{O}_6, \text{QC}) = -1107.8 \text{ kJ mol}^{-1}.$$

2.3. Experimental determination of the standard enthalpies of formation of $\Delta_f H_{298}^0$

The equilibrium constant $K_{p,T}$ is related to the reaction enthalpy, reaction entropy and temperature by the van't Hoff equation. The experimental reaction enthalpies $\Delta_r H_T^0$ for processes 1′, 2′ and 3 are calculated with eqn (8) and presented in Table 13. The values of the reaction entropies $\Delta_R S_T^0$ are calculated using quantum chemical values of entropy for ternary oxides and the experimental entropies S_T^0 of PbO(s), PbO(g), As$_4$O$_6$(g), and Sb$_4$O$_6$(g) obtained from eqn (7) and the $c_{p,T}^0$ function.[28]

$$\Delta_r H_T^0 \text{ (exp.)} = -RT \ln K_{p,T} + T\Delta_R S_T^0 \tag{8}$$

$$\Delta_f H_{T'}^0 = \Delta_f H_T^0 + \int_T^{T'} c_{p,T}^0 dT \tag{9}$$

The enthalpies of formation ($\Delta_f H_T^0$) of the ternary oxides (Table 14) were obtained using the determined enthalpies of reactions $\Delta_r H_T^0$ (Table 13) and enthalpies of formation $\Delta_f H_T^0$ of PbO(g), PbO(s), As$_4$O$_6$(g) and Sb$_4$O$_6$(g) oxides at experimental

Table 9 Experimental[28] and calculated thermodynamic characteristics of lead, arsenic and antimony oxides (def2-TZVP/RI-BP86, scaling factor = 1.053)

Molecule	S_{298}^0 (J mol^{-1} K^{-1}) (exp.//QC)	S_{1000}^0 (J mol^{-1} K^{-1}) (exp.//QC)	$c_{p,T}^0 = a + b \times 10^{-3} \times T + c \times 10^6 \times T^{-2}$ (exp.//QC)		
			a	b	c
PbO(g)	240.0//240.1	282.7//282.2	36.18//35.14	1.05//2.00	−0.36//−0.34
As$_4$O$_6$(g)	409.3//409.0	659.6//659.0	212.81//218.22	18.57//12.86	−3.98//−4.52
Sb$_4$O$_6$(g)	444.2//454.0	699.8//709.1	217.64//220.99	14.11//10.39	−3.47//−3.83

Table 10 Calculated thermodynamic characteristics of lead–arsenic and lead–antimony oxides (def2-TZVP/RI-BP86, scaling factor = 1.053)

| Molecule | $S^0_{298}//S^0_T$ (J mol^{-1} K^{-1}) | $c^0_{p,T} = a + b \times 10^{-3} \times T + c \times 10^6 \times T^{-2}$ | | |
		a	b	c
PbAs$_2$O$_4$	407.9//563.4^a	148.99	7.92	−2.79
PbSb$_2$O$_4$	424.2//614.7^b	151.03	6.12	−2.48
Pb$_3$As$_2$O$_6$(ɪ)	514.0//773.9^a	218.22	12.86	−4.52

^{a} T = 900 K. ^{b} T = 1110 K.

Table 11 Comparison of the calculated and experimental values for the standard enthalpies of the equilibrium reactions of the lead oxides (def2-TZVP/RI-BP86, scaling factor = 1.053)

Reaction	$\Delta_r H^0_{298}$ (kJ mol^{-1}) QC	$\Delta_r H^0_{298}$ (kJ mol^{-1}) Exp.^{a}
2PbO(g) ⇌ Pb$_2$O$_2$(g)	−258.3	−250.6 ± 6^3
		−265.4 ± 17^5
3PbO(g) ⇌ Pb$_3$O$_3$(g)	−470.4	−419.5 ± 25^3
		−529.2 ± 25^5
4PbO(g) ⇌ Pb$_4$O$_4$(g)	−816.7	−835.0 ± 15^3
		−845.7 ± 42^5

^{a} Mass spectrometric experiment.

temperatures, which were obtained from eqn (9) and the experimental $c^0_{p,T}$ function[28] ($\Delta_f H^0_{900}$(PbO(s)) = −187.2 kJ mol^{-1}, $\Delta_f H^0_{900}$(As$_4$O$_6$(g)) = −1070.3 kJ mol^{-1}, $\Delta_f H^0_{900}$(AsO(g)) = 75.6 kJ mol^{-1}, $\Delta_f H^0_{1110}$(PbO(g)) = 99.4 and $\Delta_f H^0_{1110}$(Sb$_4$O$_6$(g)) = −1039.2 kJ mol^{-1}). Then, the calculated enthalpies of formation $\Delta_f H^0_T$ of the ternary oxides were converted into the standard enthalpies of formation $\Delta_f H^0_{298}$ using eqn (9) and the calculated a, b and c coefficients of the $c^0_{p,T}$ function (Table 10). The deviations of the experimental values are discussed in the next section. The experimental enthalpies $\Delta_f H^0_T$ and $\Delta_f H^0_{298}$ and the quantum chemical values of $\Delta_f H^0_{298}$ of the ternary oxides are presented in Table 14 for comparison.

2.4. Error estimation by the determination of the experimental standard enthalpies of formation

In the present section we estimate errors in the determination of the standard enthalpy of formation. The proportional factors c_1 and c_2 were determined within the errors of a factor of 8 and 7 respectively. The errors of proportional factors lead to the errors of equilibrium constant $K_{p,T}$ and give the

Table 13 Experimental equilibrium constant and enthalpies of reaction

	Reaction	ln $K_{p,T}$	$\Delta_r H^0_T$ (kJ mol^{-1})
1′	PbO(s) + 1/2 As$_4$O$_6$(g) ⇌ PbAs$_2$O$_4$(g)	−5.4 ± 1.4^a	149.1 ± 19.5^a
2′	3 PbO(s) + 1/2 As$_4$O$_6$(g) ⇌ Pb$_3$As$_2$O$_6$(g)	−7.9 ± 1.2^a	132.3 ± 18.0^a
3	PbO(g) + 1/2 Sb$_4$O$_6$(g) ⇌ PbSb$_2$O$_4$(g)	7.7 ± 1.4^b	−112.8 ± 18.5^b

^{a} T = 900 K. ^{b} T = 1110 K.

deviation of ln $K_{p,T}$ ± 1.1 for reactions 1′, 2′ and ±1.0 for reaction 3. The error of the sum of ions $\sum I_i$ (eqn (6)) could reach 20%. That contributes to the errors of ln $K_{p,T}$ the values ±0.3, ±0.1 and ±0.4 for reactions 1′, 2′ and 3 respectively.

The error in determination of enthalpy of reaction $\Delta_r H^0_T$ includes both the error of equilibrium constant and the error of entropy of reaction according to eqn (8). The error of entropy of reaction 3 is lower than errors of entropy of reactions 1′ and 2′, because the entropies of reactions $\Delta_r S^0_T(1′)$ and $\Delta_r S^0_T(2′)$ include both experimental and quantum chemical calculated entropies and $\Delta_r S^0_T(3)$ is a quantum chemical value. We estimate the errors of $\Delta_r S^0_T(1′)$ and $\Delta_r S^0_T(2′)$ to be ±10 J mol^{-1} K^{-1} and the error of $\Delta_r S^0_T(3)$ to be ±5 J mol^{-1} K^{-1}.

Then the total errors of enthalpy of reactions 1′, 2′ and 3 are equal to ±19.5, ±18.0 and ±18.5 kJ mol^{-1} respectively. The errors of standard enthalpy of formation $\Delta_f H^0_{298}$ have corresponding deviations and are given in Table 14. The differences between the calculated and experimental enthalpies of formation are not very large. The biggest difference of $\Delta_f H^0_{298}$(exp) − $\Delta_f H^0_{298}$(QC) is for the Pb$_3$As$_2$O$_6$ molecule and is equal to 17.5 kJ mol^{-1}.

3. Experimental

3.1. Samples

Yellow lead monoxide (grade puriss. p.a), arsenic trioxide (grade puriss. p.a) and antimony trioxide (grade puriss. p.a) were used in the present study.

3.2. Mass spectrometry

Mass spectrometric measurements were carried out using a modified Finnigan type mass spectrometer. The vapours effusing from the Knudsen cell were ionised with 70 eV

Table 12 Calculated standard enthalpies, entropies of reaction and equilibrium constants for the equilibrium processes in which the lead–arsenic and lead–antimony oxides participate (def2-TZVP/RI-BP86, scaling factor = 1.053)

	Reaction	$\Delta_r H^0_T$ (kJ mol^{-1}) 298//T	ΔS^0_T (J mol^{-1} K^{-1}) 298//T	ln $K_{p,T}$ 298//T
1	PbO(g) + 1/2 As$_4$O$_6$(g) ⇌ PbAs$_2$O$_4$(g)	−140.7//−138.4^a	−36.7//−32.7^a	52.4//14.6^a
2	3 PbO(g) + 1/2 As$_4$O$_6$(g) ⇌ Pb$_3$As$_2$O$_6$(g)	−720.6//−703.1^a	−410.7//−378.9^a	241.5//48.4^a
3	PbO(g) + 1/2 Sb$_4$O$_6$(g) ⇌ PbSb$_2$O$_4$(g)	−115.9//−112.7^b	−42.9//−37.8^b	41.6//7.7^b

^{a} T = 900 K. ^{b} T = 1110 K.

Table 14 Experimental enthalpies of formation for lead–arsenic and lead–antimony oxides

Compound	$\Delta_f H_T^0$ (kJ mol^{-1}) Exp.	$\Delta_f H_{298}^0$ (kJ mol^{-1}) Exp.	$\Delta_f H_{298}^0$(QC) kJ mol^{-1}	$\Delta_f H_{298}^0$(exp.) − $\Delta_f H_{298}^0$(QC) kJ mol^{-1}
PbAs$_2$O$_4$	−573.2 ± 19.5^a	−659.5 ± 19.5	−668.5	9.0
Pb$_3$As$_2$O$_6$	−964.4 ± 18.0^a	−1090.3 ± 18.0	−1107.8	17.5
PbSb$_2$O$_4$	−549.9 ± 18.5^b	−669.9 ± 18.5	−653.4	−16.5

^{a} T = 900 K. ^{b} T = 1110 K.

electrons and accelerated to 3000 V. Ion currents were detected by an electron multiplier at 1.6–2.0 kV. Two systems were experimentally investigated in the gas phase: X$_2$O$_3$–PbO, where X = As or Sb. A quartz double Knudsen cell (described elsewhere[29]) with an effusion orifice 1 mm in diameter was employed in the investigation of these systems. Temperature was measured with a Pt–Pt/Rh thermocouple. X$_2$O$_3$ oxides were continuously evaporated (As$_2$O$_3$ at 423 K and Sb$_2$O$_3$ at 673 K) and flowed through solid lead oxide, which was heated to 900 K and 1110 K, respectively. The reaction products leaving the Knudsen cell were analysed by mass spectrometry. The same method with a double Knudsen cell was previously applied in the study of the Sb$_2$O$_3$–WO$_3$ system.[1] Appearance energies (AEs) of the ions of the ternary oxides were obtained by varying the electron energy to determine the onset of the ions.

3.3. Quantum chemical calculations

Quantum chemical calculations were performed using the TURBOMOLE program package.[30] All of the structures of the molecules were fully optimised using density functional theory (DFT) with the BP86 functional and the def2-TZVP triple split valence basis set with a polarisation function and small core ECP functions. RI-treatment was also applied. All computational details have been described in our previous studies.[1,2]

4.   Conclusions

The existence of three novel ternary lead–arsenic and lead–antimony oxides (PbAs$_2$O$_4$, Pb$_3$As$_2$O$_6$ and PbSb$_2$O$_4$) in the gas phase was proven by means of mass spectrometry. The gas phase of both systems primarily contained X$_4$O$_6$ and PbX$_2$O$_4$ oxides (X = As or Sb). The PbAs$_2$O$_4$ and PbSb$_2$O$_4$ oxides are isostructural, have two-coordinate atoms of Pb and three-coordinated atoms of X. Similar structures have been observed for the Sb$_2$MoO$_6$ and Sb$_2$WO$_6$ oxides.[1,2] The Pb$_3$As$_2$O$_6$ oxide has a cage-like structure with high symmetry D_{3h} and contains four-coordinate atoms of Pb (Fig. 1). The Pb$_2$X$_2$O$_5$ oxides were not detected. The oxidation state of Pb is 2+ and that of X is 3+ as in PbO and X$_4$O$_6$ oxides. The maximum number of metallic atoms found in these gaseous ternary compounds was five, similar to the results of our previous studies on antimony–molybdenum and antimony–tungsten ternary oxides.[1]

It is known that SnPO$_2$, which is isoelectronic with PbAsO$_2$, is a stable species.[11] AsO^6 also existed in the gas phase. The PbAsO$_2$$^+$ and AsO$^+$ ions have large intensities in our mass spectrum, which allowed us to suspect the presence of PbAsO$_2$ in the gas phase. However, the determination of the appearance energy of PbAsO$_2$$^+$ did not confirm our assumptions.

The PbO–As$_2$O$_3$ system has different compounds in the solid state and the gas phase. As was mentioned above, two solid compounds PbAs$_2$O$_4$ and Pb$_2$As$_2$O$_5$ were reported.[13] Our study did not confirm the presence of Pb$_2$As$_2$O$_5$ in the gas phase, but Pb$_3$As$_2$O$_6$ which is not known in the solid state was detected in the gas phase.

The enthalpies of formation of the ternary oxides in the gas phase were determined using mass spectrometry and were compared with quantum chemical calculations. The experimental and calculated standard enthalpies of formation are in very good agreement.

The partial pressures of the ternary lead–arsenic species are about 3 to 4 order of magnitude higher than the partial pressures of pure lead monoxide at the same temperature. The fraction of lead-containing species is enhanced in the presence of As$_4$O$_6$ by a factor of 5000.

References

1 E. Berezovskaya, E. Milke and M. Binnewies, *Dalton Trans.*, 2012, **41**(8), 2464.

2 E. Berezovskaya, E. Milke and M. Binnewies, *Dalton Trans.*, 2012, **41**(35), 10769.

3 A. Popovič, A. Lesar, M. Guček and L. Bencze, *Rapid Commun. Mass Spectrom.*, 1997, **11**, 459.

4 O. Knacke and A. von Richthofen, *Z. Phys. Chem.*, 1994, **187**, 257.

5 J. Drowart, R. Colin and G. Exsteen, *J. Chem. Soc., Faraday Trans.*, 1965, **61**, 1376.

6 R. D. Brittain, K. H. Lau and D. L. Hlidenbrand, *J. Phys. Chem.*, 1982, **86**, 5072.

7 G. Chiavari, D. Fabbri and G. C. Galletti, *Rapid Commun. Mass Spectrom.*, 1995, **9**, 559.

8 N. A. Asryan, A. S. Alikhanyan and G. D. Nipan, *Inorg. Mater.*, 2004, **40**, 626.

9 N. A. Asryan, A. S. Alikhanyan and G. D. Nipan, *Russ. J. Phys. Chem.*, 2003, **78**, 5.

10 G. A. Semenov, *Russ. J. Phys. Chem.*, 1985, **59**, 1520.

11 S. I. Lopatin and G. A. Semenov, *Russ. J. Gen. Chem.*, 1996, **66**, 180.

12 V. L. Stolyarova, S. I. Shornikov, G. G. Ivanov and M. M. Shultz, *Rapid Commun. Mass Spectrom.*, 1990, **4**, 510–512.

13 S. Bahfenne, L. Rintoul, J. Langhof and R. L. Frost, *J. Raman Spectrosc.*, 2011, **42**, 2119.

14 R. G. Behrens and G. M. Rosenblatt, *J. Chem. Thermodyn.*, 1972, **4**, 175.

15 R. G. Behrens and G. M. Rosenblatt, *J. Chem. Thermodyn.*, 1973, **5**, 173.

16 S. I. Lopatin, I. Ya. Mittova, F. S. Gerasimov, S. M. Shugurov, V. F. Kostryukov and S. M. Skorokhodova, *Russ. J. Inorg. Chem.*, 2006, **51**, 1749.

17 M. Binnewies, K. Rinke and H. Schäfer, *Z. Anorg. Allg. Chem.*, 1973, **395**, 50.

18 H. Liu, S. Wang, G. Zhou, J. Wu and W. Duan, *J. Chem. Phys.*, 2007, **126**, 134705.

19 J. O. Jensen, S. J. Gilliam, A. Banerjee, D. Zeroka, S. J. Kirkby and C. N. Merrow, *J. Mol. Struct. (THEOCHEM)*, 2003, **664–665**, 145.

20 S. J. Gilliam, J. O. Jensen, A. Banerjee, D. Zeroka, S. J. Kirkby and C. N. Merrow, *Spectrochim. Acta, Part A*, 2004, **60**, 425.

21 R. K. Khanna and Y. J. Park, *Spectrochim. Acta*, 1986, **42A**, 603.

22 G. C. Hampson and A. J. Stosick, *J. Am. Chem. Soc.*, 1938, **60**, 1814.

23 P. A. Akishin and V. P. Spiridonov, *J. Struct. Chem.*, 1961, **2**, 502.

24 R. J. M. Konings, E. H. P. Cordfunke and A. S. Booij, *J. Mol. Struct.*, 1992, **152**, 29.

25 R. J. M. Konings, A. S. Booij and E. H. P. Cordfunke, *Chem. Phys. Lett.*, 1993, **210**, 380.

26 A. V. Makarov and S. G. Zbezhneva, *Vysokochist. Veshchestva*, 1993, **1**, 124.

27 R. G. Egdell, M. H. Palmer and R. H. Findlay, *Inorg. Chem.*, 1980, **19**, 1314.

28 M. Binnewies and E. Milke, *Thermochemical data of Elements and Compounds*, 2nd edn, Wiley-VCH, 2002.

29 M. Binnewies, *Z. Anorg. Allg. Chem.*, 1977, **435**, 156.

30 R. Ahlrichs, M. Bär, H.-P. Baron, R. Bauernschmitt, S. Böcker, P. Deglmann, M. Ehrig, K. Eichkorn, S. Elliott, F. Furche, F. Haase, M. Häser, C. Hättig, H. Horn, C. Huber, U. Huniar, M. Kattannek, A. Köhn, C. Kölmel, M. Kollwitz, K. May, C. Ochsenfeld, H. Öhm, A. Schäfer, U. Schneider, M. Sierka, O. Treutler, B. Unterreiner, M. von Arnim, F. Weigend, P. Weis and H. Weiss, *Turbomole (vers. 5.9.1)*, Universität Karlsruhe, 2007.

Supplementary.

Table 15. Total energies of the molecular ions in the geometries of the neutral molecule.

Molecular ion	E_{tot} (a.u.)
PbO^+	-267.940878
$Pb_2O_2^+$	-536.381295
$As_4O_6^+$	-9396.109026
$Sb_4O_6^+$	-1413.122828
AsO^+	-2311.074637
$PbAs_2O_4^+$	-4966.247324
$PbAsO_2^+$	-2579.542825
$Pb_3As_2O_6(I)^+$	-5503.083897
$PbSb_2O_4^+$	-974.753730

3.4 Formation of ternary lead-molybdenum oxides $PbMoO_4$, $PbMo_2O_7$, Pb_2MoO_5 and $PbMo_3O_{10}$ in the gas phase: A mass spectrometric and quantum chemical investigation

K. Kunkel, E. Milke, M. Binnewies
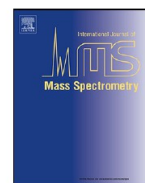
Review

Formation of ternary lead-molybdenum oxides $PbMoO_4$, $PbMo_2O_7$, Pb_2MoO_5 and $PbMo_3O_{10}$ in the gas phase: A mass spectrometric and quantum chemical investigation

K. Kunkel*, E. Milke, M. Binnewies

Institut für Anorganische Chemie, Callinstr. 9, 30167 Hannover, Germany

ABSTRACT

The formation and stability of the ternary lead-molybdenum oxides $PbMoO_4$, $PbMo_2O_7$, $PbMo_3O_{10}$ and Pb_2MoO_5 in the gas phase were studied. The $PbMoO_4$ and $PbMo_2O_7$ species were unequivocally identified in mass spectrometric experiments by the determination of m/z-values, isotopic patterns and appearance energies. Presumably, the $PbMo_3O_{10}$ and Pb_2MoO_5 species were also present in the gas phase. Thermodynamic data for the ternary oxides were obtained experimentally by means of a mass spectrometric Knudsen-cell method and were confirmed by quantum chemical calculations.
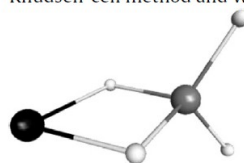
$PbMoO_4$
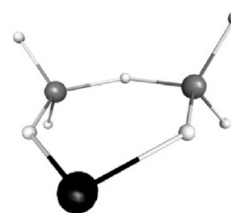
$PbMo_2O_7$
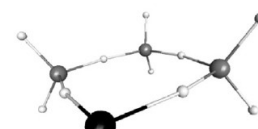
$PbMo_3O_{10}$
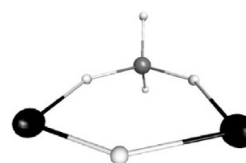
Pb_2MoO_5

* Corresponding author. Tel.: +49 5117622444; fax: +49 511 762 2254.
E-mail address: katja.kunkel@aca.uni-hannover.de (K. Kunkel).

Contents

1. Introduction

Bulk lead-molybdenum oxides $PbMoO_4$, Pb_2MoO_5 and Pb_5MoO_8 are prospective materials and widely used as acousto-optic and luminescent materials [1,2]. $PbMoO_4$ with scheelite structure shows photocatalytic activity under UV irradiation [3]. Therefore the studying of the formation lead-molybdenum oxides in the gas phase can be very important.

According to the phase diagram [4] of the $PbO–MoO_3$ system, there are three known solid compounds: $PbMoO_4$, Pb_2MoO_5 and Pb_5MoO_8. The crystal structures of solid lead-molybdenum oxides have been determined too [5–7]. All crystal structures of $PbO–MoO_3$ system have distorted tetrahedral $MoO_4{}^{2-}$ elements as well as in bulk MoO_3. The structure of lead-molybdenum compounds can be represented as a tetragonal modification of lead oxide (α-PbO), in which some of Pb atoms replaced by $MoO_4{}^{2-}$ tetrahedra. The bulk PbO in two modifications with open-packed rocksalt-like structures and bulk MoO_3 are described elsewhere [8,9].

It is known that the evaporation of lead molybdate $PbMoO_4(s)$ and lead tungstate $PbWO_4(s)$ leads to the formation of gaseous ternary oxides. Nikolaev observed three gaseous oxides, $PbMO_4$, PbM_2O_7 and Pb_2MO_5, where M = Mo, W, in a stoichiometric $PbO–MO_3$ system, with the help of mass spectrometry. Appearance energies were obtained for $PbMoO_4$ and $PbMo_2O_7$ oxides [10]. In the present work, we investigate the formation of gaseous ternary lead-molybdenum oxides in PbO-rich and MoO_3-rich systems. We present the experimental and quantum chemical calculated thermodynamic and structural characteristics of the four ternary lead-molybdenum oxides, $PbMoO_4$, $PbMo_2O_7$, $PbMo_3O_{10}$ and Pb_2MoO_5.

Several species related to lead-molybdenum gaseous ternary oxides, such as $GeMoO_4$, $GeWO_4$, GeW_2O_7, $SnMoO_4$, Sn_2MoO_5, $SnWO_4$, SnW_2O_7 and Sn_2WO_5 were also investigated thermodynamically [11–14].

2. Results and discussion

2.1. Mass spectrometric study

For the investigation of the gas phase $PbO–MoO_3$ system, several mass spectrometric experiments were conducted. The $PbO–MoO_3$ system (1:1, $PbMoO_4$) has been investigated previously [10]. In this study, we explore MoO_3-rich and PbO-rich systems. Three samples were prepared by solid state reaction and subjected to a mass spectrometric investigation. Mixtures of PbO and MoO_3 with a molar ratio of 2:3 (sample 1), 1:1 (sample 2) and 3:1 (sample 3) were heated in sealed silica ampules in vacuo at 793 K for ten days. The

obtained samples were characterised using X-ray diffraction (XRD) techniques. Comparison of the XRD patterns of the synthesised samples with literature data revealed sample 1 to be a mixture of $PbMoO_4$ and MoO_3, sample 2 to be pure $PbMoO_4$ and sample 3 to be a mixture of Pb_2MoO_5 and Pb_5MoO_8, corresponding to the phase diagram.

The vaporisation of samples 1 and 3 using a Knudsen cell was studied at 1163 and 1173 K, respectively. Sample 2 (crystal $PbMoO_4$) was investigated in a flow of MoO_3 in a double Knudsen cell (MoO_3 was evaporated at 873 K, passing the sample at 1173 K). The relative intensities of the ions in the mass spectra are presented in Table 1a. For comparison, the mass spectrum of $PbMoO_4$, which was studied by Nikolaev et al., is also presented in Table 1a. For the convenient overview of all the mass spectrometric experiments, we present the relative intensities of all the ionic species in relation to the intensity of the PbO^+ ion (Table 1b). The main ionic species are shown in Table 1b, with the intensity of PbO^+ designated as 100 in every system.

Four parent ions were detected ($PbMo_3O_{10}{}^+$, $PbMo_2O_7{}^+$, $PbMoO_4{}^+$ and $Pb_2MoO_7{}^+$) during the mass spectrometric study of the gas phase $PbO–MoO_3$ system. The appearance energies were obtained for the ions $PbMoO_4{}^+$ and $PbMo_2O_7{}^+$. Extrapolation of the linear portion of the ionisation efficiency curves to an intensity of zero gave the following value for the appearance energy (AE): $AE(PbMoO_4{}^+) = 9.6 \pm 0.5$ eV and $AE(PbMo_2O_7{}^+) = 10.3 \pm 0.5$ eV. Unfortunately, the intensities of the $PbMo_3O_{10}{}^+$ and $Pb_2MoO_5{}^+$ ions were too small to determine the appearance energy. We concluded that $PbMo_3O_{10}{}^+$ and $Pb_2MoO_5{}^+$ were the parent ions because there were no heavier ions in the mass spectra from which they could have been split. The obtained experimental enthalpies of formation based on this conclusion will be compared with quantum chemical calculated enthalpies of formation.

The dependence of the recorded ion currents on the partial pressure of the particular ion is described by the following equation:

$$p_i = c \cdot \frac{\sum I_i \cdot T}{\sigma_i \cdot S} \tag{4}$$

where p_i = the partial pressure of component i, c = the proportionality factor, $\sum I_i$ = the intensity of all of the ions formed by the ionisation and fragmentation of a gaseous molecule of i, T = temperature, σ_i = the ionisation cross section and S_i = the electron multiplier efficiency. The approximated Eq. (5) can be used in most cases (the procedure of simplification is described elsewhere [15]):

$$p_i = c \cdot \sum I_i \cdot T \tag{5}$$

The proportionality factor c was determined by a calibration experiment and found to be 1.4×10^{-13}. The deviation of factor c is

Table 1a
Relative intensities of the ionic species in the $PbO–MoO_3$ system (70 eV).

Ion	Relative intensity			
	$PbMoO_4$ (1173 K) + MoO_3 (873 K) (sample 2)	$PbMoO_4$ + MoO_3 (1163 K) (sample 1)	$PbMoO_4$ (1353 K) [10]	Pb_2MoO_5 + PbO (1173 K) (sample 3)
$PbMo_3O_{10}^+$	3.0	–	–	–
$Pb_2MoO_5^+$	–	–	2.0	9.8
$Pb_2MoO_4^+$	–	–	–	1.0
$Mo_4O_{12}^+$	9.2	8.5	–	–
$Mo_4O_{11}^+$	1.7	1.0	–	–
$PbMo_2O_7^+$	46.5	62.2	25	–
$Pb_2O_2^+$	–	–	0.9	5.1
Pb_2O^+	–	–	–	1.0
$Mo_3O_9^+$	100	18.5	1.2	–
$Mo_3O_8^+$	17.6	3.3	–	–
$PbMoO_4^+$	18.1	51.5	39	14.0
$Mo_2O_6^+$	19.1	9.1	–	–
$Mo_2O_5^+$	7.5	2.9	–	–
$Mo_2O_4^+$	4.9	1.6	–	–
PbO^+	14.1	22.2	36	100
Pb^+	15.6	100	100	39.7
MoO_3^+	4.3	–	–	–
MoO_2^+	10.8	4.3	–	–
MoO^+	5.9	1.1	–	–
Mo^+	1.4	–	–	–

Table 1b
Relative intensities of the main ionic species in the $PbO–MoO_3$ systems (overview).

Ion	Relative intensity			
	$PbMoO_4$ (1173 K) + MoO_3 (873 K)	$PbMoO_4$ + MoO_3 (1163 K)	$PbMoO_4$ (1353 K) [10]	Pb_2MoO_5 + Pb_5MoO_8 (1173 K)
$PbMo_3O_{10}^+$	21.3	–	–	–
$Pb_2MoO_5^+$	–	–	5.6	9.8
$PbMo_2O_7^+$	329.8	280.2	69.4	–
$Mo_3O_9^+$	709.2	83.3	3.3	–
$PbMoO_4^+$	128.4	232.0	108.3	14.0
PbO^+	100	100	100	100

in the range $[1.4 \times 10^{-13} \times 5; 1.4 \times 10^{-13}/5]$. The mass spectrometric measurement of pure PbO oxide was used for the calibration. Eqs. (6) and (7), describing the partial pressure of PbO as a function of temperature, and Eq. (5) were applied for the calibration [16,17]:

$$\text{for PbO} \quad lg(p/\text{bar}) = -32\,032/T + 1915 \quad (850\ldots1100\,\text{K}) \quad (6)$$

or

$$lg(p/\text{Pa}) = -13\,345/T + 11.9 \quad (900\ldots1150\,\text{K}) \quad (7)$$

Using the c value and the relative intensities $\sum I_i$ and applying Eq. (5), the partial pressures of the gaseous molecules in the

Table 2
Molecules and their ions in the gas phase over the mixture of $PbMoO_4$ and MoO_3, 1163 K, sample 1.

Molecule	Attributed ions	Partial pressure, p (bar)
$PbMoO_4$	$PbMoO_4^+$	1.7×10^{-7}
$PbMo_2O_7$	$PbMo_2O_7^+$	2.0×10^{-7}
Mo_3O_9	$Mo_3O_9^+$, $Mo_3O_8^+$, $Mo_3O_7^+$	7.0×10^{-8}
PbO	PbO^+	7.1×10^{-8}

Table 3
Molecules and their ions in the gas phase over $PbMoO_4$ (1173 K) under MoO_3 flow (873 K), sample 2.

Molecule	Attributed ions	Partial pressure, p (bar)
$PbMoO_4$	$PbMoO_4^+$	1.7×10^{-7}
$PbMo_2O_7$	$PbMo_2O_7^+$	4.5×10^{-7}
$PbMo_3O_{10}$	$PbMo_3O_{10}^+$	2.2×10^{-8}
PbO	PbO^+	1.3×10^{-7}
Mo_3O_9	$Mo_3O_9^+$, $Mo_3O_8^+$, $Mo_3O_7^+$	4.0×10^{-7}

equilibrium system $PbO–MoO_3$ can be calculated (Tables 2–4). For the calculation of the partial pressure of Mo_3O_9 over $PbMoO_4$, it was assumed that molybdenum oxide was constantly evaporating at temperature 873 K and passed through lead molybdate, $PbMoO_4$, at temperature 1173 K (Table 3).

Equilibrium conditions inside Knudsen cells have been investigated in many gaseous systems using mass spectrometry, particularly in molybdenum oxide and lead oxide systems [16,18–20]. Therefore, we assumed that the systems under consideration were in equilibrium conditions inside the Knudsen cell. Additionally, in our experiment the ratio of the sublimation area to the effusion orifice was greater than 500.

Using the partial pressures from Tables 2–4, we determined the equilibrium constants of formation of the lead-molybdenum ternary oxides, which will be given later in this paper.

2.2. Density functional theory computations

The method RI-BP86/def2-TZVP, which was used for calculations, allows good correlation between the calculated values and the experimental data for many oxides. We successfully used this

Table 4
Molecules and their ions in the gas phase over the mixture of Pb_2MoO_5 and Pb_5MoO_8, 1173 K, sample 3.

Molecule	Attributed ions	Partial pressure, p (bar)
$PbMoO_4$	$PbMoO_4^+$	1.3×10^{-7}
Pb_2MoO_5	$Pb_2MoO_5^+$, $Pb_2MoO_4^+$	9.7×10^{-8}
PbO	PbO^+	8.9×10^{-8}

Table 5
Symmetries, total energies and thermal energies of the molecules (RI-BP86/def2-TZVP).

Molecule	Point group	E_{tot}(DFT) (a.u.)	E_{298}^{therm}(DFT) (kJ mol^{-1})
PbO	$C_{\infty v}$	−267.940878	10.80
Pb$_2$O$_2$	C_{2v}	−536.690429	26.42
Pb$_3$O$_3$	D_{3h}	−805.068223	43.48
Pb$_4$O$_4$	T_d	−1073.497158	60.50
MoO$_3$	C_{3v}	−294.201556	33.81
Mo$_3$O$_9$	C_{3v}	−882.913202	118.52
Mo$_4$O$_{12}$	D_{4h}	−1177.237313	160.27
PbMoO$_4$	C_{2v}	−562.654314	51.28
PbMo$_2$O$_7$	C_2	−856.990451	93.16
PbMo$_3$O$_{10}$	C_{2v}	−1151.311179	135.38
Pb$_2$MoO$_5$	C_s	−831.045453	68.50

Table 6
Observed and calculated vibrational frequencies for gaseous As$_4$O$_6$, Sb$_4$O$_6$, Pb$_4$O$_4$, Pb$_2$O$_2$ and PbO (scaling factor = 1).

	Vibrational frequencies (cm^{-1})		
MoO$_3$			
Exp [25]	920		
Calc	945.2		
Mo$_3$O$_9$			
Exp [25]	838.0	974.7	–
Calc	839.8	992.4	1000.4
Mo$_4$O$_{12}$			
Exp [25]	870.0	–	
Calc	887.3	993.6	
Pb$_4$O$_4$			
Exp [26]	–	372	464
Calc	113.3	353.3	451.8
Pb$_2$O$_2$			
Exp [26]	–	463	558
Calc	86.6	455.2	542.7
PbO			
Exp [26]	714		
Calc	724.0		

Table 8
Calculated thermodynamic characteristics of the lead-molybdenum oxides (RI-BP86/def2-TZVP).

Molecule	S_{298}^0 (J mol^{-1} K^{-1})	$c_{p,T}^0 = a + b \times 10^{-3} \cdot T + c \times 10^6 \cdot T^{-2}$		
		a	b	c
PbMoO$_4$	363.2	123.25	7.59	−2.44
PbMo$_2$O$_7$	500.1	213.09	15.21	−4.23
PbMo$_3$O$_{10}$	635.0	301.90	23.64	−5.94
Pb$_2$MoO$_5$	472.8	171.83	8.57	−2.90

are lower than atomic charges of Mo atoms. Therefore it can be concluded that Mo—O bond is more ionic than Pb—O bond.

The experimental and calculated vibrational spectra of the gaseous molybdenum and lead oxides MoO$_3$, Mo$_3$O$_9$, Mo$_4$O$_{12}$, PbO, Pb$_2$O$_2$ and Pb$_4$O$_4$ were compared to determine the scaling factor and are presented in Table 6. The experimental frequencies and our calculated frequencies for these gaseous molecules are in good agreement. The calculated frequencies of MoO$_3$, Mo$_3$O$_9$, Mo$_4$O$_{12}$ and PbO exceed the experimental values, and the experimental frequencies of Pb$_2$O$_2$ and Pb$_4$O$_4$ exceed the calculated values insignificantly (1–3%). Therefore, the vibrational wave numbers were not calibrated (scaling factor = 1). The calculated and experimental entropies of the molybdenum and lead oxides were in good agreement (Table 7). Therefore, we did not scale thermodynamic values for the further quantum chemical investigation of the ternary oxides. But inaccuracy of the obtained entropies will be estimated in Section 2.4. The entropies and the a, b and c coefficients of the heat capacity function $c_{p,T}^0$ are given in Table 7.

The thermodynamic values of all of the compounds were obtained using the FREEH module within a temperature range from the standard temperature to the temperature of the mass spectrometric experiments at 298–1200 K. The entropy, S_T^0, can be approximated as a function of temperature:

$$S_T^0 = S_{298}^0 + \int_{298}^T c_{p,T}^0 \frac{dT}{T}$$

where

$$c_{p,T}^0 = a + b \times 10^{-3} \cdot T + c \times 10^6 \cdot T^{-2} \qquad (8)$$

The a, b and c coefficients of the heat capacity function $c_{p,T}^0$ were calculated mathematically by fitting ten values of S_T^0 in the temperature range from 298 to 1200 K. The experimental and calculated values of coefficient b for the $c_{p,T}^0$ function differed from each other but yielded correct entropy values. Therefore, the calculated coefficients a, b and c for the ternary oxides are acceptable and can be used in the calculations. The calculated entropy values and the values of the coefficients a, b and c for the ternary oxides are presented in Table 8.

The total energies of the cations Mo$_3$O$_9^+$, PbO$^+$, PbMoO$_4^+$, PbMo$_2$O$_7^+$, PbMo$_3$O$_{10}^+$ and Pb$_2$MoO$_5^+$ were computed in a doublet spin state in the geometry of a neutral molecule to determine the vertical ionisation energies (IE) of the corresponding molecules (Table 1, Supplementary). The first IE was determined as the difference between the total energy of the cation in a doublet state and the energy of the neutral molecule. Known experimental IE and AE values for lead and molybdenum oxides and the AE values for

method previously to study oxide systems containing molybdenum, lead and other oxides [21–23]. The total energies, thermal energies and point groups of molybdenum, lead and ternary lead-molybdenum oxides are presented in Table 5.

We have conducted the population analysis based on occupation numbers (PABOONs) [24] at the DFT level. Shared electron numbers (SEN) for pairs of atoms which characterise electron population between atoms and related to the bond energies were obtained. The SEN also named as bond order and can be compared to analyse bond strengths. Fig. 1 presents SEN values for MoO$_3$, Mo$_3$O$_9$, Mo$_4$O$_{12}$, PbO, Pb$_2$O$_2$, Pb$_3$O$_3$, Pb$_4$O$_4$, PbMoO$_4$, PbMo$_2$O$_7$, PbMo$_3$O$_{10}$ and Pb$_2$MoO$_5$. The formation of bonds during a reaction can be crucial for the understanding of the oxide formation. Thus we see that bonds Mo—O in Mo$_4$O$_{12}$ are weaker than in Mo$_3$O$_9$. Obviously that Pb$_4$O$_4$ is the most stable lead oxide, according to SEN values of Pb—O bonds in PbO, Pb$_2$O$_2$, Pb$_3$O$_3$ and Pb$_4$O$_4$. The PbMo$_3$O$_{10}$ has the weakest Mo—O bonds in comparison with other lead-molybdenum oxides. It means that the highest ternary oxide PbMo$_3$O$_{10}$, which was detected in the gas phase, is not so stable as PbMoO$_4$, PbMo$_2$O$_7$, and Pb$_2$MoO$_5$. The most probably higher oxides with five and more metallic atoms are even more unstable. Fig. 2 presents charge distribution in the molecules. As we see atomic charges of Pb atoms

Table 7
Experimental [27] and calculated thermodynamic characteristics of the lead and molybdenum oxides (RI-BP86/def2-TZVP, scaling factor = 1).

Molecule	S_{298}^0 (J mol^{-1} K^{-1}) (exp.//DFT)	S_{1000}^0 (J mol^{-1} K^{-1}) (exp.//DFT)	$c_{p,T}^0 = a + b \times 10^{-3} \cdot T + c \times 10^6 \cdot T^{-2}$ (exp.//DFT)		
			a	b	c
PbO(g)	240.0//240.2	282.7//282.6	36.18//35.70	1.05//1.46	−0.36//−0.36
Mo$_3$O$_9$(g)	526.7//525.5	837.3//820.0	274.48//253.44	4.23//22.60	−4.81//−5.51

Fig. 1. Shared electron numbers, analysis based on occupation numbers (RI-BP86/def2-TZVP).

Table 9
Experimental AE and calculated vertical first ionisation energies (IE) (RI-BP86/def2-TZVP).

Molecule	IE (eV) DFT	AE (eV) Exp.
PbO	9.65	9.4 ± 0.3 (EI) [28]
		9.0 ± 0.5 (EI) [20]
Mo$_3$O$_9$	10.80	12.0 ± 1 [29]
PbMoO$_4$	9.91	9.6 ± 0.5[a]
		10.8 ± 0.5 [10]
PbMo$_2$O$_7$	9.82	10.3 ± 0.5[a]
		11.4 ± 0.5 [10]
PbMo$_3$O$_{10}$	10.24	–
Pb$_2$MoO$_5$	9.08	–

[a] This work.

PbMoO$_4^+$ and PbMo$_2$O$_7^+$ from the present study were compared with the computed theoretical IE values (Table 9). The experimental AE values are in good agreement with the theoretical IE values for all the molecules. This agreement confirms that the PbMoO$_4^+$ and PbMo$_2$O$_7^+$ ions were formed by the ionisation of ternary oxides rather than by fragmentation processes.

Table 10 presents the reactions for the formation of the ternary lead-molybdenum oxides as well as the calculated enthalpies, entropies and equilibrium constants at standard and experimental temperatures for these reactions.

The quantum chemical (QC) calculated standard enthalpies of formation, $\Delta_f H^0_{298}$, of the ternary oxides were obtained using the reaction enthalpies, $\Delta_r H^0_{298}$, of processes 1–4 from Table 12 and the experimental values of $\Delta_f H^0_{298}(\text{PbO}) = 70.3$ kJ mol^{-1} [27] and $\Delta_f H^0_{298}(\text{Mo}_3\text{O}_9) = -1878.3$ kJ mol^{-1} [27] and are as follows:

$$\Delta_f H^0_{298}(\text{PbMoO}_4, \text{QC}) = -698.2 \text{ kJ mol}^{-1},$$
$$\Delta_f H^0_{298}(\text{PbMo}_2\text{O}_7, \text{QC}) = -1406.0 \text{ kJ mol}^{-1},$$
$$\Delta_f H^0_{298}(\text{PbMo}_3\text{O}_{10}, \text{QC}) = -2072.9 \text{ kJ mol}^{-1}, \text{ and}$$
$$\Delta_f H^0_{298}(\text{Pb}_2\text{MoO}_5, \text{QC}) = -874.9 \text{ kJ mol}^{-1}.$$

Processes 1–2 and 5–6 will be considered for obtaining the enthalpies of reaction in the following experimental section.

2.3. Experimental determination of the standard enthalpies of formation, $\Delta_f H^0_{298}$

The equilibrium constant $K_{p,T}$ is related to reaction enthalpy, reaction entropy and temperature by the van't Hoff equation. For the experimental determination of the standard enthalpy of
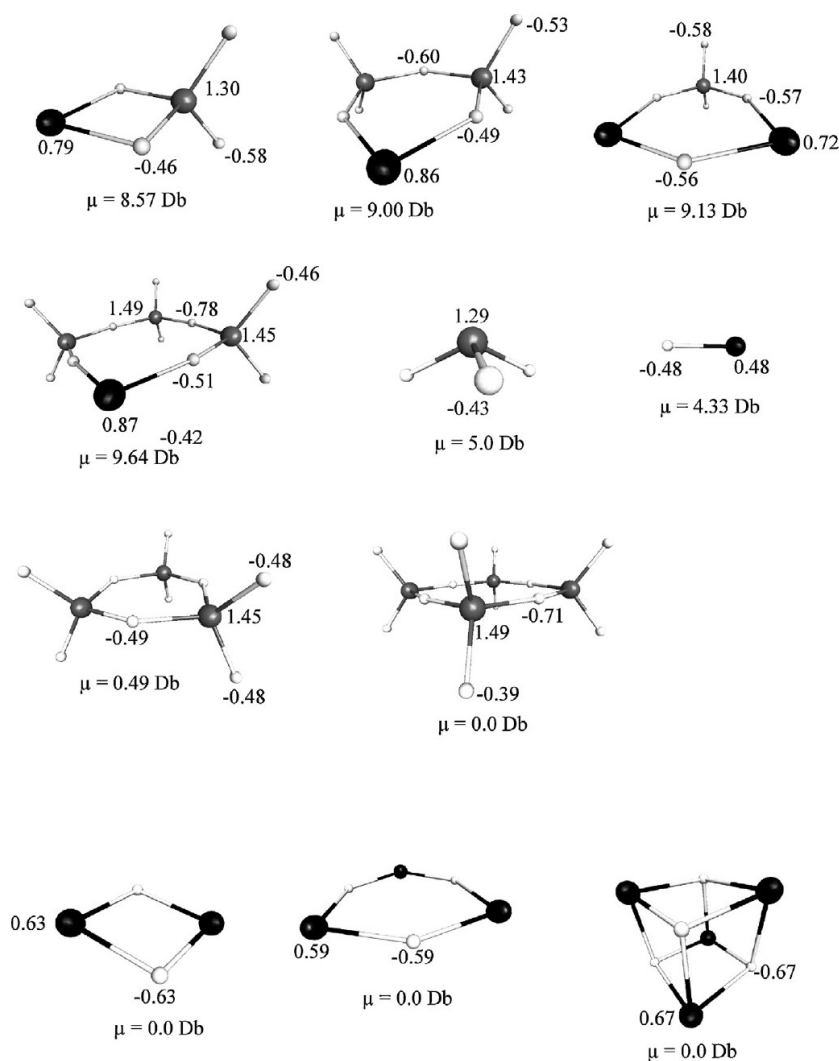
Fig. 2. Atomic charges and dipole moments of the molecules (RI-BP86/def2-TZVP).

Table 10
Calculated standard enthalpies, entropies of reaction and equilibrium constants for the equilibrium processes involving the lead-molybdenum oxides (RI-BP86/def2-TZVP).

	Reaction	$\Delta_r H_T^0$ (kJ mol^{-1})298//T	ΔS_T^0 (J mol^{-1} K^{-1})298//T	ln $K_{p,T}$ 298//T
1	PbO(g) + 1/3Mo$_3$O$_9$(g) ⇌ PbMoO$_4$(g)	−142.4//−141.2[a]	−52.2//−50.5[a]	51.2//8.5[a]
2	PbO(g) + 2/3Mo$_3$O$_9$(g) ⇌ PbMo$_2$O$_7$(g)	−224.1//−218.0[a]	−90.5//−81.1[a]	79.6//12.8[a]
3	PbO(g) + Mo$_3$O$_9$(g) ⇌ PbMo$_3$O$_{10}$(g)	−264.9//−254.3[a]	−130.7//−113.9[a]	91.2//12.6[a]
4	2PbO(g) + 1/3Mo$_3$O$_9$(g) ⇌ Pb$_2$MoO$_5$(g)	−389.4//−377.4[b]	−182.9//−164.4[b]	135.2//18.9[b]
5	PbMoO$_4$(g) + PbMo$_2$O$_7$(g) ⇌ PbMo$_3$O$_{10}$(g) + PbO(g)	101.6//105.0[b]	12.0//17.7[b]	−39.5//−8.6[b]
6	PbO(g) + MoPbO$_4$(g) ⇌ Pb$_2$MoO$_5$(g)	−247.0//−236.2[b]	−130.6//−113.9[b]	84.0//10.5[b]

[a] T = 1163 K.
[b] T = 1173 K.

Table 11
Experimental equilibrium constants and enthalpies of reaction.

	Reaction	ln $K_{p,T}$	$\Delta_r H_T^0$ (kJ mol^{-1})
1	PbO(g) + 1/3Mo$_3$O$_9$(g) ⇌ PbMoO$_4$(g)	6.6 ± 0.8[a]	−122.3 ± 7.5[a]
2	PbO(g) + 2/3Mo$_3$O$_9$(g) ⇌ PbMo$_2$O$_7$(g)	12.5 ± 1.3[a]	−215.1 ± 12.7[a]
5	PbMoO$_4$(g) + PbMo$_2$O$_7$(g) ⇌ PbMo$_3$O$_{10}$(g) + PbO(g)	−3.3 ± 0.4[b]	52.7 ± 3.7[b]
6	PbO(g) + MoPbO$_4$(g) ⇌ Pb$_2$MoO$_5$(g)	14.4 ± 1.9[b]	−273.8 ± 18.3[b]

[a] T = 1163 K.
[b] T = 1173 K.

Table 12
Experimental enthalpies of formation for the lead-molybdenum oxides.

Compound	$\Delta_f H_T^0$ (kJ mol^{-1}) Exp	$\Delta_f H_{298}^0$ (kJ mol^{-1}) Exp	$\Delta_f H_{298}^0$ (DFT) (kJ mol^{-1})	$\Delta_f H_{298}^0$ (exp) $-\Delta_f H_{298}^0$ (DFT) (kJ·mol^{-1})
PbMoO$_4$	-571.0 ± 7.5[a]	-676.3 ± 7.5	-698.2	21.9
PbMo$_2$O$_7$	-1213.9 ± 12.7[a]	-1397.2 ± 12.7	-1406.0	8.8
PbMo$_3$O$_{10}$	-1811.8 ± 3.7[b]	-2076.3 ± 3.7	-2072.9	-3.4
Pb$_2$MoO$_5$	-739.4 ± 18.3[b]	-888.0 ± 18.3	-874.9	-13.1

[a] $T = 1163$ K.
[b] $T = 1173$ K.

formation of the four ternary oxides 1, 2, 5 and 6, equilibrium processes were considered. The equilibrium constants $K_{p,T}$ of these processes were calculated using the partial pressures of the oxides from Tables 2–4. The experimental reaction enthalpies $\Delta_r H_T^0$ for processes 1, 2, 5 and 6 were calculated with Eq. (9) and are presented in Table 11. The values of the reaction entropies, $\Delta_R S_T^0$, were calculated quantum chemically (Table 10).

$$\Delta_r H_T^0(\text{exp.}) = -R \cdot T \cdot \ln K_{p,T} + T \cdot \Delta_R S_T^0(\text{QC}) \tag{9}$$

$$\Delta_f H_{T'}^0 = \Delta_f H_T^0 + \int c_{p,T}^0 dT \tag{10}$$

First, $\Delta_f H_{1163}^0$(PbMoO$_4$, exp) and $\Delta_f H_{1163}^0$(PbMo$_2$O$_7$, exp) were obtained using the determined enthalpies of reaction $\Delta_f H_{1163}^0$ for processes 1 and 2 (Table 11), the enthalpies of formation $\Delta_f H_{1163}^0$(PbO(g)) and $\Delta_f H_{1163}^0$(Mo$_3$O$_9$(g)) obtained from Eq. (10), and the experimental $c_{p,T}^0$ function [27] ($\Delta_f H_{1163}^0$(PbO(g)) = -101.4 kJ mol^{-1}, and $\Delta_f H_{1163}^0$(Mo$_3$O$_9$(g)) = -1650.2 kJ mol^{-1}). The $\Delta_f H_{1173}^0$(PbMo$_3$O$_{10}$, exp) and $\Delta_f H_{1173}^0$(Pb$_2$MoO$_5$, exp) were obtained using the determined enthalpies of reaction $\Delta_f H_{1173}^0$ for processes 5 and 6 (Table 11) and the enthalpies of formation $\Delta_f H_{1173}^0$(PbO(g)), $\Delta_f H_{1173}^0$(PbMoO$_4$, exp) and $\Delta_f H_{1173}^0$(PbMo$_2$O$_7$, exp) obtained from Eq. (10) ($\Delta_f H_{1173}^0$(PbO (g)) = 101.7 kJ mol^{-1}, $\Delta_f H_{1173}^0$(PbMoO$_4$, exp) = -569.7 kJ mol^{-1} and $\Delta_f H_{1173}^0$(PbMo$_2$O$_7$, exp) = -1211.6 kJ mol^{-1}).

Then, the calculated enthalpies of formation, $\Delta_f H_T^0$, of the ternary oxides were converted into the standard enthalpies of formation, $\Delta_f H_{298}^0$, using Eq. (10) and the calculated a, b and c coefficients for the $c_{p,T}^0$ function (Table 8). Deviations from the experimental values are discussed in the next section. The experimental enthalpies $\Delta_f H_T^0$ and $\Delta_f H_{298}^0$ are presented in Table 12, and the quantum chemical values of $\Delta_f H_{298}^0$ for the ternary oxides are given for comparison.

2.4. Error estimation by the determination of the experimental standard enthalpies of formation

In the present section, we estimate the error in the determination of the standard enthalpy of formation. As was mentioned above the value of factor c is in the range [$1.4 \times 10^{-13} \times 5$; $1.4 \times 10^{-13}/5$]. The errors in the proportional factors led to errors in the equilibrium constant $K_{p,T}$ and gave a deviation of $\ln K_{p,T} \pm 0.6$, ± 1.1, 0.0 and ± 1.6 for reactions 1, 2, 5 and 6, respectively. The error of the sum of ions $\sum I_i$ (Eq. (5)) was estimated as 10% in the present experiments. This contributes to errors in $\ln K_{p,T}$ of ± 0.2, ± 0.2, ± 0.4 and ± 0.3 for reactions 1, 2, 5 and 6, respectively. The total deviation of $\ln K_{p,T}$ is given in Table 11.

The error of determination for the enthalpy of reaction, $\Delta_f H_T^0$, includes both error in the equilibrium constant and inaccuracies of calculated entropies of reaction according to Eq. (9). The entropies of reaction, $\Delta_r S_T^0$, are quantum chemical values. Since we did not scale thermodynamic values in quantum chemical calculations,

we estimate the deviation of enthalpy of reactions $\Delta_r S_T^0$ by using scaling factors 1 ± 0.03 in that section. The differences of $\Delta_r S_T^0$ as are not big and equals to ± 1.0, ± 3.0, ± 1.0 and ± 5.0 J mol^{-1} K^{-1} for reactions 1, 2, 5 and 6, respectively.

Then, the total error of the enthalpy of reaction is equal to ± 7.5, ± 12.7, ± 3.7 and ± 18.3 kJ mol^{-1} for reactions 1, 2, 5 and 6, respectively (Table 11). The errors in the standard enthalpy of formation, $\Delta_f H_{298}^0$, and their corresponding deviations are given in Table 12. The agreement between the calculated and experimental enthalpies of formation is quite good. The biggest difference in $\Delta_f H_{298}^0$(exp) $-\Delta_f H_{298}^0$(QC) was observed for PbMoO$_5$ and is equal to 21.9 kJ mol^{-1}.

3. Experimental

3.1. Samples

Yellow lead monoxide (grade puris. p.a) and molybdenum trioxide (extra pure grade) were used in the present study.

3.2. Mass spectrometry

Mass spectrometric measurements were carried out using a modified Finnigan type mass spectrometer. The vapours effusing from the Knudsen cell were ionised with 70 eV electrons and accelerated to 3000 V. The ion currents were detected by an electron multiplier at 1.6–2.0 kV. Three systems were experimentally investigated in the gas phase. A quartz glass double Knudsen cell (described elsewhere [30]) with an effusion orifice 1 mm in diameter was employed in the investigation of these systems. The temperature was measured with a Pt/Rh-Pt thermocouple. In the first experiment, the mixture of PbMoO$_4$ and MoO$_3$ was evaporated at 1163 K. In the second experiment, MoO$_3$ was continuously evaporated at 873 K and flowed through crystalline PbMoO$_4$, which was heated to 1173 K. In the third experiment, the mixture of Pb$_2$MoO$_5$ and Pb$_5$MoO$_8$ was evaporated at a temperature of 1173 K. The reaction products leaving the Knudsen cell were analysed by mass spectrometry. The appearance energies (AEs) of the ions of the ternary oxides were obtained by varying the electron energy to determine the onset of the ions.

3.3. Quantum chemical calculations

Quantum chemical calculations were performed using the TURBOMOLE program package [31]. All of the structures of the molecules were fully optimised using density functional theory (DFT) with the BP86 functional and the def2-TZVP triple split valence basis set with a polarisation function and small core ECP functions. RI-treatment was also applied. All computational details have been described in our previous work [21–23]. Atomic coordinates of all computed molecules presented in Table 2, Supplementary.

4. Conclusions

The formation of novel ternary oxide $PbMo_3O_{10}$ in the gas phase was observed by means of mass-spectrometry (the gaseous $PbMoO_4$, $PbMo_2O_7$ and Pb_2MoO_5 were known before [10]). Additionally, we carried out a thermodynamic study for four ternary oxides $PbMoO_4$, $PbMo_2O_7$, Pb_2MoO_5 and $PbMo_3O_{10}$.

We demonstrated the presence of $PbMoO_4$ and $PbMo_2O_7$ in the gas phase by appearance energy measurements. The presence of gaseous Pb_2MoO_5 and $PbMo_3O_{10}$ was assumed. The experimental and quantum chemically calculated enthalpies of formation for all the ternary oxides were in very good agreement. Therefore, it is likely that Pb_2MoO_5 and $PbMo_3O_{10}$ were present in the gas phase as well.

The PbO–MoO_3 system, as well as other oxide systems which we have studied previously, contains different compounds in the solid state and the gas phase [21–23]. There are three solid compounds $PbMoO_4$, Pb_2MoO_5 and Pb_5MoO_8 and four gaseous compounds $PbMoO_4$, $PbMo_2O_7$, Pb_2MoO_5 and $PbMo_3O_{10}$ in the PbO–MoO_3 system.

The lead-molybdenum oxides $PbMoO_4$, $PbMo_2O_7$, $PbMo_3O_{10}$ and Pb_2MoO_5 have ring structures of alternating metal and oxygen atoms, similar to the structures of the molybdenum-tellurium oxides $MoTeO_5$, Mo_2TeO_8, Mo_3TeO_{11} and Te_2MoO_7 [21]. All gaseous molybdenum lead compounds have tetrahedral MoO_4 structural elements as well as in condense state. Because of lone pair on Pb^{2+}, lead atoms can be twofold or threefold coordinated in the gaseous compounds. All gaseous compounds of PbO–MoO_3 system, Pb_3O_3 and Pb_2O_2 have twofold coordination. Threefold coordination of Pb was observed in gaseous Pb_4O_4 and $Pb_3As_2O_6$ [23].

The Mo—O bonds in the ring structures with four metallic atoms ($PbMo_3O_{10}$ and Mo_4O_{12}) are weaker than in structures with two or three metallic atoms ($PbMoO_4$, $PbMo_2O_7$, Pb_2MoO_5 and Mo_3O_9). The ring structures with five and more metallic atoms were not observed in PbO–MoO_3 system. According to population analysis we concluded that Mo—O bonds are more ionic than Pb—O bonds.

In all the systems that were considered, the total partial pressure of the ternary lead-molybdenum species was higher than the partial pressures of PbO and Mo_3O_9. The vapour over the system with a molar ratio of $PbO:MoO_3 = 2:3$ contained the ternary species $PbMoO_4$ and $PbMo_2O_7$, with a total partial pressure ∼5 times higher than the partial pressures of pure lead monoxide and molybdenum oxide (Table 2). By increasing the partial pressure of Mo_3O_9, the partial pressures of $PbMoO_4$, $PbMo_2O_7$ and PbO also increased, and $PbMo_3O_{10}$ appeared (Table 3). In the PbO-rich system (molar ratio of $PbO:MoO_3 = 3:1$), the total partial pressures of the ternary species were ∼2.5 times higher than the partial pressure of PbO.

Appendix A. Supplementary data

Supplementary data associated with this article can be found, in the online version, at http://dx.doi.org/10.1016/j.ijms.2014.09.019.

References

[1] S. Nedilko, V. Chornii, Yu. Hizhnyi, M. Trubitsyn, I. Volnyanskaya, Opt. Mater. (2014), http://dx.doi.org/10.1016/j.optmat.2014.03.019 (in press).
[2] S. Miyazawa, H. Iwasaki, J. Cryst. Growth 8 (4) (1971) 359.
[3] D.B. Hernández-Uresti, A. Martínez-de la Cruz, J.A. Aguilar-Garib, Catal. Today 212 (2013) 70.
[4] M.A. Eissa, M.A.A. Elmasry, S.S. Younis, Thermochim. Acta 288 (1996) 169.
[5] M.R.D. Bomio, L.S. Cavalcante, M.A.P. Almeida, R.L. Tranquilin, N.C. Batista, P.S. Pizani, M. Siu Li, J. Andres, E. Longo, Polyhedron 50 (1) (2013) 532.
[6] L. Li-ji, Z. Qi-nian, Z. Peng-xiang, L. Yu-lung, T. An, J. Raman Spectrosc. 15 (6) (1984) 377.
[7] P. Vassilev, D. Nihtianova, Acta Crystallogr. C 54 (1998) 1062.
[8] M. Dieterle, G. Weinberg, G. Mestl, Phys. Chem. Chem. Phys. 4 (2002) 812.
[9] Y. Wang, X. Lin, H. Zhang, T. Wen, F. Huang, G. Li, Y. Wang, F. Liaoa, J. Lin, Cryst. Eng. Comm. 15 (2013) 3513.
[10] E.N. Nikolaev, K.V. Ovchinnikov, G.A. Semenov, Russ. J. Gen. Chem. 54 (1984) 977.
[11] S.I. Lopatin, G.A. Semenov, T.S. Pilyugina, Russ. J. Gen. Chem. 70 (2000) 529.
[12] V. Plies, Z. Anorg. Allg. Chem. 484 (1982) 165.
[13] S.I. Lopatin, S.M. Shugurov, Russ. J. Gen. Chem. 78 (2008) 705.
[14] M.N. Bulova, A.S. Alikhanyan, A.M. Gas'kov, Inorg. Mater. (Rus.) 38 (2002) 831.
[15] M. Binnewies, K. Rinke, H. Schäfer, Z. Anorg. Allg. Chem. 395 (1973) 50.
[16] A. Popovič, A. Lesar, M. Guček, L. Bencze, Rapid Commun. Mass Spectrom. 11 (1997) 459.
[17] S.I. Lopatin, I.Ya. Mittova, F.S. Gerasimov, S.M. Shugurov, V.F. Kostryukov, S.M. Skorokhodova, Russ. J. Inorg. Chem. 51 (2006) 1646.
[18] G. DeMaria, R.P. Burns, J. Drowart, M.G. Inghram, J. Chem. Phys. 32 (1960) 1373.
[19] J. Berkowitz, M.G. Inghram, W.A. Chupka, J. Chem. Phys. 26 (1957) 842.
[20] J. Drowart, R. Colin, G.J. Exsteen, Chem. Soc. Faraday Trans. 61 (1965) 1376.
[21] E. Berezovskaya, E. Milke, M. Binnewies, Dalton Trans. 41 (8) (2012) 2464.
[22] E. Berezovskaya, E. Milke, M. Binnewies, Dalton Trans. 41 (35) (2012) 10769.
[23] K. Kunkel, E. Milke, M. Binnewies, Dalton Trans. 43 (2014) 5401.
[24] C. Ehrhardt, R. Ahlrichs, Theor. Chim. Acta 68 (3) (1985) 231.
[25] D.L. Neikirk, J.C. Fagerli, M.L. Smith, D. Mosman, T.C. Devore, J. Mol. Struct. 244 (1991) 165.
[26] R.K. Khanna, Y.J. Park, Spectrochim. Acta 42A (1986) 603.
[27] M. Binnewies, E. Milke, Thermochemical Data of Elements and Compounds, 2nd ed., Wiley-VCH, 2002.
[28] A.V. Makarov, S.G. Zbezhneva, Vysokochist. Veshchestva 1 (1993) 124.
[29] R.P. Burns, G. DeMaria, J. Drowart, R.T. Grimley, J. Chem. Phys. 32 (1960) 1363.
[30] M. Binnewies, Z. Anorg. Allg. Chem. 435 (1977) 156.
[31] R. Ahlrichs, M. Bär, H.-P. Baron, R. Bauernschmitt, S. Böcker, P. Deglmann, M. Ehrig, K. Eichkorn, S. Elliott, F. Furche, F. Haase, M. Häser, C. Hättig, H. Horn, C. Huber, U. Huniar, M. Kattannek, A. Köhn, C. Kölmel, M. Kollwitz, K. May, C. Ochsenfeld, H. Öhm, A. Schäfer, U. Schneider, M. Sierka, O. Treutler, B. Unterreiner, M. von Arnim, F. Weigend, P. Weis, H. Weiss, Turbomole (vers 5.9.1), Universität Karlsruhe, 2007.

3.5 Formation and stability of gaseous ternary oxides of group 14-16 elements and related oxides of group 15 elements: mass spectrometric and quantum chemical study.

K. Kunkel*, E. Milke and M. Binnewies

EurJIC
European Journal
of Inorganic Chemistry

ChemPubSoc
Europe

FULL PAPER

Formation and Stability of Gaseous Ternary Oxides of Group 14–16 Elements and Related Oxides of Group 15 Elements: Mass Spectrometric and Quantum Chemical Study

Katerina Kunkel,*[a] Edgar Milke,[a] and Michael Binnewies[a]

The formation of four hitherto unknown lead tellurium oxides – $PbTeO_3$, $PbTe_2O_5$, Pb_2TeO_4 and $Pb_2Te_2O_6$ – was observed in the gas phase by means of a mass-spectrometric Knudsen-cell method. Other ternary oxides of group 14–16 elements were not observed in the gas phase. The enthalpies of formation for these oxides were obtained experimentally by means of a mass-spectrometric Knudsen-cell method and confirmed theoretically by using quantum chemical (QC) cal-

culations. Appearance potential measurements were conducted for $PbTeO_3$ and Pb_2TeO_4. The structures of the ternary oxides that represent the minima on the potential-energy surfaces were found by using QC calculations. The behaviour of the related compounds $PbTeO_3$, X_2O_3, $Pb_2Te_2O_6$ and X_4O_6 in the gas phase has been discussed (for which X = P, As, Sb, Bi).

1. Introduction

Evaporation of oxides of group 15 elements X_2O_3 (for which X = P, As, Sb, Bi) is widely studied. In the present work, we study the formation of gaseous ternary oxides of group 14–16 elements, which are isoelectronic to X_4O_6 and X_2O_3 oxides. Scotlandit $PbSO_3$, fairbankite $PbTeO_3$ and molybdomenite $PbSeO_3$ are known as very rare minerals and are isoelectronic to group 15 element oxides, X_2O_3. The crystalline structures of $PbSO_3$, $PbSeO_3$ and $PbTeO_3$ with Pb^{2+}, Te^{4+} and Se^{4+} are reported elsewhere.[1–3] Two other bulk higher oxides with Pb^{2+}, Se^{4+} and Te^{4+} are also known: Pb_3SeO_5 and $Pb_2Te_3O_8$.[4,5] Other bulk ternary oxides of group 14–16 elements with oxidation states of 2+ and 4+, respectively, are not known.

The evaporation behaviour of X_2O_3 is well known: the gas phase contains primarily X_4O_6 molecules with a well-known cage structure and molecular symmetry T_d. In the saturated vapour over phosphorus, arsenic and antimony trioxides, no other species besides P_4O_6, As_4O_6 and Sb_4O_6, respectively,[6–8] were detected. In the saturated vapour of bismuth oxide, small concentrations of other Bi/O species, including Bi_2O_3, were found.[9] The gaseous ternary oxides As_3SbO_6, $As_2Sb_2O_6$ and $AsSb_3O_6$, congeners of X_4O_6, have been observed by Drowart et al.[10]

To understand the formation of ternary oxides, we need to understand the behaviour of individual oxides in the gas
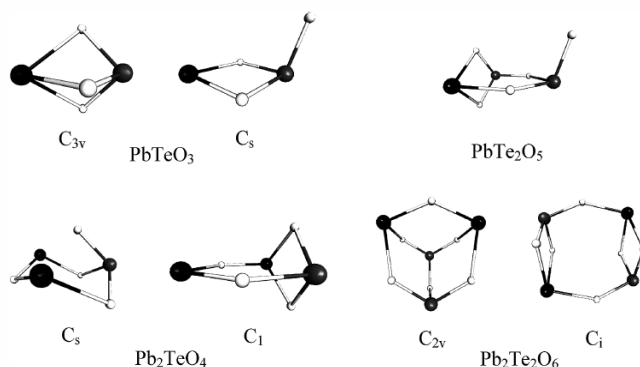
phase. The main gaseous components of the vapour of sulfur, selenium and tellurium dioxides are monomers SO_2, SeO_2 and TeO_2. The vapour above $SO_{2(l)}$ contains only monomeric species $SO_2(g)$; the vapour above $SeO_2(s)$ contains small amounts of dimer Se_2O_4; and the vapour of $TeO_2(s)$ contains $(TeO_2)_x$ (x = 2–4), $(TeO)_x$ (x = 1–4) and Te_2.[11–13] The gas phase over solid lead monoxide consists of mainly PbO, Pb_2O_2 and Pb_4O_4 molecules and a small amount of the oligomers Pb_3O_3, Pb_5O_5 and Pb_6O_6.[14,15] By evaporation of the lead oxide, PbO partly dissociates to form Pb(g) and O_2. Analogously, SnO evaporates to form gaseous SnO, Sn_2O_2, Sn_3O_3 and Sn_4O_4.[16] By the vaporisation of the mixture Ge+GeO_2, GeO was detected as the main compound; Ge_2O_2 and Ge_3O_3 are also presented in the gas phase.[17] Thus the amount of oligomers increases from GeO to SnO and PbO.

In the present work we combined mass-spectrometric experimental and quantum chemical calculations and obtained experimental and theoretical reaction enthalpies

[a] Institut für Anorganische Chemie,
Callinstrasse 9, 30167 Hannover, Germany
E-mail: katja.kunkel@aca.uni-hannover.de
http://www.aci.uni-hannover.de/
Supporting information for this article is available on the WWW under http://dx.doi.org/10.1002/ejic.201402734.

59

$\Delta_r H_T^0$ and standard formation enthalpies $\Delta_f H_{298}^0$ of the ternary oxides. The mass-spectrometric study of the ternary oxides is limited by the narrow temperature range. In such a case it is not possible to obtain the reaction enthalpy by means of the second law of thermodynamics for which the temperature dependence of equilibrium constants has to be determined. Therefore we applied the third law of thermodynamics. The difficulty of that approach is the determination of the reaction entropy $\Delta_r S_T^0$. We used quantum chemical calculations to obtain the reaction entropy.

2. Results and Discussion

2.1 Mass-Spectrometric Study

The formation of gaseous ternary oxides was observed only in the PbO–TeO_2 system. The PbO–TeO_2 system inclined toward glass formation, therefore a mixture of two solid oxides, PbO and TeO_2 (1:1), was heated in a Knudsen cell at 1063 K. The gaseous products of chemical interaction of the oxides were analysed after leaving the Knudsen cell. The relative intensities of the ionic species in the PbO–TeO_2 system are given in Table 1.

Table 1. Intensities of the ionic species over a molten mixture of PbO–TeO_2 (1:1 mol), 70 eV, 1063 K.

Ion	Relative intensity
$Pb_2Te_2O_6^+$	3.3
$Pb_2TeO_4^+$	34.4
$Pb_2TeO_3^+$	2.1
$PbTe_2O_5^+$	6.8
$Pb_2O_2^+$	10.4
Pb_2O^+	3.3
$PbTeO_3^+$	43.1
$PbTeO_2^+$	9.4
$PbTeO^+$	16.9
Te_2^+	20.2
PbO^+	17.9
Pb^+	10.8
TeO_2^+	100
TeO^+	66.4
Te^+	26.4

The following oxide systems have been also studied by means of mass spectrometry using simple and double Knudsen cells (described elsewhere):[18] PbO–SeO_2 (at 900/390 K), SnO–TeO_2 (at 1033 K), SnO–SeO_2 (at 1040/390 K), GeO_2+Ge–TeO_2 (at 950 K) and GeO_2+Ge–SeO_2 (at 950/360 K). Ternary oxides have not been observed in the gas phase in these systems. For the study of the PbO–SO_2 system, $PbSO_3$(s) was evaporated in the Knudsen cell at 450 K. In this experiment only individual oxides were detected.

The fragmentation pathways of the ionised species in the system PbO–TeO_2 are not simple. As previously mentioned, PbO and TeO_2 not only vaporise to form monomers and oligomers but also dissociate into Pb, $(TeO)_x$ (x = 1–4) and Te_2. The Pb^+ ion is formed by the fragmentation and ionisation processes.[15] Muenow et al. attributed the TeO_2^+ ion to TeO_2(g); the TeO^+ ion was attributed to both TeO_2(g) and TeO(g), and the Te^+ ion to TeO(g).[12] Lakshmi

Narasimhan et al. reported the partial pressures of the gaseous components in the vaporisation of TeO_2.[13,19] They obtained the same order of the partial pressure of TeO_2(g) and TeO(g) [$p(TeO)/p(TeO_2) \approx 0.6$–0.7] at temperatures of 885 to 940 K. Thus, the gas phase in the PbO–TeO_2 system, which contained significant concentrations of TeO_2, TeO, Te_2, PbO, Pb and ternary oxides, is complex. In addition to ternary oxides with Te^{4+} and Pb^{2+}, some ternary oxides can contain Te^{2+}. There are six ions in the mass spectrum that are suspected to be parent ions: $PbTeO_3^+$, $Pb_2TeO_4^+$, $PbTe_2O_5^+$, $Pb_2Te_2O_6^+$, $Pb_2TeO_3^+$ and $PbTeO_2^+$.

To distinguish between a parent ion and a fragment ion, we carried out appearance-potential measurements. Unfortunately, appearance potentials were only obtained for two ions with high intensities, $Pb_2TeO_4^+$ and $PbTeO_3^+$, while the intensities of $Pb_2Te_2O_6^+$, $PbTe_2O_5^+$, $Pb_2TeO_3^+$ and $PbTeO_2^+$ were too small. The appearance potentials were derived by linear extrapolation of the ionisation efficiency curves to be the following: $AP(PbTeO_3^+) = (8.9 \pm 0.5)$ eV and $AP(Pb_2TeO_4) = (8.3 \pm 0.5)$ eV. These values agree well with the ionisation energies obtained by quantum chemical calculations (see section 2.2). Therefore, it can be concluded that $Pb_2TeO_4^+$ and $PbTeO_3^+$ are parent ions, formed by the ionisation of Pb_2TeO_4(g) and $PbTeO_3$(g). The biggest indicator that $Pb_2Te_2O_6^+$ is also a parent ion is the mass spectrum, where ions which heavier than the $Pb_2Te_2O_6^+$ ion were not observed. Additionally, the formula $Pb_2Te_2O_6$ is isoelectronic with well-known molecules such as As_4O_6 or Sb_4O_6. The other ions, $PbTe_2O_5^+$, $Pb_2TeO_3^+$ and $PbTeO_2^+$, can be both parent and fragmented ion species. First, we suppose that $PbTe_2O_5^+$, $Pb_2TeO_3^+$ and $PbTeO_2^+$ ions are formed by the ionisation of the hypothetical molecules $PbTe_2O_5$, Pb_2TeO_3 and $PbTeO_2$. By using quantum chemical calculations, we can calculate theoretical thermodynamic values to characterise the hypothetical molecules and compare them with experimental data obtained from the mass spectra.

There is a dependence of the recorded ion current on the partial pressure and temperature, which can be approximated by Equation (1)[20]

$$p_i = c \cdot \Sigma I_i \cdot T \qquad (1)$$

in which p_i is the partial pressure, T is the equilibrium temperature, ΣI_i is the intensity of the ions formed by ionisation and fragmentation and c is the proportionality factor.

The proportionality factor c was determined by a calibration experiment and found to be 1.8×10^{-10}. The deviation of factor c is in the range [$1.8 \times 10^{-10} \times 5$; $1.8 \times 10^{-10}/5$]. The mass-spectrometric measurement of pure PbO oxide was used for the calibration. Equation (2) or Equation (3), which describe the partial pressure of PbO as a function of temperature, were applied for the calibration.

$$\lg(p \, [\text{bar}]) = -32032/T + 1915 \ (850\text{–}1100 \text{ K})^{[14]} \qquad (2)$$

$$\lg(p \, [\text{Pa}]) = -13345/T + 11.89 \ (900\text{–}1150 \text{ K})^{[21]} \qquad (3)$$

By using the c value, the relative intensities ΣI_i, and by applying Equation (1), the partial pressures of the gaseous

molecules in the PbO–TeO$_2$ equilibrium system can be calculated. Table 2 presents the gas molecules, the ions attributed to them (parent ions and their fragments) and the partial pressures of these molecules. The PbO$^+$ ion was considered to be a molecular ion because the ratio of intensities $I(\text{PbO}^+)/I(\text{Pb}_2\text{O}_2{}^+)$ in the mass spectra of ternary oxides was close to this ratio in calibration experiments. Additionally, it was considered that PbTe$_2$O$_5{}^+$, Pb$_2$TeO$_3{}^+$ and PbTeO$_2{}^+$ are the parent ions of the hypothetical molecules PbTe$_2$O$_5$, Pb$_2$TeO$_3$ and PbTeO$_2$. If this hypothesis is not correct, then the obtained partial pressures of the hypothetical molecules must be added to the partial pressures of the existing molecules Pb$_2$Te$_2$O$_6$, Pb$_2$TeO$_4$ and PbTeO$_3$. The TeO$^+$ ion corresponded to both TeO$_2{}^+$ and TeO$^+$ ions. The ratio $p(\text{TeO})/p(\text{TeO}_2)$ was taken to be equal to 0.7, as in the study by Lakshmi Narasimhan et al.[19]

Table 2. Molecules and their ions in the gas phase of a PbO–TeO$_2$ mixture.

Molecule	Attributed ions	Partial pressure, p [bar] (1063 K)
PbO	PbO$^+$	2.4×10^{-6}
TeO$_2$	TeO$_2{}^+$, TeO$^+$	1.5×10^{-5}
TeO	TeO$^+$, Te$^+$	1.1×10^{-5}
Te$_2$	Te$_2{}^+$	2.7×10^{-6}
Pb$_2$Te$_2$O$_6$	Pb$_2$Te$_2$O$_6{}^+$	3.8×10^{-7}
PbTe$_2$O$_5$[a]	PbTe$_2$O$_5{}^+$	7.3×10^{-7}
Pb$_2$TeO$_4$	Pb$_2$TeO$_4{}^+$	4.7×10^{-6}
PbTeO$_3$	PbTeO$_3{}^+$	5.8×10^{-6}
PbTeO$_2$[a]	PbTeO$_2{}^+$	1.3×10^{-6}
Pb$_2$TeO$_3$[a]	Pb$_2$TeO$_3{}^+$	2.9×10^{-7}
Pb$_2$O$_2$	Pb$_2$O$_2{}^+$, Pb$_2$O$^+$	1.8×10^{-6}

[a] Hypothetical molecule.

We neglected the intensity of the PbTeO$^+$ ion since that ion can be a fragment of several ternary oxides. We suppose that PbTeO$^+$ is formed mostly by splitting of Pb$_2$TeO$_4{}^+$ and PbTeO$_3{}^+$ molecules because these molecular ions have high intensities. We will take into account the neglect of the PbTeO$^+$ ion by error estimation.

By using the partial pressures from Table 2, the equilibrium constants of the formation of the ternary oxides could be calculated and are given later.

2.2 Density Functional Theory Computation

2.2.1. Lead, Tellurium and Ternary Lead Tellurium Oxides

The def2-TZVP/RI-BP86 method is very suitable for calculations of ternary oxide systems and gives a good correlation between the experimental and theoretical values. We have previously used this method for calculations of molybdenum, tungsten, tellurium, arsenic, antimony and lead oxides, as well as some ternary oxides formed from them.[22–24] The following lead and tellurium oxides and their ternary oxides (including hypothetical molecules) were calculated with full optimisation of their geometries: PbO, Pb$_2$O$_2$, Pb$_3$O$_3$, Pb$_4$O$_4$, TeO, TeO$_2$, Te$_2$O$_4$, PbTeO$_3$, Pb$_2$TeO$_4$, PbTe$_2$O$_5$, Pb$_2$Te$_2$O$_6$, PbTeO$_2$ and Pb$_2$TeO$_3$. The TeO molecule has a minimum in its potential-energy surface

in the triplet state, as does the related molecule O$_2$. The total energies, thermal energies and point groups of the calculated molecules are presented in Tables 3 and 4.

Table 3. Symmetries, total energies and thermal energies of the lead and tellurium oxides (def2-TZVP/RI-BP86).

Molecule	Point group	Structure	E_{tot} [a.u.]	E_{298}^{therm} [kJ mol^{-1}]
PbO	$C_{\infty v}$		−268.29556	10.80
TeO$_2$	C_{2v}		−418.646847	20.54
TeO	$C_{\infty v}$		−343.394307	13.58
Pb$_2$O$_2$	D_{2h}		−536.690429	26.42
Te$_2$O$_4$	C_i		−837.371218	48.78
Pb$_3$O$_3$	D_{3h}		−805.068232	43.48
Pb$_4$O$_4$	C_{2v}		−1073.496828	59.72

For PbTeO$_3$, Pb$_2$TeO$_4$ and Pb$_2$Te$_2$O$_6$, two structural isomers were found. The difference in the total energies of the two isomers for all the ternary oxides is not large: $E_{\text{tot}}[\text{PbTeO}_3(C_{3v})] - E_{\text{tot}}[\text{PbTeO}_3(C_s)] = -20.9\ \text{kJ mol}^{-1}$, $E_{\text{tot}}[\text{Pb}_2\text{TeO}_4(C_s)] - E_{\text{tot}}[\text{Pb}_2\text{TeO}_4(C_1)] = -8.2\ \text{kJ mol}^{-1}$ and $E_{\text{tot}}[\text{Pb}_2\text{Te}_2\text{O}_6(C_{2v})] - E_{\text{tot}}[\text{Pb}_2\text{Te}_2\text{O}_6(C_i)] = -8.4\ \text{kJ mol}^{-1}$. The Gibbs free-energy values of the isomer transitions at our experimental temperature ($\Delta_i G_{1063}$) for the reactions PbTeO$_3(C_{3v}) \rightleftharpoons$ PbTeO$_3(C_s)$, Pb$_2$TeO$_4(C_1) \rightleftharpoons$ Pb$_2$TeO$_4(C_s)$ and Pb$_2$Te$_2$O$_6(C_i) \rightleftharpoons$ Pb$_2$Te$_2$O$_6(C_{2v})$ are equal to 0.9, 4.6 and 14.5 kJ mol^{-1}, respectively.

According to the values of $\Delta_i G_T$, the theoretical ratio of the partial pressures of the isomers can be calculated at 1063 K: $p[\text{PbTeO}_3(C_{3v})]/p[\text{PbTeO}_3(C_s)] \approx 10{:}9$, $p[\text{Pb}_2\text{TeO}_4(C_1)]/p[\text{Pb}_2\text{TeO}_4(C_s)] \approx 5{:}3$ and $p[\text{Pb}_2\text{Te}_2\text{O}_6(\text{Ci})]/p[\text{Pb}_2\text{Te}_2\text{O}_6(C_{2v})] \approx 5{:}1$. These ratios were used in the experimental determination of the enthalpies of formation of PbTeO$_3$, Pb$_2$TeO$_4$ and Pb$_2$Te$_2$O$_6$.

We have conducted the population analysis based on occupation numbers (PABOONs)[25] at the DFT level. Shared electron numbers (SEN) for pairs of atoms that characterise electron population between atoms and related to the bond energies were obtained. The SEN also determined the bond order and can be compared to analyse

Table 4. Symmetries, total energies and thermal energies of the ternary oxides (def2-TZVP/RI-BP86).

Molecule	Point group	Structure	E_{tot} [a.u.]	E_{298}^{therm} [kJ mol^{-1}]
PbTeO$_3$	C_{3v}		−687.050513	37.72
PbTeO$_3$	C_s		−687.042570	37.82
PbTe$_2$O$_5$	C_1		−1105.781409	65.90
Pb$_2$TeO$_4$	C_s		−955.448539	54.80
Pb$_2$TeO$_4$	C_1		−955.445417	54.86
Pb$_2$Te$_2$O$_6$	C_{2v}		−1374.185073	82.82
Pb$_2$Te$_2$O$_6$	C_i		−1374.181886	83.13
PbTeO$_2$	C_{2v}		−611.773248	27.21
Pb$_2$TeO$_3$	C_1		−880.148555	41.36

Figure 1. Shared electron numbers. Analysis based on occupation numbers (RI-BP86/def2-TZVP).

bond strengths. Figure 1 presents SEN values for the ternary oxides including hypothetical PbTeO$_2$ and Pb$_2$TeO$_3$. The formation of bonds during a reaction can be crucial in understanding the oxide formation. Figure 2 presents charge distribution in the molecules. As we can see, atomic charges of Pb atoms are lower than atomic charges of Te atoms. Therefore it can be concluded that the Te–O bond is more ionic than the Pb–O bond.

The known literature experimental data and calculated vibration spectra of the gaseous tellurium and lead oxides TeO$_2$, PbO, Pb$_2$O$_2$ and Pb$_4$O$_4$ were compared to determine the scaling factor and are presented in Table 5. The experimental frequencies and our calculated frequencies for these gaseous molecules are in good agreement. The calculated frequencies of PbO exceed the experimental values, and the experimental frequencies of TeO$_2$, Pb$_2$O$_2$ and Pb$_4$O$_4$ exceed the calculated values insignificantly (1–3 %). Therefore, the vibrational wavenumbers were not calibrated (scaling fac-

tor: 1). Experimental and unscaled calculated entropies of the tellurium and lead oxides are in good agreement (Table 6). Therefore, we have not scaled the calculated thermodynamic data of the ternary oxides as well.

Thermodynamic values for all the compounds were obtained with help of the FREEH module in a range from standard temperature to the temperature of the mass-spectrometric experiment (298–1060 K). The entropy S_T^0 can be approximated as a function of temperature as in Equation (4).

$$S_T^0 = S_{298}^0 + \int_{298}^{T} c_{p,T}^0 \frac{dT}{T} \qquad (4)$$

in which $c_{p,T}^0 = a + b \times 10^{-3} \times T + c \times 10^6 \times T^{-2}$.

The coefficients a, b and c were calculated mathematically by fitting ten points of S_T^0 and using Equation (4). The calculated entropies and coefficients of the $c_{p,T}^0$ function were compared with the experimental literature values to demonstrate the adequacy of the chosen calculation method (def2-TZVP/RI-BP86) (Table 6). The agreement between the experiment and quantum chemical calculations is quite good. Applying the calculated $c_{p,T}^0$ function gave quantum chemical values of S_T^0 that are close to the experimental values of S_T^0. Therefore, calculated coefficients a, b and c for the ternary oxides are also acceptable and can be used. Calculated entropies and coefficients a, b and c for ternary oxides are presented in Table 7.

127
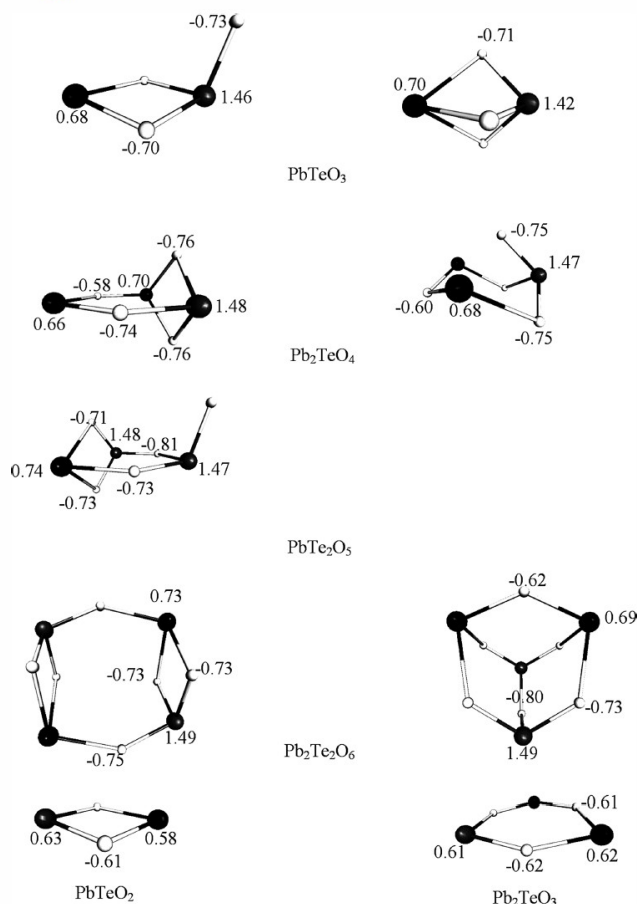
Figure 2. Atomic charges and dipole moments of the molecules (RI-BP86/def2-TZVP).

Table 5. Observed and calculated vibrational frequencies for gaseous As_4O_6, Sb_4O_6, Pb_4O_4, Pb_2O_2 and PbO (scaling factor: 1).

		Vibrational frequencies [cm^{-1}]		
TeO_2	exp.[26]	279	853	–
	calcd.	276.4	833.8	–
Pb_4O_4	exp.[27]	–	372	464
	calcd.	113.3	353.3	451.8
Pb_2O_2	exp.[27]	–	463	558
	calcd.	86.6	455.2	542.7
PbO	exp.[27]	714	–	–
	calcd.	724.0	–	–

The total energies of the cations TeO_2^+, PbO^+, $PbTeO_3^+$, $PbTe_2O_5^+$, $Pb_2TeO_4^+$, $Pb_2Te_2O_6^+$, $PbTeO_2^+$ and $Pb_2TeO_3^+$ were computed in the doublet spin state using the geometry of the neutral molecule to determine the vertical ionisation energies (IEs) of the corresponding molecules (Table S1 in the Supporting Information). Hypothetical molecules were also considered. The first IE was determined as the difference between the total energy of the cation in the doublet state and the energy of the neutral molecule. The experimental appearance energies (AEs) of $PbTeO_3$ and Pb_2TeO_4 were compared with the computed theoretical IEs (Table 8).

Table 6. Experimental[28] and calculated thermodynamic characteristics of gaseous lead and tellurium oxides (def2-TZVP/RI-BP86).

Molecule	S_{298}^0	$c_{p,T}^0 = a + b \cdot 10^{-3} \cdot T + c \cdot 10^6 \cdot T^{-2}$		
	[J mol^{-1} K^{-1}] (exp.//QC)	(exp.//QC)		
		a	b	c
PbO	240.0//240.2	36.2//35.7	1.1//1.5	–0.4//–0.4
TeO_2	275.0//273.7	54.8//53.2	2.4//4.2	–1.2//–0.9
Te_2O_4	376.7//378.7	131.8//124.5	0.7//7.4	–1.7//–2.1
TeO	240.7//233.4	35.3//35.3	1.3//1.8	–0.4//–0.4

Table 7. Calculated thermodynamic characteristics of gaseous lead and tellurium oxides (def2-TZVP/RI-BP86).

Molecule	S_{298}^0 [J mol^{-1} K^{-1}]	$c_{p,T}^0 = a + b \cdot 10^{-3} \cdot T + c \cdot 10^6 \cdot T^{-2}$		
		a	b	c
$PbTeO_3(C_{3v})$	340.1	103.31	4.10	–1.63
$PbTeO_3(C_s)$	360.7	103.04	4.29	–1.60
$PbTe_2O_5$	462.5	174.05	7.48	–2.70
$Pb_2TeO_4 (C_s)$	434.7	152.44	4.72	–2.17
$Pb_2TeO_4 (C_1)$	446.8	151.94	5.16	–2.11
$Pb_2Te_2O_6 (C_{2v})$	521.7	222.98	8.35	–3.18
$Pb_2Te_2O_6 (C_i)$	543.8	223.03	8.32	–3.29
$PbTeO_2$	327.9	80.62	2.19	–1.07
Pb_2TeO_3	422.6	120.65	3.54	–1.36

These values are in good agreement, thereby confirming that the $PbTeO_3^+$ and $Pb_2TeO_4^+$ ions were formed by the ionisation of the ternary oxides rather than a fragmentation process.

Table 8. Calculated vertical first ionisation potentials (IP) (def2-TZVP/RI-BP86) and experimental appearance energy (AE).

Molecule	IE [eV] QC	AE [eV] exp.
PbO	9.65	9.2 ± 0.2[14]
		9.0 ± 0.5[15]
TeO_2	10.81	11.0 ± 0.5[12]
TeO	9.54	9.5 ± 0.5[12]
$PbTeO_3(C_{3v})$	9.56	8.9 ± 0.5[a]
$PbTeO_3(C_s)$	9.07	
$PbTe_2O_5$	9.02	–
$Pb_2TeO_4 (C_s)$	8.63	8.3 ± 0.5[a]
$Pb_2TeO_4 (C_1)$	8.57	
$Pb_2Te_2O_6 (C_{2v})$	8.41	–
$Pb_2Te_2O_6 (C_i)$	8.61	–
$PbTeO_2 (C_{2v})$	6.97	–
$Pb_2TeO_3 (C_1)$	6.36	–

[a] This work.

Table 9 presents the formation reactions of the ternary lead tellurium oxides and the calculated enthalpies, entropies and equilibrium constants at standard and experimental temperatures for these reactions.

The calculated standard enthalpies of formation, $\Delta_f H_{298}^0$, of the ternary oxides can be obtained using the reaction enthalpies $\Delta_f H_{298}^0$ of processes 1–6 from Table 9 and the experimental values of $\Delta_f H_{298}^0(PbO) = 70.3$, $\Delta_f H_{298}^0(TeO_2) = -61.3$ and $\Delta_f H_{298}^0(TeO) = 74.5$.[28]

$\Delta_f H_{298}^0[PbTeO_3(C_{3v}),QC] = -270.9 \text{ kJ mol}^{-1}$

$\Delta_f H_{298}^0[PbTeO_3(C_s),QC] = -249.9 \text{ kJ mol}^{-1}$

$\Delta_f H_{298}^0[PbTe_2O_5(C_s),QC] = -547.7 \text{ kJ mol}^{-1}$

Table 9. Calculated standard enthalpies and entropies of the gaseous reaction and equilibrium constants for the equilibrium processes of lead tellurium oxides (def2-TZVP/RI-BP86).

	Reaction	$\Delta_r H_T^0$ [kJ mol^{-1}] 298//1063 K	ΔS_T^0 [J mol^{-1} K^{-1}] 298//1063 K	$\ln K_{p,T}$ 298//1063 K
1.1	$PbO + TeO_2 \rightleftharpoons PbTeO_3(C_{3v})$	−279.9//−261.8	−173.9//−154.9	92.0//11.0
1.2	$PbO + TeO_2 \rightleftharpoons PbTeO_3(C_s)$	−258.9//−240.9	−153.2//−138.3	86.1//10.6
2	$PbO + 2TeO_2 \rightleftharpoons PbTe_2O_5$	−495.4//−456.0	−325.1//−289.4	160.9//16.8
3.1	$2PbO + TeO_2 \rightleftharpoons Pb_2TeO_4(C_s)$	−545.1//−508.7	−319.5//−288.9	181.6//22.8
3.2	$2PbO + TeO_2 \rightleftharpoons Pb_2TeO_4(C_1)$	−536.8//−500.5	−307.3//−276.8	179.7//23.3
4.1	$2PbO + 2TeO_2 \rightleftharpoons Pb_2Te_2O_6(C_{2v})$	−775.6//−717.8	−506.2//−454.8	252.2//26.5
4.2	$2PbO + 2TeO_2 \rightleftharpoons Pb_2Te_2O_6(C_i)$	−766.9//−709.3	−484.1//−433.2	251.3//28.2
5	$PbO + TeO \rightleftharpoons PbTeO_2(C_{2v})$	−216.1//−201.2	−142.4//−138.4	70.1//6.1
6	$2PbO + TeO \rightleftharpoons Pb_2TeO_3(C_1)$	−424.5//−397.5	−287.9//−278.2	136.7//11.5

$\Delta_f H_{298}^0[Pb_2TeO_4(C_s),QC] = -465.8$ kJ mol^{-1}

$\Delta_f H_{298}^0[Pb_2TeO_4(C_1),QC] = -457.6$ kJ mol^{-1}

$\Delta_f H_{298}^0[Pb_2Te_2O_6(C_{2v}),QC] = -757.6$ kJ mol^{-1}

$\Delta_f H_{298}^0[Pb_2Te_2O_6(C_i),QC] = -748.9$ kJ mol^{-1}

$\Delta_f H_{298}^0(PbTeO_2,QC) = -71.2$ kJ mol^{-1}

$\Delta_f H_{298}^0(Pb_2TeO_3,QC) = -209.4$ kJ mol^{-1}

2.2.2. Other Ternary Oxides of Group 14–16 Elements

Other ternary oxides ABO$_3$ (in which A = Ge, Sn, Pb; B = S, Se, Te) of group 14–16 elements that were not detected in the gas phase by means of mass-spectrometric experiments were also quantum chemically studied. The total energies, thermal energies and entropies of these molecules are presented in Table S2 of the Supporting Information. ABO$_3$ oxides can exist in two isomeric forms: in C_s and C_{3v} symmetries similar to PbTeO$_3$ (see Table 4). The difference in total energies ΔE_{tot} of these isomeric forms does not exceed 21 kJ mol^{-1} for PbSO$_3$, PbSeO$_3$, PbTeO$_3$, SnSO$_3$, SnSeO$_3$ and SnTeO$_3$, and their C_{3v} isomers (except of SnSO$_3$) have lower energies. For GeSO$_3$, GeSeO$_3$ and GeTeO$_3$ the differences in ΔE_{tot} are higher and C_s configuration is more favourable.

The formation of ABO$_3$ ternary oxides (isoelectronic to X$_2$O$_3$) is presented in Table 10 for the sake of comparison. For most of oxides (except of PbTeO$_3$), formation of the C_s isomer is more favourable at 298–1000 K. According to thermodynamic values presented in Table 10, we have concluded that the formation of lead tellurium ternary oxides is more favourable than formation of other ternary oxides of group 14–16 elements, because the values of $\ln K_{p,1000}$ for the PbTeO$_3$ formation reaction are bigger than for the formation reactions of other ABO$_3$ oxides. The stability of the

gaseous ternary oxides increases in the series: Pb > Sn > Ge and Te > Se > S. Although the theoretically calculated equilibrium constant $K_{p,1000}$ of the formation reaction of SnTeO$_3$(C_s) is quite high (Table 10), SnTeO$_3$ was not detected at 1033 K. The reason for that is low pressure of monoxide SnO. Let us consider the following reaction:

$PbO + SnTeO_3(C_s) \rightleftharpoons PbTeO_3(C_{3v}) + SnO$.
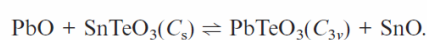
The equilibrium constant $K_{p,1000}$ of this reaction can be calculated by using reactions from Table 10 and it is equal to 3, that is, $\dfrac{p(SnO)}{p[SnTeO_3(C_s)]} \times \dfrac{p(PbTeO_3)}{p(PbO)} = 3$.

By using the preceding equation and partial pressures $p(PbTeO_3)$ and $p(PbO)$ measured at 1063 K, we concluded that partial pressures $p(SnTeO_3)$ and $p(SnO)$ are values on the same order. SnO was not detected in our experiment at 1033 K. It is probable that the partial pressure of SnTeO$_3$ is also too low to detect that ternary oxide. The $K_{p,1000}$ for other reactions from Table 10 is even lower, therefore ternary oxides could not be detected at temperatures about 1000 K.

2.2.3. X$_4$O$_6$ and X$_2$O$_3$ Molecules (X = P, As, Sb, Bi)

In this section, we consider oxides that are related to lead tellurium ternary oxides. X$_4$O$_6$ and X$_2$O$_3$ are isoelectronic (in which X = P, As, Sb, Bi) with Pb$_2$Te$_2$O$_6$ and PbTeO$_3$, respectively. We compare the behaviour of these groups of compounds in the gas phase. Table 11 presents the calculated structures and energetic and thermodynamic characteristics of X$_4$O$_6$ and X$_2$O$_3$. By using these data, the enthalpies, entropies and equilibrium constants of the two reactions, $1/2X_4O_6(T_d) \rightleftharpoons X_2O_3(D_{3h})$ and $X_4O_6(T_d) \rightleftharpoons X_4O_6(D_{2h})$, were calculated. The thermodynamic character-

Table 10. Comparison of the formation reactions of gaseous ternary oxides of group 14–16 elements (def2-TZVP/RI-BP86).

Reaction	$\Delta_r H_{298}^0$ [kJ mol^{-1}]	ΔS_{298}^0 [J mol^{-1} K^{-1}]	$\ln K_{p,298}$//$\ln K_{p,1000}$
$PbO + SO_2 \rightleftharpoons PbSO_3(C_s)$	−139.5	−155.9	37.6//−2.3
$PbO + SeO_2 \rightleftharpoons PbSeO_3(C_{3v})$	−217.0	−172.7	66.8//5.0
$PbO + TeO_2 \rightleftharpoons PbTeO_3(C_{3v})$	−279.9	−158.8	92.0//12.5
$SnO + SO_2 \rightleftharpoons SnSO_3(C_s)$	−129.4	−156.5	33.4//−3.6
$SnO + SeO_2 \rightleftharpoons SnSeO_3(C_s)$	−192.5	−155.2	59.0//4.3
$SnO + TeO_2 \rightleftharpoons SnTeO_3(C_s)$	−252.4	−154.9	83.3//11.4
$GeO + SO_2 \rightleftharpoons GeSO_3(C_s)$	−81.3	−157.3	13.9//−9.5
$GeO + SeO_2 \rightleftharpoons GeSeO_3(C_s)$	−147.6	−1.3	40.8//0.3
$GeO + TeO_2 \rightleftharpoons GeTeO_3(C_s)$	−207.9	−156.0	65.1//5.9

64

istics of these reactions were compared with those of analogous reactions with $PbTeO_3(C_{3v})$, $PbTeO_3(C_s)$, $Pb_2Te_2O_6$-(C_{2v}) and $Pb_2Te_2O_6(C_i)$ (Tables 12 and 13).

Table 11. Point groups, total energies, structures, thermal energies and entropies of X_2O_3 and X_4O_6 oxides, in which X = P, As, Sb, Bi (def2-TZVP/RI-BP86).

Molecule	Point group	Structure	E_{tot} [a.u.]	E^{therm}_{298} [kJ mol^{-1}]	S^0_{298} [J mol^{-1} K^{-1}]
P_2O_3	D_{3h}		−908.660019	44.03	281.3
As_2O_3	D_{3h}		−4698.159549	39.81	303.2
Sb_2O_3	D_{3h}		−706.653441	38.08	318.9
Bi_2O_3	D_{3h}		−655.463908	36.81	336.3
P_4O_6	T_d		−1817.490177	98.37	356.6
As_4O_6	T_d		−9396.461653	87.58	416.5
Sb_4O_6	T_d		−1413.450842	84.18	461.8
Bi_4O_6	T_d		−1311.057395	81.28	506.0
P_4O_6	D_{2h}		−1817.452905	98.13	386.5
As_4O_6	D_{2h}		−9396.425238	87.75	446.0
Sb_4O_6	D_{2h}		−1413.408816	84.14	492.8
Bi_4O_6	D_{2h}		−1311.015205	81.26	535.5

According to the calculated thermodynamic data presented in Table 12, it is clear that the dimerisation of X_2O_3 is much more favourable than the dimerisation of $PbTeO_3$ at standard and high temperatures. Therefore, the presence of $PbTeO_3$ and very small concentrations of X_2O_3 in the gas phase at high temperatures can be expected, as was confirmed experimentally.

The thermodynamics of the isomerisation processes of isoelectronic X_4O_6 and $Pb_2Te_2O_6$ are also different. The structure of X_4O_6 is tetrahedral (T_d) at standard and high temperatures. The structure of $Pb_2Te_2O_6(C_{2v})$, which is analogous to the structure of $X_4O_6(T_d)$, is not the most stable. $Pb_2Te_2O_6(C_i)$ also exists in the gas phase, and it is more stable than $Pb_2Te_2O_6(C_{2v})$ at temperatures above 1000 K.

2.3. Experimental Determination of the Standard Enthalpies of Formation $\Delta_f H^0_{298}$

The equilibrium constant $K_{p,T}$ is related to the reaction enthalpy, reaction entropy and temperature by the van 't Hoff equation. The experimental natural logarithms of the equilibrium constant and enthalpies $\Delta_r H^0_T$ for processes 1–6 were calculated using Equation (5). The values of the reaction entropies $\Delta_r S^0_T(QC)$ are taken from the quantum chemical calculations (Table 9). The enthalpy of reactions $\Delta_r H^0_{1063}$ were obtained using Equation (6) and were converted to $\Delta_r H^0_{298}$ using the calculated $c^0_{p,T}$ functions for the components of the reactions taken from Tables 6 and 7. The standard reaction enthalpies $\Delta_r H^0_{298}$ as well as the reaction enthalpy $\Delta_r H^0_{1063}$ and the natural logarithm of the equilibrium constant $\ln K_{p,1063}$ are presented in Table 14.

$$\Delta_r H^0_T(\text{exp.}) = -RT\ln K_{p,T}(\text{exp.}) + T\Delta_r S^0_T(QC) \tag{5}$$

$$\Delta_r H^0_{T'} = \Delta_r H^0_T + \int_{T'}^{T} c^0_{p,T} dT \tag{6}$$

The experimental standard enthalpies of formation $\Delta_f H^0_{298}$ of the ternary oxides were obtained by using the reaction enthalpies $\Delta_r H^0_{298}$ from Table 14 and the experimental values $\Delta_f H^0_{298}(PbO) = 70.3$, $\Delta_f H^0_{298}(TeO_2) = -61.3$ and $\Delta_f H^0_{298}(TeO) = 74.5$.[28]

We now discuss the possibility of the hypothetical molecules existing in the gas phase. First, we consider reactions 2 and 4 of Table 14, in which the hypothetical molecules $PbTe_2O_5$ and $Pb_2Te_2O_6$ participate. The calculated and experimental enthalpies and equilibrium constant of reactions 2 and 4 are in very good agreement (Tables 9 and 14). The experimental and calculated enthalpies of formation of $Pb_2Te_2O_6$ and $PbTe_2O_5$ are also in good agreement (Table 15). If $PbTe_2O_5$ does not exist, then $PbTe_2O_5^+$ is a fragment ion of $Pb_2Te_2O_6$, and the partial pressure $p(PbTe_2O_5)$ has to be added to the partial pressure $p(Pb_2Te_2O_6)$. In that case, the agreement between the experimental and calculated values of $\Delta_r H^0_{298}$, $\Delta_r H^0_{1063}$ and

Table 12. Comparison of the dimerisation of isoelectronic molecules (def2-TZVP/RI-BP86).

Reaction	$\Delta_r H^0_{298}$ [kJ mol^{-1}]	ΔS^0_{298} [J mol^{-1} K^{-1}]	$\ln K_{p,298}$//$\ln K_{p,1000}$
$P_2O_3(D_{3h}) \rightleftharpoons 1/2P_4O_6(T_d)$	−219.4	−103.0	76.2//14.3
$As_2O_3(D_{3h}) \rightleftharpoons 1/2As_4O_6(T_d)$	−184.5	−94.9	63.1//11.3
$Sb_2O_3(D_{3h}) \rightleftharpoons 1/2Sb_4O_6(T_d)$	−186.2	−88.0	64.6//12.3
$Bi_2O_3(D_{3h}) \rightleftharpoons 1/2Bi_4O_6(T_d)$	−167.5	−83.3	57.2//10.6
$PbTeO_3(C_{3v}) \rightleftharpoons 1/2Pb_2Te_2O_6(C_{2v})$	−107.9	−79.3	34.0//3.0

Table 13. Comparison of the isomerisation reactions (def2-TZVP/RI-BP86).

Reaction	$\Delta_r H^0_{298}$ [kJ mol^{-1}]	ΔS^0_{298} [J mol^{-1} K^{-1}]	$\ln K_{p,298}$//$\ln K_{p,1000}$
$Pb_2Te_2O_6(C_i) \rightleftharpoons Pb_2Te_2O_6(C_{2v})$	−8.7	−22.1	0.8//−1.6
$P_4O_6(D_{2h}) \rightleftharpoons P_4O_6(T_d)$	−97.6	−30.0	35.8//8.1
$As_4O_6(D_{2h}) \rightleftharpoons As_4O_6(T_d)$	−95.8	−29.6	35.1//8.0
$Sb_4O_6(D_{2h}) \rightleftharpoons Sb_4O_6(T_d)$	−110.3	−31.0	40.8//9.5
$Bi_4O_6(D_{2h}) \rightleftharpoons Bi_4O_6(T_d)$	−110.8	−29.5	41.2//10.6

Table 14. Experimental equilibrium constants and enthalpies of gaseous reaction.

	Reaction	$\ln K_{p,1063}$	$\Delta_r H^0_{1063}$ [kJ mol^{-1}]	$\Delta_r H^0_{298}$ [kJ mol^{-1}]
1.1	$PbO + TeO_2 \rightleftharpoons PbTeO_3(C_{3v})$	11.4	−269.7	−278.0
1.2	$PbO + TeO_2 \rightleftharpoons PbTeO_3(C_s)$	11.5	−248.8	−258.0
2	$PbO + 2TeO_2 \rightleftharpoons PbTe_2O_5$[a]	21.0	−493.0	−514.8
3(I)	$2PbO + TeO_2 \rightleftharpoons Pb_2TeO_4(C_s)$	23.7	−517.0	−535.6
3(II)	$2PbO + TeO_2 \rightleftharpoons Pb_2TeO_4(C_1)$	24.3	−508.7	−527.4
4(I)	$2PbO + 2TeO_2 \rightleftharpoons Pb_2Te_2O_6(C_{2v})$	31.4	−761.2	−792.5
4(II)	$2PbO + 2TeO_2 \rightleftharpoons Pb_2Te_2O_6(Ci)$	33.1	−752.8	−783.8
5	$PbO + TeO \rightleftharpoons PbTeO_2$[a]	10.8	−242.5	−248.5
6	$2PbO + TeO \rightleftharpoons Pb_2TeO_3$[a]	22.3	−492.4	−502.7

[a] Hypothetical molecule.

$\ln K_{p,1063}$ of processes 4.1 and 4.2 becomes worse. Therefore, we take this as evidence that PbTe$_2$O$_5$ is present in the vapour.

Table 15. Comparison of the calculated and experimental standard enthalpies of formation of ternary lead tellurium oxides.

Compound	$\Delta_f H^0_{298}$ [kJ mol^{-1}]	$\Delta_f H^0_{298}$(QC) [kJ mol^{-1}]	$\Delta_f H^0_{298}$(exp) − $\Delta_f H^0_{298}$(QC) [kJ mol^{-1}]
PbTeO$_3$(C_{3v})	−269.9 ± 18.5	−270.9	1.0
PbTeO$_3$(C_s)	−248.9 ± 18.5	−249.9	1.0
PbTe$_2$O$_5$	−567.1 ± 34.3	−547.7	−19.4
Pb$_2$TeO$_4$(C_s)	−456.3 ± 34.2	−465.8	9.5
Pb$_2$TeO$_4$(C_1)	−448.1 ± 34.2	−457.6	9.5
Pb$_2$Te$_2$O$_6$(C_{2v})	−770.8 ± 50.6	−757.6	−16.9
Pb$_2$Te$_2$O$_6$(C_i)	−762.1 ± 50.6	−748.9	−16.9

The experimental thermodynamic values for reactions 5 and 6 of Table 14, in which the hypothetical PbTeO$_2$ and Pb$_2$TeO$_3$ are found, do not agree with each other. The experimental value of $\ln K_{p,1063}$ noticeably exceeds the theoretical value, that is, the partial pressures of hypothetical PbTeO$_2$ and Pb$_2$TeO$_3$ are too high in the experiment. This deviation leads to a large discrepancy between the experimental and theoretical enthalpies of formation of hypothetical PbTeO$_2$ and Pb$_2$TeO$_3$, that is, the theoretical values exceed the experimental ones (32 and 78 kJ mol^{-1}, respectively). Thus, the partial pressure of PbTeO$_2$ and Pb$_2$TeO$_3$ must be low. Therefore, we assume that PbTeO$_2^+$ and Pb$_2$TeO$_3^+$ are fragments, and the partial pressures of PbTeO$_2$ and Pb$_2$TeO$_3$ from Table 2 must be added to the partial pressures of PbTeO$_3$ and Pb$_2$TeO$_4$, respectively.

The case in which PbTeO$_2^+$ and Pb$_2$TeO$_3^+$ ions are formed both by the ionisation and fragmentation is also possible. Then the partial pressures of PbTeO$_2$ and Pb$_2$TeO$_3$ molecules have to be approximately 10^{-8} and approximately 10^{-11} bar, respectively, according to the estimation made with the help of theoretical values of $\ln K_{p,T}$ of reactions 5 and 6 (Table 9). Therefore we neglect the existence of PbTeO$_2$ and Pb$_2$TeO$_3$ molecules in the present system.

Under these assumptions, the experimental thermodynamic values were calculated for reactions 1.1, 1.2, 3.1 and 3.2 in Table 9, and the results agreed well with the theoretical values. The experimental and calculated enthalpies of formation of PbTeO$_3$ and Pb$_2$TeO$_4$ are also in good agreement (Table 15).

The differences between the calculated and experimental enthalpies of formation are not very large. The greatest difference of $\Delta_f H^0_{298}$(exp) − $\Delta_f H^0_{298}$(QC) does not exceed 20 kJ mol^{-1}. The deviations of the experimental values are discussed below.

2.4. Error Estimation by the Experimental Determination of the Standard Enthalpies of Formation

Here we will estimate the error presented in the determination of the standard enthalpies of formation. The error in determining the enthalpy of reaction $\Delta_r H^0_T$ includes both the error in the equilibrium constant and the inaccuracy of the calculated entropy of the reaction according to Equation (5). The value of factor c, which is in the range [1.8 × 10^{-10} × 5; 1.8 × 10^{-10}/5], and the error of the sum of

Table 16. Errors in the determination of the equilibrium constants, the enthalpies and entropies of gaseous reaction $E(\ln K_{p,T})$, $E(\Delta_r S^0_T)$ and $E(\Delta_r H^0_T)$.

	Reaction	$E(\ln K_{p,T})$ from factor c	$E(\ln K_{p,T})$ from ΣI_i	$E(\Delta_r S^0_T)$ [J mol^{-1} K^{-1}]	$E(\Delta_r H^0_T)$ [kJ mol^{-1}]
1.1	$PbO + TeO_2 \rightleftharpoons PbTeO_3(C_{3v})$	±1.6	±0.3	±1.1	±18.5
1.2	$PbO + TeO_2 \rightleftharpoons PbTeO_3(C_s)$	±1.6	±0.3	±1.1	±18.5
2	$PbO + 2TeO_2 \rightleftharpoons PbTe_2O_5$[a]	±3.2	±0.4	±2.4	±34.3
3.1	$2PbO + TeO_2 \rightleftharpoons Pb_2TeO_4(C_s)$	±3.2	±0.4	±2.2	±34.2
3.1	$2PbO + TeO_2 \rightleftharpoons Pb_2TeO_4(C_1)$	±3.2	±0.4	±2.2	±34.2
4.1	$2PbO + 2TeO_2 \rightleftharpoons Pb_2Te_2O_6(C_{2v})$	±4.8	±0.5	±3.5	±50.6
4.2	$2PbO + 2TeO_2 \rightleftharpoons Pb_2Te_2O_6(C_i)$	±4.3	±0.5	±3.5	±50.6
5	$PbO + TeO \rightleftharpoons PbTeO_2$[a]	±1.6	±0.2	±1.0	±16.9
6	$2PbO + TeO \rightleftharpoons Pb_2TeO_3$[a]	±3.2	±0.3	±2.0	±33.1

[a] Hypothetical molecule.

the ions ΣI_i [Equation (1)], which is estimated to be 10%, lead to the deviation of $\ln K_{p,T}$ (Table 16). The entropies of reactions, $\Delta_r S_T^0$, are quantum chemical values. Since we did not scale thermodynamic values in quantum chemical calculations, we estimated the deviation of enthalpy of reactions $\Delta_r S_T^0$ by using scaling factors of 1 ± 0.03. According to that, the deviations in the entropies of reactions $E(\Delta_r S_T^0)$ are not very large (Table 16). The errors in the equilibrium constants, the enthalpy of reactions and the entropy of reactions are presented in Table 15. The errors in the standard enthalpies of formation $\Delta_f H_{298}^0$ have corresponding deviations and are given in Table 15.

As mentioned above, we neglected the intensity of the PbTeO$^+$ ion and suppose that this ion is formed by the fragmentation of different ternary oxides. The obtained experimental enthalpies of formation change insignificantly if PbTeO$^+$ corresponds to one ternary oxide entirely: in 2.5, 12.6, 3.4 and 8.5 kJ mol^{-1}, respectively, for PbTeO$_3$, PbTe$_2$O$_5$, Pb$_2$TeO$_4$ and Pb$_2$Te$_2$O$_6$. Actually, the error is even smaller if we distribute PbTeO$^+$ between ternary oxides and keep in mind that molecular ions PbTeO$_3^+$ and Pb$_2$TeO$_4^+$ have high intensities.

4. Conclusion

Ternary oxides of group 14–16 elements were investigated. The gaseous ternary oxides were detected only in the PbO–TeO$_2$ system, which corresponds to our conclusions about the stability of ternary oxides ABO$_3$ (in which A = Ge, Sn, Pb; B = S, Se, Te) made with the help of quantum chemical calculations. The stability of gaseous ternary oxide increases in the series: Pb > Sn > Ge and Te > Se > S. The existence of four hitherto unknown ternary lead tellurium oxides – PbTeO$_3$, PbTe$_2$O$_5$, Pb$_2$TeO$_4$ and Pb$_2$Te$_2$O$_6$ – in the gas phase was proven by means of a mass-spectrometric Knudsen-cell method and confirmed by quantum chemical calculations. Each of the three compounds – PbTeO$_3$, Pb$_2$TeO$_4$ and Pb$_2$Te$_2$O$_6$ – exist in two isomeric configurations. The tellurium and lead atoms in all the ternary oxides have oxidation states of 4+ and 2+, respectively. All the ternary oxides have three-coordinate Te^{4+}, just as in all oligomers of tellurium oxide. The Pb^{2+} is two-coordinate (like in Pb$_2$O$_2$ and Pb$_3$O$_3$) or three-coordinate (like in Pb$_4$O$_4$).

According to population analysis we concluded that Te–O bonds are more ionic than Pb–O bonds in ternary lead tellurium oxides.

The thermodynamics of the dimerisation of isoelectronic PbTeO$_3$ and X$_2$O$_3$ and the isomerisation of isoelectronic Pb$_2$Te$_2$O$_6$ and X$_4$O$_6$ were studied with the help of quantum chemical calculations. Although the structures of the isoelectronic molecules are similar, their behaviour in the gas phase is different. Pb$_2$Te$_2$O$_6$ has two stable isomers with C_{2v} and C_i symmetries, and X$_4$O$_6$ compounds have only one stable isomer with T_d symmetry. Both Pb$_2$Te$_2$O$_6$ and PbTeO$_3$ exist in the gas phase and can be detected. According to the quantum chemical calculations, the dimerisation

of X$_2$O$_3$ is very favourable, unlike the dimerisation of PbTeO$_3$. PbTeO$_3$ is a dominant ternary oxide in the gas phase unlike X$_2$O$_3$, which could be detected in small concentrations only by evaporation of bismuth oxide.[9]

The gas phase of the system contains a significant concentration of binary oxides TeO$_2$, TeO, PbO and elemental gaseous Pb and Te$_2$. Therefore, the possibility of the formation of gaseous ternary oxides with Te^{2+} was considered. The presence of the ionic species Pb$_2$TeO$_3^+$ and PbTeO$_2^+$ in the mass spectra indicated that possibility. By analysing the results of the mass-spectrometric experiment and by using quantum chemical calculations, we have concluded that Pb$_2$TeO$_3^+$ and PbTeO$_2^+$ are fragment ions and that there are no gaseous ternary oxides that contain Te^{2+}.

The enthalpies of formation of the ternary oxides PbTeO$_3$, PbTe$_2$O$_5$, Pb$_2$TeO$_4$ and Pb$_2$Te$_2$O$_6$ in the gas phase were determined by using a mass-spectrometric Knudsen-cell method and were compared with the quantum chemical calculations. The experimental and calculated standard enthalpies of formation are in very good agreement.

Experimental Section

Sample Preparation: Yellow lead monoxide (grade puriss. p.a.), tin monoxide (grade purum), metallic germanium, germanium dioxide (grade puriss. p.a.), selenium dioxide (grade puriss. p.a.) and tellurium dioxide (grade purum) were used in the present study. PbSO$_3$ was obtained by means of a double replacement reaction by using Na$_2$SO$_3$ (grade puris. p.a.) and Pb(NO$_3$)$_2$ (grade puriss. p.a.).

Mass Spectrometry: Mass spectrometric measurements were carried out with a modified Finnigan-type 212 mass spectrometer. The vapours that effused from the Knudsen cells were ionised with 70 eV electrons and accelerated to 3000 V. Ion currents were detected by means of an electron multiplier at 1.6–2.0 kV. A quartz glass simple and double Knudsen cells with an effusion orifice 1 mm in diameter was employed in the investigation of these systems. The temperature was measured with a Pt/Rh–Pt thermocouple. The appearance energies (AEs) of the ions of the ternary oxides were obtained by varying the electron energy to determine the onset of the ions.

Quantum Chemical Calculations: Quantum chemical calculations were performed by using the TURBOMOLE program package.[29] All of the structures of the molecules were fully optimised by using density functional theory (DFT) with the BP86 functional and the def2-TZVP triple-split valence basis set with a polarisation function and small-core effective core potential (ECP) functions. RI treatment, which was also applied, allowed us to speed up computation by a factor of at least 10 without sacrificing accuracy. The total electronic energy E_{tot} was calculated according to theoretical methods and basis sets. Computations of the harmonic vibrational frequencies were performed analytically using the TURBOMOLE module *aoforce*. Thermodynamic values for all the compounds were obtained with help of module FREEH in a range from standard temperature to the temperature of the mass-spectrometric experiments (298–1060 K). Thermal energies include thermal corrections and were calculated within the standard harmonic-oscillator approximation for each molecule in the gas phase. The vibrational frequencies were used unscaled.

Acknowledgments

[1] F. Pertlik, J. Zemann, *Tschermaks Mineral. Petrogr. Mitt.* **1985**, *34*, 289–295.

[2] M. Pasero, N. Rotiroti, *Neues Jahrb. Mineral. Monatsh.* **2003**, 145–152.

[3] V. E. Zavodnik, S. A. Ivanov, A. I. Stash, *Acta Crystallogr., Sect. E* **2008**, *64*, i16.

[4] S.-H. Kim, J. Yeon, P. S. Halasyamani, P. Shiv, *Chem. Mater.* **2009**, *21*, 5335–5342.

[5] J.-C. Champarnaud-Mesjard, P. Thomas, M. Colas-Dutreilh, A. Oufkir, *Z. Kristallogr. New Cryst. Struct.* **2001**, *216*, 185–186.

[6] D. W. Muenow, O. M. Uy, J. L. Margrave, *J. Inorg. Nucl. Chem.* **1970**, *32*, 3459–3467.

[7] R. D. Brittain, K. H. Lau, D. L. Hlidenbrand, *J. Phys. Chem.* **1982**, *86*, 5072–5075.

[8] N. A. Asryan, A. S. Alikhanyan, G. D. Nipan, *Russ. J. Phys. Chem.* **2004**, *78*, 5–11.

[9] L. N. Sidorov, I. I. Minayeva, E. Z. Zasorin, I. D. Sorokin, A. Ya. Borshchevsky, *High Temp. Sci.* **1980**, *12*, 175–196.

[10] J. Drowart, S. Smoes, A. Vanderauwera-Mahieu, *J. Chem. Thermodyn.* **1978**, *10*, 453–464.

[11] E. K. Kazenas, Y. V. Tsvetkov, *Thermodynamics of Evaporation of Oxides*, **2007**, LKI, Moscow, p. 178.

[12] D. W. Muenow, J. W. Hastie, R. Hauge, R. Bautista, J. L. Margrave, *Trans. Faraday Soc.* **1969**, *65*, 3210–3220.

[13] T. S. Lakshmi Narasimhan, R. Balasubramanian, S. Nalini, M. Sai Baba, *J. Nucl. Mater.* **1997**, *247*, 28–32.

[14] A. Popovič, A. Lesar, M. Guček, L. Bencze, *Rapid Commun. Mass Spectrom.* **1997**, *11*, 459–468.

[15] J. Drowart, R. Colin, G. Exsteen, *J. Chem. Soc. Faraday Trans.* **1965**, *61*, 1376–1383.

[16] R. Colin, J. Drowart, G. Verhaegen, *Trans. Faraday Soc.* **1965**, *61*, 1364–1371.

[17] J. Drowart, F. Degrève, G. Verhaegen, R. Colin, *Trans. Faraday Soc.* **1965**, *61*, 1072–1085

[18] M. Binnewies, *Z. Anorg. Allg. Chem.* **1977**, *435*, 156–160.

[19] T. S. Lakshmi Narasimhan, M. Sai Baba, R. Viswanathan, *Thermochim. Acta* **2005**, *427*, 137–147.

[20] M. Binnewies, K. Kinke, H. Schäfer, *Z. Anorg. Allg. Chem.* **1973**, *395*, 50–62.

[21] S. I. Lopatin, I. Ya. Mittova, F. S. Gerasimov, S. M. Shugurov, V. F. Kostryukov, S. M. Skorokhodova, *Russ. J. Inorg. Chem.* **2006**, *51*, 1749–1756.

[22] E. Berezovskaya, E. Milke, M. Binnewies, *Dalton Trans.* **2012**, *41*, 2464–2471.

[23] E. Berezovskaya, E. Milke, M. Binnewies, *Dalton Trans.* **2012**, *41*, 10769–10776.

[24] K. Kunkel, E. Milke, M. Binnewies, *Dalton Trans.* **2014**, *43*, 5401–5408.

[25] C. Ehrhardt, R. Ahlrichs, *Theor. Chim. Acta* **1985**, *68*, 231–245.

[26] R. J. M. Konings, A. S. Booij, A. Kovács, *J. Chem. Phys. Lett.* **1998**, *292*, 447–453

[27] R. K. Khanna, Y. J. Park, *Spectrochim. Acta Part A* **1986**, *42*, 603–606.

[28] M. Binnewies, E. Milke, *Thermochemical Data of Elements and Compounds*, 2nd ed., Wiley-VCH, Weinheim, Germany, **2002**.

[29] R. Ahlrichs, M. Bär, H.-P. Baron, R. Bauernschmitt, S. Böcker, P. Deglmann, M. Ehrig, K. Eichkorn, S. Elliott, F. Furche, F. Haase, M. Häser, C. Hättig, H. Horn, C. Huber, U. Huniar, M. Kattannek, A. Köhn, C. Kölmel, M. Kollwitz, K. May, C. Ochsenfeld, H. Öhm, A. Schäfer, U. Schneider, M. Sierka, O. Treutler, B. Unterreiner, M. von Arnim, F. Weigend, P. Weis, H. Weiss, *Turbomole*, v. 5.9.1, University of Karlsruhe, Germany, **2007**.
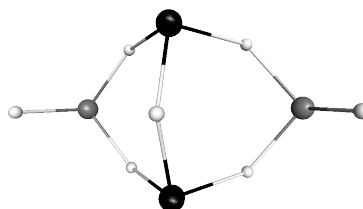
3.6 Formation and stability of antimony tellurium ternary oxides Sb₂TeO₅ and Sb₂Te₂O₇ in the gas phase. Quantum chemical and mass spectrometric studies.
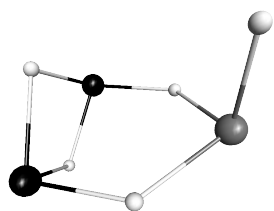
Sb$_2$TeO$_5$ Sb$_2$Te$_2$O$_7$

3.6.1 Summary

The present section concerns the gaseous ternary antimony tellurium oxides. The detailed information about composition of the gas phase of individual antimony and tellurium oxides was reported before. The gas phase over the mixture of solid oxides Sb$_2$O$_3$ and TeO$_2$ contains high concentrations of TeO$_2$ and Sb$_4$O$_6$ similar like the gas phase of individual antimony and tellurium oxides. Additionally two ternary oxides (Sb$_2$TeO$_5$ and Sb$_2$Te$_2$O$_7$) in small concentration were detected. It is known one relative compound of Sb$_2$TeO$_5$ oxide. The gaseous PbTe$_2$O$_5$, which was studied previously is isoelectronic with Sb$_2$TeO$_5$ and has very similar structure.

3.6.2 Mass spectrometric study.

The formation of the ternary antimony tellurium oxides was observed in the gas phase with a help of mass spectrometry. The mixture of two solid oxides Sb$_2$O$_3$ and TeO$_2$ (1:1) was heated in a Knudsen cell by the temperature of 933 K. The gaseous products of interaction of the oxides were analysed after leaving the Knudsen cell. The relative intensities of ion species in system Sb$_2$O$_3$-TeO$_2$ are given in Table 3.1. Unfortunately the appearance potentials could not be obtained for ternary oxides, since the intensities of Sb$_2$TeO$_5^+$ and Sb$_2$Te$_2$O$_7^+$ were too small. It is concluded that Sb$_2$Te$_2$O$_7^+$ is the parent ion because there were no heavier ions in the mass spectra from which they could have been spitted. Presumably the Sb$_2$TeO$_5^+$ is parent ion too. The obtained experimental enthalpies of formation based on this conclusion will be compared with quantum chemical calculated enthalpies of formation.

Table 3.1. Intensities of the ion species in the mixture $Sb_2O_3 - TeO_2$ (1:1 mol), 70 eV, 933 K.

Ion	Relative intensity
$Sb_2Te_2O_7^+$	1.3
$Sb_4O_6^+$	35.9
$Sb_2TeO_5^+$	3.5
$Sb_3O_4^+$	8.2
$Te_2O_4^+$	7.5
$Te_2O_2^+$	4.1
Te_2^+	32.2
TeO_2^+	100
TeO^+	61.3
Te^+	16.0

The partial pressures of the gaseous compounds were calculated using approximated eq. 3.1, which was also used for the investigation of other oxide systems (see above).

$$p_i = c \cdot \sum I_i \cdot T \qquad (3.1)$$

The proportionality factor c was determined by a calibration experiment and was found to be $2.4 \cdot 10^{-10}$ bar·K^{-1}. The mass spectrometric measurement of pure antimony oxide was used for the calibration. The procedure of calibration was described before.

Table 3.2 presents the parent ions, their fragments, which contributed to the gaseous molecules, and the partial pressures of these molecules. The TeO^+ ions are both parent and fragmented ions according to previous studies [73]. The ratio $p(TeO)/p(TeO_2)$ is close to 0.7 in wide temperature range as was reported by Lakshmi Narasimhan *et. al*. [74]. Therefore the contribution of TeO^+ was distributed between partial pressures of TeO and TeO_2 according to mentioned ratio. Using the partial pressures, we determined the equilibrium constants of the formation of the antimony tellurium ternary oxides, which will be given later (Table 3.6).

Table 3.2. Molecules and their ions in the gas phase of the Sb_2O_3- TeO_2 system.

Molecule	Attributed ions	Partial pressure, p (bar) (933 K)
Sb_4O_6	$Sb_4O_6^+$, $Sb_3O_4^+$	$1.0 \cdot 10^{-5}$
TeO_2	TeO_2^+, TeO^+	$2.5 \cdot 10^{-5}$
TeO	TeO^+, Te^+	$1.6 \cdot 10^{-5}$
Sb_2TeO_5	$Sb_2TeO_5^+$	$8.1 \cdot 10^{-7}$
$Sb_2Te_2O_7$	$Sb_2Te_2O_7^+$	$2.9 \cdot 10^{-7}$

3.6.3 Density functional theory computations.

Method def2-TZVP/RI-BP86 which is used for the theoretical investigation of other oxide system, was used for the study of Sb_2O_3-TeO_2 system. The Table 3.3 presents calculated total energies and thermal energies of gaseous components, which were detected experimentally. The good agreement between experimental and theoretical values for individual oxides (Sb_4O_6 and TeO_2) was demonstrated before. Therefore the chosen method of quantum chemical calculations was used for the Sb_2TeO_5 and $Sb_2Te_2O_7$ oxides. The thermodynamic characteristics of the ternary oxides presented in Table 3.4.

Table 3.3. Point group, total energies and thermal energies of the molecules (def2-TZVP/RI-BP86).

Molecule	Point group	E_{tot} (a.u.)	E^{therm}_{298} (kJ·mol^{-1})
TeO_2	C_{2v}	-418.646847	20.54
Sb_4O_6	T_d	-1413.450842	84.18
Sb_2TeO_5	C_s	-1125.397790	66.52
$Sb_2Te_2O_7$	C_1	-1544.122986	94.79

Table 3.4. Calculated thermodynamic characteristics of antimony tellurium oxides (def2-TZVP/RI-BP86).

Molecule	S^0_{298} // S^0_{933} (J·mol^{-1}·K^{-1})	$c^0_{p,T} = a + b·10^{-3}·T + c·10^6·T^{-2}$		
		a	b	c
Sb_2TeO_5	442.2 // 630.9	172.51	9.12	-2.74
$Sb_2Te_2O_7$	544.5 // 810.6	242.00	13.75	-3.75

Table 3.5 presents the reactions for the formation of the ternary antimony tellurium oxides as well as the calculated enthalpies, entropies and equilibrium constants at standard and experimental temperatures for these reactions.

Table 3.5. Calculated standard enthalpies, entropies of reaction and equilibrium constants for the equilibrium processes in the TeO_2 - Sb_4O_6 system in the gas phase (def2-TZVP/RI-BP86).

	Reaction	$\Delta_r H^0_T$ (kJ·mol^{-1}) 298 // 933	ΔS^0_{933} (J·mol^{-1}·K^{-1}) 298 // 933	$lnK_{p.933}$ 298 // 933
1	$TeO_2(g) + 1/2\ Sb_4O_6(g) \rightleftharpoons Sb_2TeO_5(g)$	-64.4 // -59.3	-62.5 // -53.5	18.5 // 1.2
2	$2\ TeO_2(g) + 1/2\ Sb_4O_6(g) \rightleftharpoons Sb_2Te_2O_7(g)$	-264.8 // -249.4	-233.9 // -206.5	78.8 // 7.3

The calculated standard enthalpies of formation $\Delta_f H^0{}_{298}$ of the ternary oxides have been obtained with the help of the reaction enthalpies $\Delta_r H^0{}_{298}$ of the processes from Table 3.5 and the experimental values of $\Delta_f H^0{}_{298}(Sb_4O_6)$ = -1215.5 kJ·mol^{-1} [75], and $\Delta_f H^0{}_{298}(TeO_2)$ = -61.3 kJ·mol^{-1} [75] and are as follows:

$\Delta_f H^0{}_{298}(Sb_2TeO_5,QC)$ = -733.4 kJ·mol^{-1}, and

$\Delta_f H^0{}_{298}(Sb_2Te_2O_7,QC)$ = -995.2 kJ·mol^{-1}.

3.6.4 Experimental determination of the standard enthalpies of formation

The experimental reaction enthalpies $\Delta_r H^0{}_T$ for processes 1 and 2 are calculated with eq. 3.2 and presented in Table 3.6. The values of the reaction entropies $\Delta_R S^0{}_T$ are calculated using quantum chemical values of entropies for ternary oxides.

$$\Delta_r H^0{}_T(\text{exp.}) = -RT \cdot \ln K_{p,T} + T \cdot \Delta_R S^0{}_T \qquad (3.2)$$

$$\Delta_f H^0{}_{T'} = \Delta_f H^0{}_T + \int_T^{T'} c^0{}_{p,T}\, dT \qquad (3.3)$$

Table 3.6. Experimental equilibrium constants and enthalpies of gaseous reactions.

	Reaction	$\ln K_{p,933}$	$\Delta_r H^0{}_{933}$ (kJ·mol^{-1})
1	$TeO_2(g) + 1/2\ Sb_4O_6(g) \rightleftharpoons Sb_2TeO_5(g)$	2.4	-68.6
2	$2\ TeO_2(g) + 1/2\ Sb_4O_6(g) \rightleftharpoons Sb_2Te_2O_7(g)$	12.1	-286.4

Table 3.7. Experimental enthalpies of formation for oxides.

Compound	$\Delta_f H^0{}_{933}$ (kJ·mol^{-1}) exp	$\Delta_f H^0{}_{298}$ (kJ·mol^{-1}) exp	$\Delta_f H^0{}_{298}(QC)$ kJ·mol^{-1}	$\Delta_f H^0{}_{298}(exp)-\Delta_f H^0{}_{298}(QC)$ kJ·mol^{-1}
Sb_2TeO_5	-636.7	-743.6	-733.4	-10.2
$Sb_2Te_2O_7(g)$	-882.8	-1033.4	-995.2	-38.3

The enthalpies of formation ($\Delta_f H^0{}_T$) of the ternary oxides (Table 3.7) were obtained using the determined enthalpies of reactions $\Delta_r H^0{}_T$ (Table 3.5) and enthalpies of formation $\Delta_f H^0{}_{933}$ of $TeO_2(g)$ and $Sb_4O_6(g)$ oxides, which were obtained from eq. 3.3 and the experimental $c^0{}_{p,T}$ functions [75]: ($\Delta_f H^0{}_{933}(TeO_2(g))$ = -28.3 kJ·mol^{-1} and $\Delta_f H^0{}_{933}(Sb_4O_6(g))$ = -1079.7 kJ·mol^{-1}). Then, the calculated enthalpies of formation $\Delta_f H^0{}_{933}$ of the ternary oxides were converted into the standard enthalpies of formation $\Delta_f H^0{}_{298}$ using eq. 3.3 and the calculated a, b and c coefficients of the $c^0{}_{p,T}$ function (Table 3.4). The experimental enthalpies

$\Delta_f H^0_{933}$ and $\Delta_f H^0_{298}$ and the quantum chemical values of $\Delta_f H^0_{298}$ of the ternary oxides are presented in Table 3.6 for comparison.

3.6.5 Conclusions

Two gaseous ternary antimony tellurium oxides (Sb_2TeO_5 and $Sb_2Te_2O_7$) were detected in the gas phase. Atom of tellurium in both ternary oxides has oxidation state 4+ and atom of antimony 3+. Both structures of ternary oxides have three-coordinated Te^{4+} and Sb^{3+} like oligomers of tellurium dioxide and antimony oxide. The structure of Sb_2TeO_5 is similar with the structure of relative isoelectronic $PbTe_2O_5$ oxide, which was studied before.
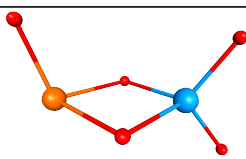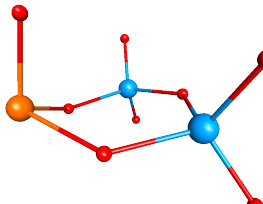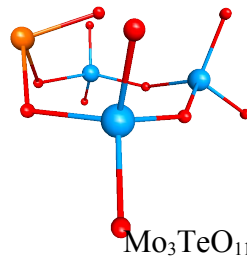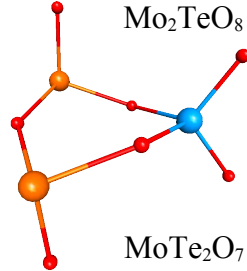
The gas phase of the system contains significant concentration of binary oxides TeO_2, TeO and Sb_4O_6 and small concentration of ternary oxides. Since the intensities of $Sb_2TeO_5^+$ and $Sb_2Te_2O_7^+$ were too small, it was not possible the determination of appearance energies of these ions. But we suppose that Sb_2TeO_5 and $Sb_2Te_2O_7$ oxides exist in the gas phase, because experimental and theoretical enthalpies of formation are in good agreement.

4 Discussion and results

In this thesis the formation and stability of the row of hitherto unknown ternary oxides in the gas phase has been studied. 24 novel ternary gaseous oxides, which were detected by means of mass spectrometry presented in Table 4.1.

All structures are formed of alternating metal/metalloid and oxygen atoms. The structures are built as "rings", "cages" and "open cage" structures. The ring structures presented by $MoTeO_5$, Mo_2TeO_8, Mo_3TeO_{11}, $MoTe_2O_7$, $PbMoO_4$, $PbMo_2O_7$, $PbMo_3O_{10}$, Pb_2MoO_5, $PbTeO_3(C_s)$ and $Pb_2TeO_4(C_s)$ molecules. As we see all compounds of MoO_3-TeO_2 and PbO-MoO_3 systems are built as rings with four-coordinated Mo^{6+}, three-coordinated Te^{4+} and two-coordinated Pb^{2+}. Two molecules of PbO-TeO_2 system ($PbTeO_3(C_s)$ and $Pb_2TeO_4(C_s)$) are ring structures with three-coordinated Te^{4+} and two-coordinated Pb^{2+}. The PbO-TeO_2 system has the structures with cage and open cage geometries too. In these structures Pb^{2+} is three-coordinated (like in Pb_4O_4) and has no lone pair unlike in ring structures with Pb atoms. The Pb^{2+} is four-coordinated in $Pb_3As_2O_6$ and all valence electrons of Pb are shared with oxygen atoms. The cage structures are h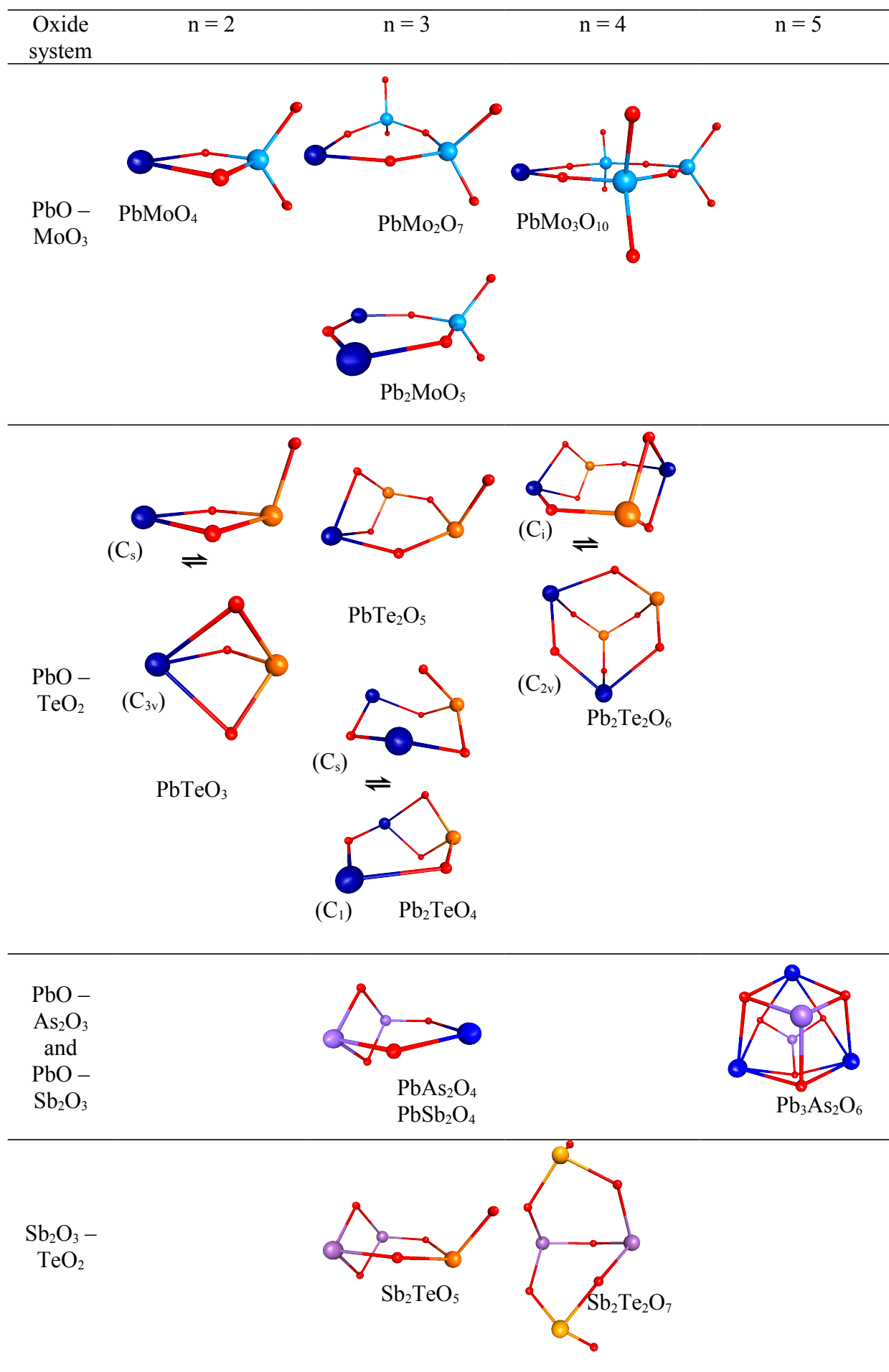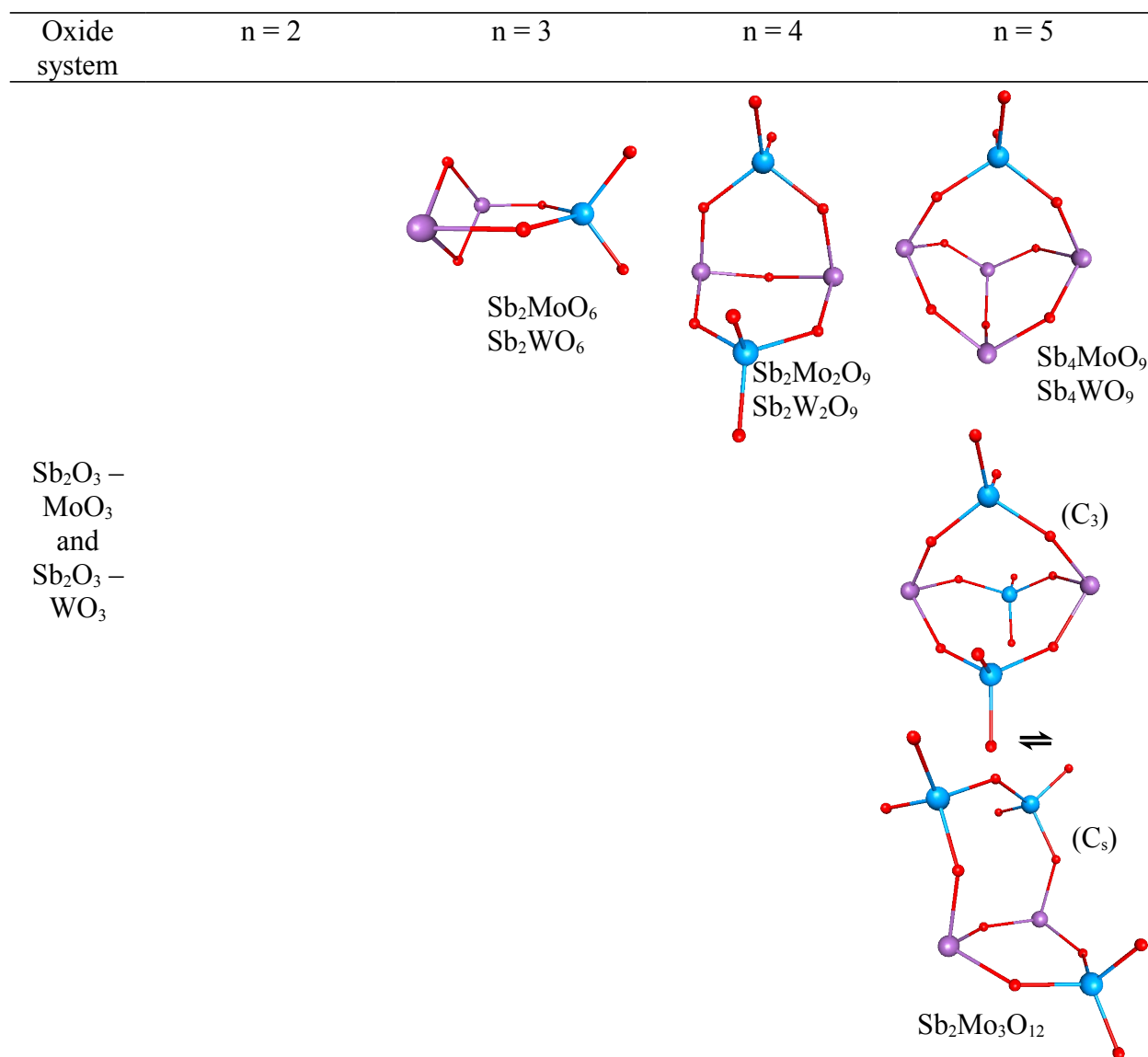igh symmetrical and presented by $PbTeO_3(C_{3v})$, $Pb_2Te_2O_6(C_{3v})$, $Pb_3As_2O_6$ and $Sb_2Mo_3O_{12}(C_{3v})$ molecules. The As^{3+} and Sb^{3+} are three-coordinated in ternary oxides, which are either in cage (like in As_4O_6 and Sb_4O_6) or open cage geometries. All other structures were corresponded to open cage structures: $PbTe_2O_5$, $Pb_2TeO_4(C_1)$, $Pb_2Te_2O_6(C_i)$, $PbAs_2O_4$, $PbSb_2O_4$, Sb_2MoO_6, $Sb_2Mo_2O_9$, $Sb_2Mo_3O_{12}(C_s)$, Sb_4MoO_9, Sb_2WO_6, $Sb_2W_2O_9$, Sb_4WO_9, Sb_2TeO_5 and $Sb_2Te_2O_7$ molecules. The number of metallic/metalloid atoms in gaseous ternary oxides is from one to five atoms.

Table 4.1. Structures of the thernary oxides (n – quantity of metal/metalloid atoms).

Oxide system	n = 2	n = 3	n = 4	n = 5
MoO_3 – TeO_2				

$MoTeO_5$

Mo_2TeO_8

Mo_3TeO_{11}

$MoTe_2O_7$

Oxide system	n = 2	n = 3	n = 4	n = 5
PbO – MoO$_3$	PbMoO$_4$	PbMo$_2$O$_7$	PbMo$_3$O$_{10}$	
		Pb$_2$MoO$_5$		
PbO – TeO$_2$	(C$_s$) ⇌	PbTe$_2$O$_5$	(C$_i$) ⇌	
	(C$_{3v}$) PbTeO$_3$	(C$_s$) ⇌ (C$_1$) Pb$_2$TeO$_4$	(C$_{2v}$) Pb$_2$Te$_2$O$_6$	
PbO – As$_2$O$_3$ and PbO – Sb$_2$O$_3$		PbAs$_2$O$_4$ PbSb$_2$O$_4$		Pb$_3$As$_2$O$_6$
Sb$_2$O$_3$ – TeO$_2$		Sb$_2$TeO$_5$	Sb$_2$Te$_2$O$_7$	

Oxide system	n = 2	n = 3	n = 4	n = 5

Sb$_2$MoO$_6$
Sb$_2$WO$_6$

Sb$_2$Mo$_2$O$_9$
Sb$_2$W$_2$O$_9$

Sb$_4$MoO$_9$
Sb$_4$WO$_9$

(C$_3$)

(C$_s$)

Sb$_2$Mo$_3$O$_{12}$

Sb$_2$O$_3$ –
MoO$_3$
and
Sb$_2$O$_3$ –
WO$_3$

The enthalpies of formation for all gaseous ternary oxides were obtained experimentally and confirmed using quantum chemical calculations. Table 4.2 presents experimental and calculated standard enthalpies of formation and entropies of ternary oxides. The existence of most of gaseous ternary oxides which were studied in that work was proved by appearance energies measurements. The experimental AE values are in very good agreement with theoretical values. For the following ions AEs were measured: Mo$_2$TeO$_8^+$, Mo$_3$TeO$_{11}^+$, Sb$_2$Mo$_2$O$_9^+$, Sb$_4$MoO$_9^+$, Sb$_2$Mo$_3$O$_{12}^+$, Sb$_2$WO$_6^+$, Sb$_2$W$_2$O$_9^+$, PbAs$_2$O$_4^+$, PbMoO$_4^+$, PbMo$_2$O$_7^+$, PbTeO$_3^+$ and Pb$_2$TeO$_4^+$. The intensities of several ions of ternary oxides were too small, therefore their AEs measurements were not possible: MoTeO$_5^+$, MoTe$_2$O$_7^+$, Sb$_2$MoO$_6^+$, Sb$_4$WO$_9^+$, PbSb$_2$O$_4^+$, Pb$_3$As$_2$O$_6^+$, PbMo$_3$O$_{10}^+$, Pb$_2$MoO$_5^+$, PbTe$_2$O$_5^+$, Pb$_2$Te$_2$O$_6^+$, Sb$_2$TeO$_5^+$ and Sb$_2$Te$_2$O$_7^+$. However it was proved that these ions are parent species.

Table 4.2. Experimental and calculated (def2-TZVP/RI-BP86) standard enthalpies of formation and entropies of ternary oxides.

Ternary oxide	$\Delta_f H^0_{298}$	$\Delta_f H^0_{298}$	S^0_{298}
	$kJ \cdot mol^{-1}$	$kJ \cdot mol^{-1}$	$J \cdot mol^{-1} \cdot K^{-1}$
	exp	(QC)	(QC)
$MoTeO_5$	-730.2	-735.4	389.5
Mo_2TeO_8	-1436.3	-1436.1	517.1
$MoTe_2O_7$	-999.7	-1002.7	504.8
Mo_3TeO_{11}	-2132.7	-2110.7	629.3
$PbMoO_4$	-676.3	-698.2	363.2
$PbMo_2O_7$	-1397.2	-1406.0	500.1
Pb_2MoO_5	-888.0	-874.9	472.8
$PbMo_3O_{10}$	-2076.3	-2072.9	635.0
$PbTeO_3(C_s)$	-248.9	-249.9	360.7
$PbTeO_3(C_{3v})$	-269.9	-270.9	340.1
$PbTe_2O_5$	-567.1	-547.7	462.5
$Pb_2TeO_4(C_s)$	-456.3	-465.8	434.7
$Pb_2TeO_4(C_1)$	-448.1	-457.6	446.8
$Pb_2Te_2O_6(C_i)$	-762.1	-757.6	543.8
$Pb_2Te_2O_6(C_{2v})$	-770.8	-748.9	521.7
$PbAs_2O_4$	-659.5	-668.5	407.9
$PbSb_2O_4$	-669.9	-653.4	424.2
$Pb_3As_2O_6$	-1090.3	-1107.8	514.0
Sb_2TeO_5	-743.6	-733.4	442.2
$Sb_2Te_2O_7$	-1033.4	-995.2	544.5
Sb_2MoO_6	-1187.9	-1197.9	440.9
Sb_2WO_6	-1240.7	-1251.1	448.9
$Sb_2Mo_2O_9$	-1905.9	-1907.8	566.4
$Sb_2W_2O_9$	-1994.3	-2012.1	593.0
Sb_4MoO_9	-1881.6	-1888.9	626.3
Sb_4WO_9	-1926.8	-1945.5	569.2
$Sb_2Mo_3O_{12}(C_3)$	-2583.1	-2570.2	691.0
$Sb_2Mo_3O_{12}(C_s)$	-2573.7	-2560.8	699.9

Bibliography

[1] S. Ramanathan, **"***Thin Film Metal-Oxides: Fundamentals and Applications in Electronics and Energy***"**, 2010, Springer Since+Business Media, LLC.

[2] J. F. Wager, Bao Yeh, R. L. Hoffman, D. A. Keszler, *Current Opinion in Solid State and Materials Science*, 2014, 18(2), 53-61.

[3] M. Willander, O. Nur, Q. X. Zhao, L. L. Yang, M. Lorenz, B. Q. Cao, J. Z. Pérez, C. Czekalla, G. Zimmermann, M. Grundmann, A. Bakin, A. Behrends, M. Al-Suleiman, A. El-Shaer, A. Che Mofor, B. Postels, A. Waag, N. Boukos, A. Travlos, H. S. Kwack, J. Guinard, D. Le Si Dang, *Nanotechnology*, 2009, 20, 332001.

[4] Sh.-Q. Li, P. Guo, D. B. Buchholz, W. Zhou, Y. Hua, T. W. Odom, J. B. Ketterson, L. E. Ocola, K. Sakoda, R. P. H. Chang, *ACS Photonics*, 2014, 1 (3), 163–172.

[5] C. Clavero, *Nature Photonics*, 2014, 8, 95–103.

[6] S. D. Jackson, J. S. J. Hargreaves, "*Metal Oxide Catalysis*", 2009, Wiley-VCH.

[7] I. E. Wachs, *Catalysis Today*, 2005, 100, 79–94.

[8] R. Jaaniso, O. K. Tan, "*Semiconductor Gas Sensors*", Woodhead Publishing Series in Electronic and Optical Materials, 2013.

[9] K. Wetchakun, T. Samerjai, N. Tamaekong, C. Liewhiran, C. Siriwong, V. Kruefu, A. Wisitsoraat, A. Tuantranont, S. Phanichphant, *Sensors and Actuators B: Chemical,* 2011, 160(1), 580–591.

[10] Y.-B. Hahn, R. Ahmad, N. Tripathy, *Chem. Commun.*, 2012, 48, 10369-10385

[11] G. E. Moore, H. W. Allison, *Phys. Rev.*, 1950, 77, 246 – 258.

[12] J. Jiang, Y. Li, J. Liu, X. Huang, C. Yuan, X. W. Lou, *Advanced Materials*, 2012, 24 (38), 5166–5180.

[13] A. J. Carrillo, J. Moya, A. Bayón, P. Jana, V. A. de la Peña O'Shea, M. Romero, J. Gonzalez-Aguilar, D. P. Serrano, P. Pizarro, J. M. Coronado, *Solar Energy Materials and Solar Cells*, 2014, 123, 47–57.

[14] T. Block, N. Knoblauch, M. Schmücker, *Thermochimica Acta*, 2014, 577, 25–32

[15] S. Mitra, K. Sridharan, J. Unnam, K. Ghosh, *Thin Solid Films*, 2008, 516 (5), 798–802

[16] T. Kondo, Y. Sawada, K. Akiyama, H. Funakubo, T. Kiguchi, S. Seki, M.H. Wang, T. Uchida, *Thin Solid Films*, 2008, 516 (17), 5864–5867.

[17] N. Yoshida, S. Terazawa, K. Hayashi, T. Hamaguchi, H. Natsuhara, S. Nonomura, *Journal of Non-Crystalline Solids*, 2012, 358 (17), 1987–1989.

[18] K. Iizuka, M. Kambara, T. Yoshida, *Sensors and Actuators B: Chemical*, 2011, 155 (2), 551–556.

[19] D. Horwat, D.I. Zakharov, J.L. Endrino, F. Soldera, A. Anders, S. Migot, R. Karoum, Ph. Vernoux, J.F. Pierson, *Surface and Coatings Technology*, 2011, 205 (2), S171–S177

[20] Y. J. Lee, W. T. Nichols, D.- G. Kim, Y. Do Kim, *J. Phys. D: Appl. Phys.*, 2009, 42, 115419.

[21] B.J. Chen, X.W. Sun, C.X. Xu, B.K. Tay, *Physica E: Low-dimensional Systems and Nanostructures*, 2004, 21 (1), 103–107.

[22] G.F. Pérez-Sánchez, F. Chávez, D. Cortés-Salinas, P. Zaca-Morán, A. Morales-Acevedo, R. Peña-Sierra, O. Goiz, A.T. Huerta, *Vacuum*, 2014, 107, 236–241.

[23] E.K. Kazenas, Yu.V. Tsvetkov, *Thermodynamics of the vaporization of oxides, LKI*: Moscow, 2008.

[24] S. I. Lopatin, S. M. Shugurov, *The Open Thermodynamics Journal,* 2013, *7,* (Suppl 1, M5) 35-56

[25] E.K. Kazenas *Thermodynamics of Vaporization of the Binary oxides*, Nauka: Moscow, 2004.

[26] M. Binnewies, K. Rinke, H. Schäfer, *Z. Anorg. Allg. Chem.*, 1973, 395, 50 – 62.

[27] G. F. Fine, L. M. Cavanagh, A. Afonja, R. Binions, *Sensors*, 2010, 10, 5469-5502.

[28] M. Itoh, K. Hayakawa, Sh. Oishi, *J. Phys.: Condens. Matter*, 2001, 13, 6853–6864.

[29] P. P. González-Borrero, F. Sato, A. N. Medina, M. L. Baesso, A. C. Bento, G. Baldissera, C. Persson, G. A. Niklasson, C. G. Granqvist, A. Ferreira da Silva, *Applied Physics Letters*, 2010, 96, 061909.

[30] S. Barazzouk, R.P. Tandon, S. Hotchandani, *Sensors and Actuators B: Chemical*, 2006, 119 (2), 691–694.

[31] B.T. Marquis, J.F. Vetelino, *Sens. Actuators B*, 2001, 77, 100–110.

[32] S.S. Sunu, E. Prabhu, V. Jayaraman, K.I. Gnanasekar, T.K. Seshagiri, T. Gnanasekaran, *Sensors and Actuators B: Chemical*, 2004, 101 (1-2) 161–174.

[33] Sh. Bai, Ch. Chen, D. Zhang, R. Luo, D. Li, A. Chen, Ch.-Ch. Liu, *Sensors and Actuators B: Chemical*, 2014, 204, 754–762.

[34] J.L. Solis, S. Saukko, L.B. Kish, C.G. Granqvist, V. Lantto, *Sens. Actuators B*, 2001, 77, 316–321.

[35] D. Davazoglou, T. Dritsas, *Sens. Actuators B*, 2001, 77, 359–362.

[36] E. Comini, L. Yubao, Y. Brando, G. Sberveglieri, *Chemical Physics Letters*, 2005, 407 (4-6), 368–371.

[37] V. Oison, L. Saadi, C. Lambert-Mauriat, R. Hayn, *Sensors and Actuators B: Chemical*, 2011, 160 (1), 505–510.

[38] R. Ionescu, A. Hoel, C.G. Granqvist, E. Llobet, P. Heszler, *Sensors and Actuators B: Chemical*, 2005, 104 (1), 132–139.

[39] T. Itoh, J. Wang, I. Matsubara, W. Shin, N. Izu, M. Nishibori, N. Murayama, *Materials Letters*, 2008, 62 (17-18), 3021–3023.

[40] K. Kanda, T. Maekawa, *Sensors and Actuators B: Chemical*, 2005, 108 (1-2), 97–101.

[41] Y. Shimizu, N. Matsunaga, T. Hyodo, M. Egashira, *Sens. Actuators B*, 2001, 77, 35–40.

[42] F. Bender, C. Kim, T. Mlsna, J.F. Vetelino, *Sens. Actuators B*, 2001, 77, 281–286.

[43] Sh.-Y. Lin, Ch.-M. Wang, K.-Sh. Kao, Y.-Ch. Chen, Ch.-Ch. Liu, *Journal of Sol-Gel Science and Technology*, 2010, 53 (1), 51-58.

[44] S. Papaefthimiou, G. Leftheriotis, P. Yianoulis, *Electrochimica Acta*, 2001, 46, 2145-2150.

[45] Gavrilyuk, U. Tritthart, W. Gey, *Solar Energy Materials and Solar Cells*, 2011, 95 (7), 1846–1851.

[46] A.I Gavrilyuk, *Electrochimica Acta*, 1999, 44 (18), 3027–3037.

[47] J. Song, X. Ni, D. Zhang, H. Zheng, *Solid State Sciences*, 2006, 8 (10), 1164-1167.

[48] J. Zhang, W. Zhang, Z. Yang, Z. Yu, X. Zhang, T. Chia Chang, A. Javey, *Sensors and Actuators B: Chemical*, 2014, 202, 708-713.

[49] G. Blasse, M. Wiegel, *Journal of Alloys and Compounds*, 1995, 224 (2), 342-344.

[50] T. Fransen, P. Mars, P. J. Gellings, *Journal of Colloid and Interface Science*, 1979, 70 (1), 97-104.

[51] S. L. Jain, J. K. Joseph, B. Sain, *Catalysis Letters*, 2007, 115 (1-2), 8-12.

[52] I. E. Wachs, T. Kim, E. I. Ross, *Catalysis Today*, 2006, 116, 162–168.

[53] Zh. Liu, T. Yamazaki, Y. Shen, T. Kikuta, N. Nakatani, T. Kawabata, *Appl. Phys. Lett.*, 2007, 90, 173119.

[54] T. Siciliano, M. Di Giulio, M. Tepore, E. Filippo, G. Micocci, A. Tepore, *Sensors and Actuators B: Chemical*, 2009, 137 (2), 644-648.

[55] T. Siciliano, M. Di Giulio, M. Tepore, E. Filippo, G. Micocci, A. Tepore, *Sensors and Actuators B: Chemical*, 2009, 138 (2), 550-555.

[56] Sh. Sen, M. Sharma, V. Kumar, K.P. Muthe, P.V. Satyam, U. M. Bhatta, M. Roy, N.K. Gaur, S.K. Gupta, J.V. Yakhmi, *Talanta*, 2009, 77 (5), 1567-1572.

[57] K. Arshak, O. Korostynska, *IEEE Sensors J.*, 2003, 3, 717–721.

[58] N. Uchida, Y. Ohmachi, *J. Appl. Phys.*, 1969, 40, 4692–4695.

[59] N. Dewan, K. Sreenivas, V. Gupta, *J. Cryst. Growth*, 2007, 305, 237-241.

[60] R. Nayak, V. Gupta, A.L. Dawar, K. Sreenivas, *Thin Solid Films*, 2003, 445, 118-126.

[61] J. E. Shelby, *"Introduction to Glass Science and Technology"*, Royal Society of Chemistry, UK, 2005.

[62] B.V. Raghavaiah, P. Nageswara Rao, P. Yadgiri Reddy, N. Veeraiah, *Optical Materials*, 2007, 29 (5), 566-572.

[63] G. Little Flower, G. Sahaya Baskaran, N. Krishna Mohan, N. Veeraiah, *Materials Chemistry and Physics*, 2006, 100 (2–3), 211–216.

[64] E Culea, Al Nicula, *Solid State Communications*, 1984, 50 (10), 929–932.

[65] T.Honma, R. Sato, Y. Benino, T. Komatsu, V. Dimitrov, *Journal of Non-Crystalline Solids*, 2000, 272 (1), 1-13.

[66] R. Vijay, P. R. Babu, B.V. Raghavaiah, P.M. Vinaya Teja, M. Piasecki, N. Veeraiah, D. Krishna Rao, *Journal of Non-Crystalline Solids*, 2014, 386, 67-75.

[67] S. Bala Murali Krishna, P.M. Vinaya Teja, D. Krishna Rao, *Materials Research Bulletin*, 2010, 45 (12), 1783-1791.

[68] G. S. Baskaran, M.V. Ramana Reddy, D. Krishna Rao, N. Veeraiah, *Solid State Communications*, 2008, 145 (7-8), 401-406.

[69] A.E. Ersundu, M. Çelikbilek, M. Baazouzi, M.T. Soltani, J. Troles, S. Aydin, *Journal of Alloys and Compounds*, 2014, 615, 712-718.

[70] M. Srinivasa Reddy, G. Naga Raju, G. Nagarjuna, N. Veeraiah, *Journal of Alloys and Compounds*, 2007,438, (1-2), 41-51.

[71] T. Satyanarayana, I.V. Kityk, K. Ozga, M. Piasecki, P. Bragiel, M.G. Brik, V. Ravi Kumar, A.H. Reshak, N. Veeraiah, *Journal of Alloys and Compounds*, 2009 482 (1-2), 283-297.

[72] R. Yousefi, Ali Khorsand Zak, F. Jamali-Sheini, N. M. Huang, W. J. Basirun, M. Sookhakian, 2014, *Ceramics International*, 40 (8 A), 11699-11703.

[73] D.W. Muenow, J.W. Hastie, R. Hauge, R. Bautista, J.L. Margrave. *Trans. Faraday Soc.* 65 (1969), 3210

[74] T. S. Lakshmi Narasimhan, M. Sai Baba, R. Viswanathan, *Thermochimica Acta*, 2005, 427, 137

[75] M. Binnewies, E. Milke., *Thermochemical Data of Elements and Compounds*, 2nd ed., Wiley-VCH, 2002.

Lebenslauf

Persönliche Daten:

Name:	Katerina Alexandrovna Kunkel (geb. Berezovskaya)
Geburtsdatum:	29.10.1979
Staatsangehörigkeit:	russisch

Praktische Erfahrungen:

5/2010-3/2015	Wissenschaftliche Mitarbeiterin am Institut für Anorganische Chemie, Leibniz Universität Hannover. Massenspektrometrische Untersuchungen zur Thermodynamik von Hochtemperaturreaktionen. Quantenchemischen Rechnungen. Betreuung von Praktika für fortgeschrittene Studierende im Fach Anorganische Chemie, Betreuung von Bachelor-Arbeiten
9/2007 – 9/2009	Wissenschaftliche Mitarbeiterin am Deutschen Kunststoff Institut, Abteilung Physik, Darmstadt Bearbeitung eines AiF-geförderten Forschungsprojektes zur Untersuchung und Weiterentwicklung von Naturklebstoffen auf Basis von Kasein
1/2006 – 7/2006	Hilfswissenschaftler an der staatlichen Universität St. Petersburg, Fachbereich Physik
5/2005	Stipendium an der V.A. Fock-School für quanten- und rechnergestützte Chemie (INTAS), Novgorod, Russland
5/2004 – 7/2004	Stipendium an der Freien Universität Berlin in der Forschungsgruppe "Hydrogen Bonding and Hydrogen Transfer" am Institut für Chemie und Biochemie (DAAD)
12/2002 – 12/2005	Stipendium an der staatlichen Universität St. Petersburg, Doktorarbeit
10/2002 – 12/2002	Hilfswissenschaftler an der staatlichen Universität St. Petersburg, "Russisches Laserphysikzentrum", Russland

Akademischer Bildungsweg:

03/2015	Promotion zum Dr. rer. nat, Leibniz Universität Hannover. **Thema der Promotion**: "Formation of ternary oxides in the gas phase. Mass spectrometric and quantum chemical investigation"
2/2005	Diplom kandidata nauk im Fachbereich Physik-Mathematik, staatliche Universität St. Petersburg, Russland **Thema der Diplomarbeit**: "Fragmentierungsspektren von organischen Molekülen und Molekülkomplexen bei Elektronen und Ionenbeschuss"
9/1997 – 7/2002	Studium der anorganischen Chemie, staatlichen Universität St. Petersburg, Russland **Thema der Diplomarbeit**: "Donator-Akzeptor-Verbindungen von 4,4'-bipy und Aluminium- und Galliumtrihalogeniden"

Sprachkenntnisse:	Russisch (Muttersprache) Deutsch (verhandlungssicher) Englisch (fließend)

Fachkenntnisse:	• anorganische und organische Synthese, luftempfindliche Synthese in Vacuum
	• Massenspektroskopie
	•Quanten-chemische Berechnung mit den Programmpaketen TURBOMOLE, GAMESS und GAUSSIAN
	• Ultraschall Transmissions- und Ultraschall Reflexionsverfahren
	• Dynamisch-Mechanisch-Thermische Analyse (DMTA, ARES Rheometer)
	• Thermoanalyse mittels Differential Scanning Calorimetry (DSC)
	• Lichtstreuung (NANOPHOX Sympatec)
	• Flüssigkeits-NMR
Zusatzqualifikationen:	Microsoft Office-Paket
	Origin 8
	Photoshop
	Software Point (LIMS)
	Quantenchemische Berechnungssoftware
	Diverse Messsoftware
Hobbys:	joggen, schwimmen, lesen